



저작자표시-비영리-변경금지 2.0 대한민국

이용자는 아래의 조건을 따르는 경우에 한하여 자유롭게

- 이 저작물을 복제, 배포, 전송, 전시, 공연 및 방송할 수 있습니다.

다음과 같은 조건을 따라야 합니다:



저작자표시. 귀하는 원저작자를 표시하여야 합니다.



비영리. 귀하는 이 저작물을 영리 목적으로 이용할 수 없습니다.



변경금지. 귀하는 이 저작물을 개작, 변형 또는 가공할 수 없습니다.

- 귀하는, 이 저작물의 재이용이나 배포의 경우, 이 저작물에 적용된 이용허락조건을 명확하게 나타내어야 합니다.
- 저작권자로부터 별도의 허가를 받으면 이러한 조건들은 적용되지 않습니다.

저작권법에 따른 이용자의 권리는 위의 내용에 의하여 영향을 받지 않습니다.

이것은 [이용허락규약\(Legal Code\)](#)을 이해하기 쉽게 요약한 것입니다.

[Disclaimer](#)

**Thesis for the Degree of Master of Science**

**Damage of stiffened plates due to lateral collision  
and their residual strength under axial compression**

The Graduate School  
University of Ulsan

Department of Naval Architecture and Ocean Engineering

MAY THU CHO

**Damage of stiffened plates due to lateral collision  
and their residual strength under axial compression**

Supervisors: Professor Sang Rai Cho

A Thesis

Submitted to  
the Graduate School of the University of Ulsan  
in Partial Fulfillment of the Requirements  
for the Degree of Master

By

May Thu Cho

Department of Naval Architecture  
and Ocean Engineering,  
University of Ulsan  
Ulsan, Korea

December 2017


# **Damage of stiffened plates due to lateral collision and their residual strength under axial compression**

This certifies that the thesis of May Thu Cho is approved.



---

Committee Chair. Prof. Joo Sung Lee



---

Committee Member. Prof. Hyun Kyoung Shin



---

Committee Member. Prof. Sang-Rai Cho

Department of Naval Architecture  
and Ocean Engineering,  
University of Ulsan  
Ulsan, Korea

December, 2017

# Abstract

Stiffened plate is very conservative tool for engineering constructions. This type of structure is a standard element to start the investigation of the whole structures. Due to their strong demands, many researchers have paid attention to the ultimate strength of stiffened plate in several decades. In marine service life, most of the structures are contributed with stiffened plates.

Stiffened plate structures have to face dynamic loading during their service life. Moreover, the accidental cases such as collision, grounding and falling objects cannot be avoided. In this scenario, the residual ultimate strength becomes crucial factor to withstand the various loading in service life.

Among various structural elements of marine structures, only stiffened plates will be tested and analyzed in this study. Collision accident will be considered as the most probable one. Although damaged stiffened plates have to experience various kinds of loading, however, axial compression will be considered in this study.

At the first stage, lateral collision test are conducted and the results are used to validate the numerical tool for collision analyses. Simultaneously, the axial compression tests were performed and ultimate strength simulation is carried out using displacement control method according to the experimental environment.

# Acknowledgements

The work of this thesis includes all of the efforts of so many people beside the author. I am thankful to every individual, who supports this thesis in various ways and gave me a guide line during this endeavour, with sincere appreciation.

This effort was carried out at the Department of Naval Architecture and Ocean Engineering, the Graduate School, University of Ulsan, during the period of March 2016 to October 2017. I am sincerely thankful to my academic supervisor Professor Sang-Rai Cho for his guidance, great support and kind advice throughout my MSc research studies. It was a real privilege and an honour for me to share his knowledge and kind-hearted patience throughout my study.

I am also grateful and appreciative to my thesis committee, Professor Joo Sung Lee and Professor Hyun Kyoung Shin for their knowledge sharing during this final work.

A special thank to all of my laboratory colleagues from The Ultimate Limit State Analysis Laboratory, (ULSAN LAB) for their constant support, availability and constructive suggestions which were dominant for the accomplishment of the work presented in this thesis.

I would like to express my sincere gratitude to Myanmar Maritime University for giving me a precious chance to study abroad.

Finally, I would like to thank my family for their endless support and encouragement.

May Thu Cho,  
Ulsan, December 2017

# Contents

- Abstract .....i
- Acknowledgements .....ii
- Contents.....iii
- List of figures ..... v
- List of tables .....vii
- List of symbols .....viii
- Chapter 1 Introduction..... 1
  - 1.1 Back ground and motivation..... 1
  - 1.2 Aims and scope of work ..... 3
- Chapter 2 Lateral collision tests on stiffened plates .....4
  - 2.1 Introduction.....4
    - 2.1.1 Material Properties .....4
    - 2.1.2 Dimension of the models .....5
    - 2.1.3 Initial imperfection measurement .....6
  - 2.2 Set up of the experiment .....8
  - 2.3 Lateral collision test results ..... 11
- Chapter 3 Residual strength tests of damaged stiffened plates under axial compression ..... 15
  - 3.1 Geometric measurement of damaged stiffened plates ..... 15
  - 3.2 Set up of the experiment ..... 15
  - 3.3 Residual strength test results ..... 18
- Chapter 4 Numerical analysis of lateral collision tests .....24
  - 4.1 Lateral collision simulation .....24
    - 4.1.1 Assembly of finite element model .....24
    - 4.1.2 Material definition.....25
    - 4.1.3 Boundary Condition.....27
    - 4.1.4 Convergence study .....28
    - 4.1.5 Comparison of predictions and tests .....28
  - 4.2 Intermediate step for releasing boundries ..... 31
- Chapter 5 Residual strength analysis of damaged stiffened plates .....32
  - 5.1 Residual strength simulation.....32
    - 5.1.1 Assembly of finite element model .....32
    - 5.1.2 Material definition.....32
    - 5.1.3 Boundary conditions .....33

5.1.4 Comparison of predictions and tests .....	33
Chapter 6 Discussion.....	42
6.1 Introduction.....	42
6.2 Comparison of numerical predictions with test results.....	42
6.3 Comparison with design formulations.....	43
Chapter 7 Conclusions and recommendations for future works .....	45
7.1 Conclusions.....	45
7.2 Recommendations for future works.....	46
References .....	47
Appendix-A Initial imperfection measurement results (mm) .....	49
Appendix-B Measurement of damaged plates before releasing boundary conditions (mm) .....	52
Appendix-C Measurement of damaged plates after releasing boundary conditions (mm).....	54
Appendix-D Tensile test results .....	56
Appendix-E Strain history of lateral collision tests ( <i>SP-A2</i> and <i>SP-A3</i> ).....	57
Appendix-F Strain history of lateral collision tests ( <i>SP-B2</i> and <i>SP-B3</i> ).....	58
Appendix-G Strain history of axial compression test ( <i>SP-A1</i> , <i>SP-A2</i> and <i>SP-A3</i> ) .....	59
Appendix-H Strain history of axial compression test ( <i>SP-B1</i> , <i>SP-B2</i> and <i>SP-B3</i> ) .....	60
Appendix-I Details of existing design formulations .....	61
Appendix-J Summary of data.....	63



# List of figures

Fig. 1.1 Typical stiffened plate.....	1
Fig. 2.1 (a) Universal tensile machine (b) tensile coupon tests.....	4
Fig. 2.2 Engineering stress-strain curve of plates ( <i>TC-1</i> ), longitudinal stiffeners ( <i>TC-2</i> ) and transverse girders ( <i>TC-3</i> ).....	5
Fig. 2.3 Geometry of the test models (a) lateral collision test (b) axial compression test .....	5
Fig. 2.4 Initial imperfection measurements.....	7
Fig. 2.5 Measurement of deflection.....	7
Fig. 2.6 Lateral collision test (a) striker-head shape (b) boundary conditions .....	8
Fig. 2.7 Experimental set-up for lateral collision test .....	9
Fig. 2.8 Position of impact point and arrangement of striker (a) all the supports are in tension (b) the support on one side is slightly released. ....	10
Fig. 2.9 Strain gauge arrangement for lateral collision test.....	10
Fig. 2.10 The location of the impact point .....	11
Fig. 2.11 Comparison of depth of dent (a) <i>SP-A2</i> (b) <i>SP-A3</i> (c) <i>SP-B2</i> (d) <i>SP-B3</i> .....	12
Fig. 2.12 Model <i>SP-A2</i> (a) Plate side (b) Stiffener side (c) Lateral view of deformation.....	13
Fig. 2.13 Model <i>SP-A3</i> (a) Plate side (b) Stiffener side (c) Lateral view of deformation.....	13
Fig. 2.14 Model <i>SP-B2</i> (a) Plate side (b) Stiffener side (c) Lateral view of deformation.....	14
Fig. 2.15 Model <i>SP-B3</i> (a) Plate side (b) Stiffener side (c) Lateral view of deformation.....	14
Fig. 3.1 Measurement of damaged stiffened plate .....	15
Fig. 3.2 Ultimate strength test set-up .....	16
Fig. 3.3 Arrangement of boundary conditions .....	16
Fig. 3.4 Strain gauge arrangement for axial compression test .....	17
Fig. 3.5 Position of measurement points .....	18
Fig. 3.6 Load axial shortening curve (a) <i>SP-A</i> series (b) <i>SP-B</i> series .....	20
Fig. 3.7 Collapse shape of Model <i>SP-A1</i> (a) Plate side (b) Stiffener side.....	21
Fig. 3.8 Collapse shape of Model <i>SP-A2</i> (a) Plate side (b) Stiffener side.....	21
Fig. 3.9 Collapse shape of Model <i>SP-A3</i> (a) Plate side (b) Stiffener side.....	22
Fig. 3.10 Collapse shape of Model <i>SP-B1</i> (a) Plate side (b) Stiffener side.....	22
Fig. 3.11 . Collapse shape of Model <i>SP-B2</i> (a) Plate side (b) Stiffener side.....	23
Fig. 3.12 Collapse shape of Model <i>SP-B3</i> (a) Plate side (b) Stiffener side.....	23
Fig. 4.1 Assembly of model for lateral collision test .....	24
Fig. 4.2 Boundary condition ‘A’ (a) Tie constraint (b) Fixed boundary condition .....	27
Fig. 4.3 Boundary condition ‘B’ (a) Tie constraint (b) Fixed boundary condition .....	27

Fig. 4.4 Convergence study on finite element models .....	28
Fig. 4.5 Deformation pattern of <i>SP- A2</i> (a) Numerical analysis (b) Experiment .....	30
Fig. 4.6 Deformation pattern of <i>SP- A3</i> (a) Numerical analysis (b) Experiment .....	30
Fig. 4.7 Deformation pattern of <i>SP- B2</i> (a) Numerical analysis (b) Experiment .....	30
Fig. 4.8 Deformation pattern of <i>SP- B3</i> (a) Numerical analysis (b) Experiment .....	30
Fig. 4.9 Deformation of Model- <i>SP-A2</i> (a) before releasing boundary conditions (b) after releasing boundary conditions .....	31
Fig. 5.1 Assembly model for residual strength analysis ( <i>SP-A2</i> ).....	32
Fig. 5.2 Boundary conditions for residual strength analysis ( <i>SP-A2</i> ) .....	33
Fig. 5.3 Distribution of welding residual strength with initial imperfection ( <i>SP-B1</i> ).....	34
Fig. 5.4 Stress-strain curves ( <i>SP-A1</i> ).....	35
Fig. 5.5 Stress-strain curves ( <i>SP-B1</i> ).....	35
Fig. 5.6 Stress distribution across the whole model under uniform axial compression ( <i>SP-A1</i> ) ..	36
Fig. 5.7 Stress distribution across the whole model under uniform axial compression ( <i>SP-A2</i> ) ..	36
Fig. 5.8 Stress distribution across the whole model under uniform axial compression ( <i>SP-A3</i> ) ..	37
Fig. 5.9 Stress distribution across the whole model under uniform axial compression ( <i>SP-B1</i> ) ..	37
Fig. 5.10 Stress distribution across the whole model under uniform axial compression ( <i>SP-B2</i> )	38
Fig. 5.11 Stress distribution across the whole model under uniform axial compression ( <i>SP-B3</i> )	38
Fig. 5.12 Comparison of stress-strain curves ( <i>SP-A1</i> ) .....	39
Fig. 5.13 Comparison of stress-strain curves ( <i>SP-A2</i> ) .....	39
Fig. 5.14 Comparison of stress-strain curves ( <i>SP-A3</i> ) .....	39
Fig. 5.15 Comparisons of stress-strain curves ( <i>SP-B1</i> ).....	40
Fig. 5.16 Comparison of stress-strain curves ( <i>SP-B2</i> ) .....	40
Fig. 5.17 Comparison of stress-strain curves ( <i>SP-B3</i> ) .....	40

# List of tables

Table 2.1 Material Properties .....	4
Table 2.2 Range of parameters.....	5
Table 2.3 Detail description of the models.....	6
Table 2.4 Maximum values of initial deflection measurements (mm).....	7
Table 2.5 Summary of test variables .....	9
Table 2.6 Test results.....	11
Table 3.1 Requirements for axial compression test .....	16
Table 4.1 Comparison of test results and predictions: Strain rate sensitivity (with <i>B.C. 'A'</i> ) .....	27
Table 4.2 Comparison of test results and predictions: Boundary conditions (with <i>M.P. - I</i> ) .....	28
Table 4.3 Comparison of depth of dent at the impact point .....	29
Table 4.4 Comparison of depth of dent at the impact point after releasing boundary conditions	31
Table 5.1 Comparison of residual strength test and numerical analysis results.....	41
Table 6.1 Comparison of various existing design formulae.....	44

# List of symbols

$s_L$	: spacing of longitudinal stiffener
$s_T$	: spacing of transverse girder
$n_{sL}$	: number of longitudinal stiffeners
$w_o$	: lateral displacement of stiffened plate
$w_o^s$	: lateral displacement of stiffener
$w_o^b$	: lateral displacement of the plate
$n_{sT}$	: number of transverse stiffeners
$b_i$	: amplitude (constant) for the stiffener
$C_n$	: amplitude (constant) for the plate
$F_{max}$	: maximum axial force applied along the round bar
$t$	: thickness of the plate
$E$	: modulus of elasticity
$\beta$	: $\frac{s_L}{t} \sqrt{\frac{\sigma_Y}{E}}$ , plate slenderness ratio parameter
$\lambda_c$	: $\sqrt{\frac{\sigma_Y}{\sigma_{ec}}}$ , column slenderness parameter of the stiffener including associated plate
$\lambda_t$	: $\sqrt{\frac{\sigma_Y}{\sigma_{et}}}$ , tripping slenderness parameter of the stiffener
$n_{sL}$	: number of stiffeners in longitudinal direction
$n_{sT}$	: number of girders in transverse direction
$m$	: mass of the element
$g$	: gravitational force assumed 9.81 m/s <sup>2</sup>
$\sigma_x$	: applied axial compressive stress
$\sigma_{ec}$	: Euler column buckling stress of stiffener including associate plating
$\sigma_Y$	: mean yield stress
$\sigma_T$	: ultimate strength of the element
$\sigma_{et}$	: elastic tripping stress of stiffener
$I_w$	: polar moment of inertia of stiffener web
$I_f$	: polar moment of inertia of stiffener flange
$e_s$	: distance between stiffener centroid (plate excluded) and its toe
$\sigma_{eoax}$	: overall grillage buckling stress
$L$	: overall length
$B$	: overall breadth

$a_x$  : average cross sectional area per unit width of plating and longitudinal stiffener  
 $\rho_c$  : knock down factor for column buckling of stiffener  
 $\rho_t$  : knock down factor for tripping of stiffener  
 $\rho_{oa}$  : knock down for overall buckling of stiffened plate under axial compression  
 $R_{eHA}$  : Equivalent minimum yield stress, in N/mm<sup>2</sup> of the considered element  
 $b_{effl}$  : Effective width of the attached shell plating  
 $b_f$  : Width of the flange  
 $h_w$  : Height of the web  
 $h_{we}$  : Effective height of the web  
 $R_{eHp}$  : Minimum yield stress of the material of the considered plate  
 $R_{eHs}$  : Minimum yield stress of the material of the considered stiffener  
 $s$  : plate breadth as the spacing between the stiffeners  
 $l$  : Longer side of the plate  
 $\sigma_x$  : axial stress  
 $t_w$  : thickness of web  
 $t_p$  : thickness of plate  
 $ISI$  : initial shape imperfection  
 $COV$  : coefficient of variance  
 $L_{oa}$  : length overall  
 $B_{oa}$  : breadth overall  
 $t_p$  : thickness of plate  
 $l_{spa}$  : longitudinal stiffener spacing  
 $lh_w$  : longitudinal stiffener web height  
 $lt_w$  : longitudinal stiffener web thickness  
 $lw_f$  : longitudinal stiffener flange width  
 $lt_f$  : longitudinal stiffener flange thickness  
 $t_{spa}$  : transverse frame spacing  
 $th_w$  : transverse web height  
 $tt_w$  : transverse web thickness  
 $t_{wf}$  : transverse flange width  
 $tt_f$  : transverse flange thickness  
 $\sigma_{YP}$  : yield strength of plate element  
 $\sigma_{YI}$  : yield strength of longitudinal stiffeners

- $\sigma_{Yg}$  : yield strength of transverse girders  
 $\sigma_a$  : effective axial stress  
 $\sigma_b$  : bending stress in the stiffener  
 $\sigma_w$  : stress due to torsional deformation  
 $D_x, D_y$  : effective flexural rigidity per unit width of stiffeners with attached plating in longitudinal (x) and transverse (y) direction  
 $D_{xy}$  : twisting rigidity per unit width  
 $G$  : shear modulus of the material  
 $J$  :  $\frac{h_{sf}t_{sf}^3+h_{sw}t_{sw}^3}{3}$  ; St. Venant Torsional moment  
 $M_{equ}$  :  $M_e + \frac{Pba^2}{16}$  ; equivalent bending stress due to end bending moment and lateral pressure  
 $M_e$  : the applied end bending moment  
 $C_w$  :  $I_f \left( \frac{h_w+t_f}{2} \right)^2$  ; Torsional wrapping constant  
 $p$  : applied lateral pressure  
 $X_m$  : the ratio of actual to predicted ultimate strength  
 $M_p$  : fully plastic bending moment  
 $I_o$  : moment of inertia of the stiffener  
 $\sigma_{ec}$  : Euler column buckling stress of stiffener including associated plate  
 $\sigma_{et}$  : Elastic tripping stress of stiffener  
 $\sigma_{eoax}$  : overall grillage buckling stress  
 $\sigma_{xa}$  : applied axial compressive stress

# Chapter 1 Introduction

## 1.1 Back ground and motivation

Stiffened plate is the very conservative way of ingredient in marine service life. It is inevitable that this type of structures have to face the various loading condition and dynamic impact during their service situations. Therefore, the structural behaviour and predicting the stiffness and strength of the stiffened plate is very important for marine structural engineering.

Typical stiffened plate (Fig. 1.1) is composed of longitudinal stiffeners reinforced by the transverse stiffeners. The existence of bending moment and shear force is dominant according to the sizes of ships. Hogging and sagging conditions may also tell the behaviour of the plate on the deck and bottom shell plate. Although the collapse mode of structures under combined loading is really complicated and rare to find out the open literatures, collapse mode under axial compression can be differentiated by column buckling, stiffener tripping and overall buckling.

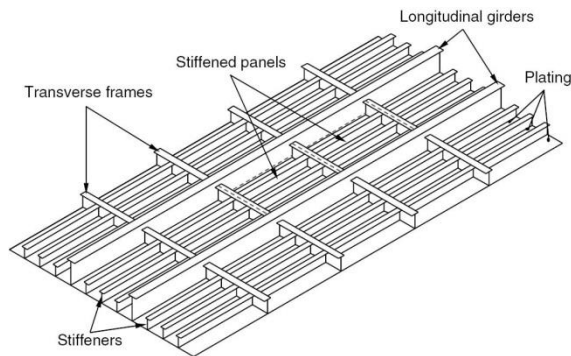


Fig. 1.1 Typical stiffened plate

According to the fact that stiffened plate is one of the most common marine structural elements, the strength of ship plate takes part in a vital role in ultimate strength analysis of ship structures. Theoretical and experimental research with various types of damage not only on stiffened plate but also on the grillage had been performed to understand the behaviour and estimate the residual strength within more than several decades. Although there are many published papers represented for generating different damage using numerical approach, only few papers study on the experimental points of views compared with others.

Marine transportations are still prevalent due to their convenience and price competitiveness. To keep the prevalence, however, it is required for shipbuilding industries to improve the design technology against various accidents including collision and grounding. Probabilistic approaches seem necessary for more rational structural design against accidents. The design process of marine structures consists of the predictions of the accident occurrence probability, the extents of damage due to the accident and the residual strength of the damaged structure. To perform probabilistic approaches in marine structural design considering accidents simple tools are necessary for the predictions. This study is related with the predictions of the extents of damage due to collision accident and the residual strength of the damaged structure.

In realistic condition, ship structures have to experience combination of longitudinal stress, transverse stress, shear stress and lateral pressure before and after collision. Failure of stiffened plate can lead to the destruction of the whole ship. To lessen the consequences of damage, the ship

structure should withstand some degree of damage. Therefore, it is a prerequisite to evaluate and understand the residual strength of damaged stiffened plate in order to improve the design tolerance and rehabilitation of damaged ships.

“Damages” refer to the corrosion due to environmental effects, local dent due to collision and grounding or falling objects, fatigue cracks due to dynamic loads that may leads to the reduction in loading capacity of the structures. The initial imperfection due to fabrication and welding process can sustain the initiation of the cracking damage. This imperfection with the repeated dynamic loading can grow the damage up in an unstable way which progresses the catastrophic failure of the structure.

To specify the ultimate limit state throughout their design life, the cracking damage should be taken into consideration. The longitudinal edge crack along the weld intersections between plates and support members can decrease the plate ultimate strength significantly which is kind of the most common damage in actual steel-plated structures [1].

A single crack consideration is very conservative since the structural members may have gone through the multiple crack damages during their service conditions. Therefore, the crack propagation characteristics and the interaction between propagation cracks take part as a vital role in the plastic collapse mechanism. Numerical study on the multiple cracks of the structures [2] also point out the fact that the existence of disturbing cracks in higher stress region declines the ultimate strength of the whole structures substantially.

Damage caused by corrosion is inevitable not only in marine service life but also on various scopes and therefore many researchers have a great interest on this. Moreover, a series of investigations on several kind of corrosion have been conducted and the results also indicated that the corrosion is greatly dependent upon the geometric properties of the plate thickness

Denting is a type of structural degradation, and should be investigated to prevent an unexpected structural failure. The mass and shape of the striker, the range of the impact velocity, the position of the impact on the target, the boundary conditions, and a nonlinearity of the geometrical and material properties are factors affecting the formulation of dented structures.

The rate of reduction of the ultimate strength is also affected by different type of dents [3]. The shape of a spherical or conical depression does not affect the collapse strength of a plate [4]. A collision caused by a sharp edge can greatly decrease the residual strength of the plate compared with other collision types. The global displacement response of the plate is dependent on the type of collision test, namely, dynamic or quasi-static [5-6]. A stiffened plate with greater or smaller rigidity does not significantly affect the deformation profile of the plate, although the resistance against a collision differs [7].

The plate geometry, loading position, and indenter geometry are crucial factors of a metal sheet under lateral indentation. In past decades, studies on blunt or sharp shape strikers were a popular trend when considering a collision on a stiffened or unstiffened plate. These days, however, a hemispherical or spherical shape is more approachable according to the advanced technologies of marine industries. The radius of the striker is greater, and the resistance of the plate has also increased [8].

The failure model of a stiffened plate is quite, complicated and the residual strength of this type of structures undergoing damage is a problem to consider. The indentation on a stiffener causes a higher loss of the panel strength compared with a panel damaged on a plate between stiffeners, and the initial imperfection has no influence on the dynamic test results [9].



Probabilistic approaches seem necessary for determining a more rational structural design accident occurrence probability, the extent of damage from an accident, and the residual strength of the damaged structure. To apply probabilistic approaches to a marine structural design when considering an accident, simple tools are necessary for predictions. The aim of our study is to attain the extent of damage and the influencing factors affecting the reduction of the ultimate strength of a stiffened plate under a lateral collision.

Several types of numerical, analytical, experimental and non-linear finite element approaches on plates and stiffened panels have been conducted regarding with variety of imperfections, different loading conditions and boundary conditions [10-13]. However, only very limited literatures are available on the ultimate compressive strength of orthotropic stiffened plates with geometric imperfection and material nonlinearity. The residual strength of this type of structures will be focused on this study.

## **1.2 Aims and scope of work**

This thesis is focused on the residual compressive strength of one and two half bays stiffened plate. Two kinds of experimental investigations have been conducted with the facility of ULSAN LAB. The objectives of the present work are:

- To provide experimental information of the resistance of the stiffened plates against lateral impact loadings.
- To provide experimental information of the residual strength of damaged stiffened plates under axial compression.
- To predict the extent of damage due to lateral collision and residual strength of damaged stiffened plates under axial compression.

A brief description of this study is summarized as follows;

Chapter 1 represents for the trace of history and research background in order to understand the scenario of lateral collision and ultimate strength simulations.

A detailed explanation in the design of the models and lateral collision test scenario is described in Chapter 2. In this chapter, the description of the models, initial imperfection measurement, tensile test results and an overview of lateral collision test are presented.

In Chapter 3, the residual strength of damaged stiffened plates under uniform axial compression is mentioned. In this chapter, the residual strength and failure mode of each model are described in details.

The procedure of FEM analysis based upon the experimental condition is analysed in Chapters 4 and 5.

# Chapter 2 Lateral collision tests on stiffened plates

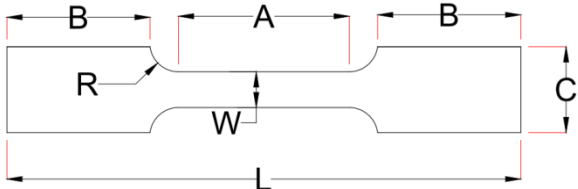
## 2.1 Introduction

### 2.1.1 Material Properties

The strength of the material is the primary concern in terms of the stress necessary to attain plastic deformation or the maximum stress that the material can withstand. A quasi-static tensile test was conducted to obtain the mechanical properties. According to the KS B 0801 [14], tensile coupons were designed. Steel is the main composer in all models. A total of fifteen tensile coupons (five from the plate, five from the stiffeners, and the others from the transverse) were prepared and tested using a Universal Testing Machine (Fig. 2.1).



(a)



- L, overall length : 180 mm
- C, width of grid section : 30 mm
- B, length of grid section : 50 mm
- A, length of reduced section : 60 mm
- w, width of reduced section : 13 mm
- R, radius of fillet : 10 mm

(b)

Fig. 2.1 (a) Universal tensile machine (b) tensile coupon tests

The average material properties of the steel plate and stiffeners attained from three different groups are listed in Table 2.1. The results indicated that the thickness of the plate is quite important in a tensile section. A thinner plate can resist the tension and stress better than a thicker plate; however, a suddenly drop occurs when a fracture is initiated as shown in Fig. 2.2. The average ultimate tensile strength of all tensile coupons is approximately 1.7 times larger than their average yield strength.

Table 2.1 Material Properties

Item	Plate	Stiffener	
		Longitudinal	Transverse
$t$ (mm)	2.85	2.93	9.68
$\sigma_Y$ (MPa)	351	347	257
$\sigma_T$ (MPa)	416	415	434
$E$ (MPa)	228850	234285	217012

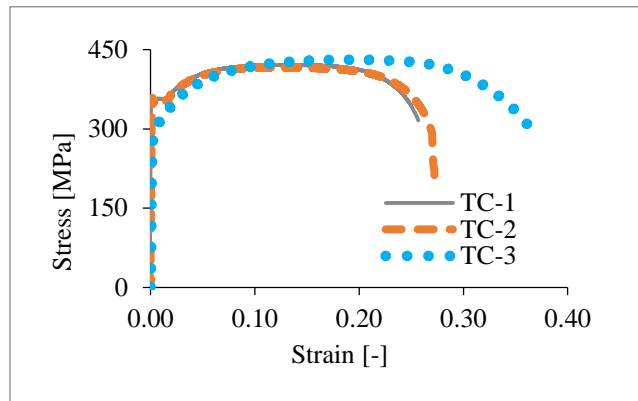


Fig. 2.2 Engineering stress-strain curve of plates (TC-1), longitudinal stiffeners (TC-2) and transverse girders (TC-3)

### 2.1.2 Dimension of the models

Stiffened plates are extensively used as structural components of marine structures. These kinds of structures normally suffer from various types of damage. Among such types, a lateral collision is a crucial scenario that can lead to catastrophic failure of an entire structure. Therefore, the stiffened plate of a VLCC hull form [15] was extracted and scaled down to simulate a prototype similar to a real case. However, variations in the dimensions were applied to study the effects on the lateral collision test. The parameter ranges are as shown in Table 2.2.

Table 2.2 Range of parameters

	$\beta$	$\lambda_c$	$\lambda_T$
<i>VLCC</i>	1.4-1.5	0.3-1.2	0.3-3.8
<i>SP-A</i>	1.3	0.34	0.37
<i>SP-B</i>	1.3	0.24	0.28

The experimental models as shown in Fig. 2.3, approximately one-fifteen scale of stiffened plate in *VLCC*, is shaped with six longitudinal stiffeners and two transverse girders. This type of one and two half bays stiffened plate is divided into two series according to their different scantlings.

In the letter “*SP-A*” and “*SP-B*”, *SP* refers to the stiffened plate, “*A*” for IA-30x15x2.93 mm and “*B*” for IA-40x20x2.93 mm respectively. However, the same transverse section properties is possessed. The detail descriptions of experimental models are presented in Table. 2.3.

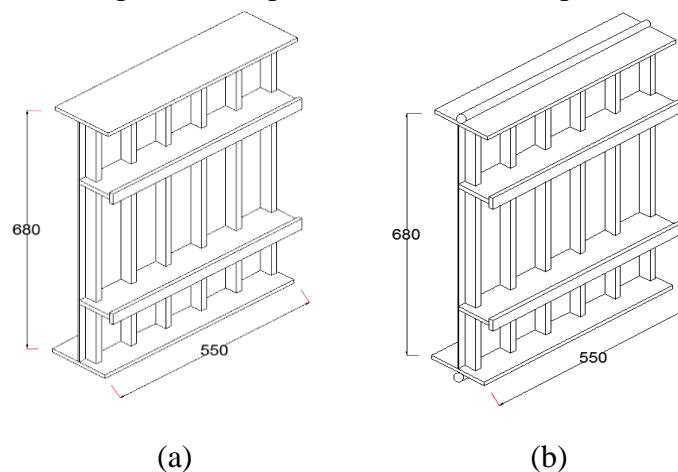


Fig. 2.3 Geometry of the test models (a) lateral collision test (b) axial compression test

Table 2.3 Detail description of the models

Model	Plate	Stiffener		$n_{sL}$	$n_{sT}$
		Longitudinal ( $s_L$ )	Transverse ( $s_T$ )		
	(mm)	(mm)	(mm)		
<i>SP-A1</i>	680x550x2.85	30x15x2.93 IA (100)	90x30x9.68 T (340)	6	2
<i>SP-A2</i>					
<i>SP-A3</i>					
<i>SP-B1</i>		40x20x2.93 IA (100)			
<i>SP-B2</i>					
<i>SP-B3</i>					

End plates are fitted at both ends of the models in order to provide the rigid boundary conditions for lateral collision test (Fig. 2.3(a)). Additional arrangement of round bars to the end plates can be seen in Fig. 2.3 (b) which is intended to apply in axial compression test.

### 2.1.3 Initial imperfection measurement

Fabrication process may induce the initial shape imperfection and residual stresses in plates. The geometry of a distorted stiffened plate can be described by means of two components, one that causes due to the lateral displacement of the plate and the other with lateral displacement of stiffeners. The interaction between this distortions of plate can be functioned as below.

$$w_0 = w_0^s(x, y) + w_0^b(x, y) \quad (1)$$

The lateral displacement of a stiffener may be assumed as half sinusoidal wave and therefore the reference plane between two adjacent stiffeners may be steady increment of sinusoidal function within a specific amplitude.

$$w_0^s = \left\{ b_i + (b_{i+1} - b_i) \frac{x}{a} \right\} \sin \frac{\pi y}{b} \quad (2)$$

The lateral displacement of plate relative to the reference plane between two adjacent stiffeners can be presented as below.

$$w_0^b = \sum_{n=1}^N C_n \sin \frac{\pi x}{a} \sin \frac{n\pi y}{b} \quad (3)$$

Therefore, the total lateral displacement of the plate becomes

$$w_0(x, y) = \left\{ b_i + (b_{i+1} - b_i) \frac{x}{a} \right\} \sin \frac{\pi y}{b} + \sum_{n=1}^N C_n \sin \frac{\pi x}{a} \sin \frac{n\pi y}{b} \quad (4)$$

The shape profile of the plate can alter the collapse mode of stiffened plate and then the amplitude of the plate becomes crucial roles in predicting the ultimate strength. Antoniou (1980, 1984) investigated more than 2000 plate panels of a 30000 DWT class product carrier, a 37000 DWT class bulk carrier, a floating crane and hatch covers. In his study, the derivation of four categories; deflection shapes of sinusoidal, dished and horse-shaped and multi-waves, are dominant according to their aspect ratio of the plate panels. However, the results indicated that the uncertainty of the proposed equation is in high condition.

DNV [16] rules also consider the imperfection effect into the reduced slenderness parameter in order to predict the buckling strength of stiffened panels. The out-of-straightness of stiffeners or girder flange relative to the web plane shall not exceed the value 0.0015 time of the transverse spacing. Moreover, the out of plane displacement of unstiffened plate panels shall not exceed 0.02 time of the longitudinal stiffeners spacing. It is also recommended that the buckling strength of a fabricated structure with larger imperfections may be determined by use of the actually measured imperfection amplitude.

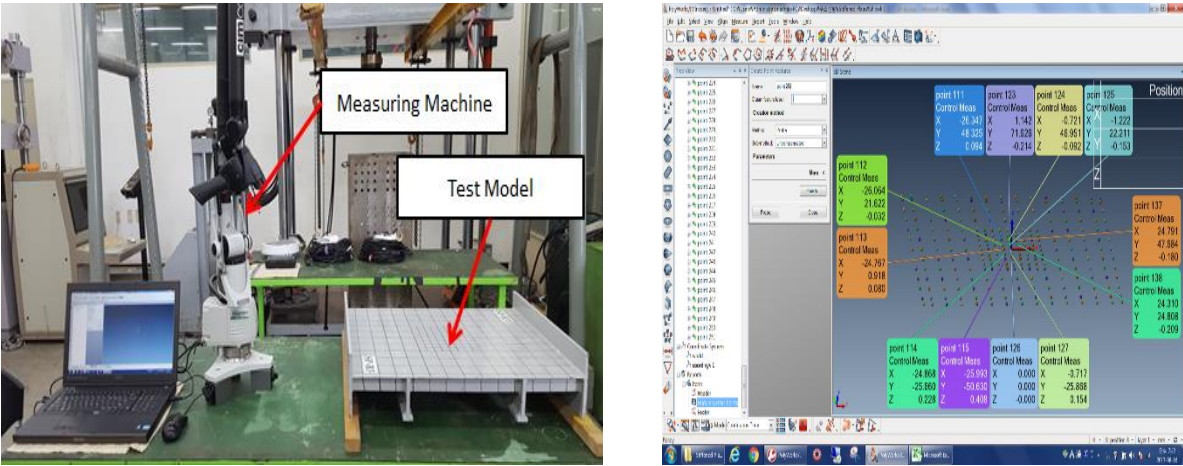


Fig. 2.4 Initial imperfection measurements

In our experiment, the grid line plan has been assigned on the raw model in order to detect the initial geometric imperfection throughout the structure. Initial imperfection due to fabrication process is taken into account since their magnitude and shape can disturb the collapse mode of stiffened plates. The data of out of flatness of the plate and out of straightness of the stiffeners along the grid lines shown in Fig. 2.4 are collected using measuring machine in order to reduce the geometric uncertainty of the models.

The measurement data pointed out the fact that all models possess the horse-shape deflection. The edges of the models have higher deformed shape because of the welding connection between stiffened plate and end plate. The stiffener side way of *SP-B3* is severe compared with the others. The maximum values of initial deflection measurements (Fig. 2.5) are shown in Table 2.4.

Table 2.4 Maximum values of initial deflection measurements (mm)

	<i>SP-A1</i>	<i>SP-A2</i>	<i>SP-A3</i>	<i>SP-B1</i>	<i>SP-B2</i>	<i>SP-B3</i>
Max. lateral deflection of plate	3.92	4.10	2.08	4.09	3.85	2.71
Max. lateral deflection of stiffener	10.09	7.01	2.65	3.13	5.30	5.36
Max. transverse deflection of stiffeners	9.71	7.77	8.98	8.16	11.81	7.49
Max. transverse deflection of girders	20.55	17.34	17.52	17.94	14.39	17.20

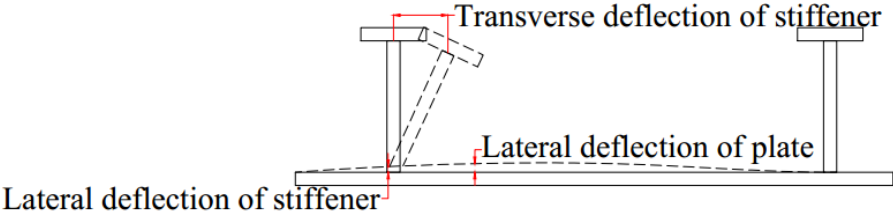


Fig. 2.5 Measurement of deflection

## 2.2 Set up of the experiment

The aim of our study is to predict the extent of damage due to lateral collision and the residual strength of damaged stiffened plate. In order to conduct this purpose, the experiment is divided into two portions.

1-Collision test : to generate the permanent damage extent on the mid length between stiffeners

2-Axial compression test : to attain the residual strength of damaged stiffened plates under uniaxial compression

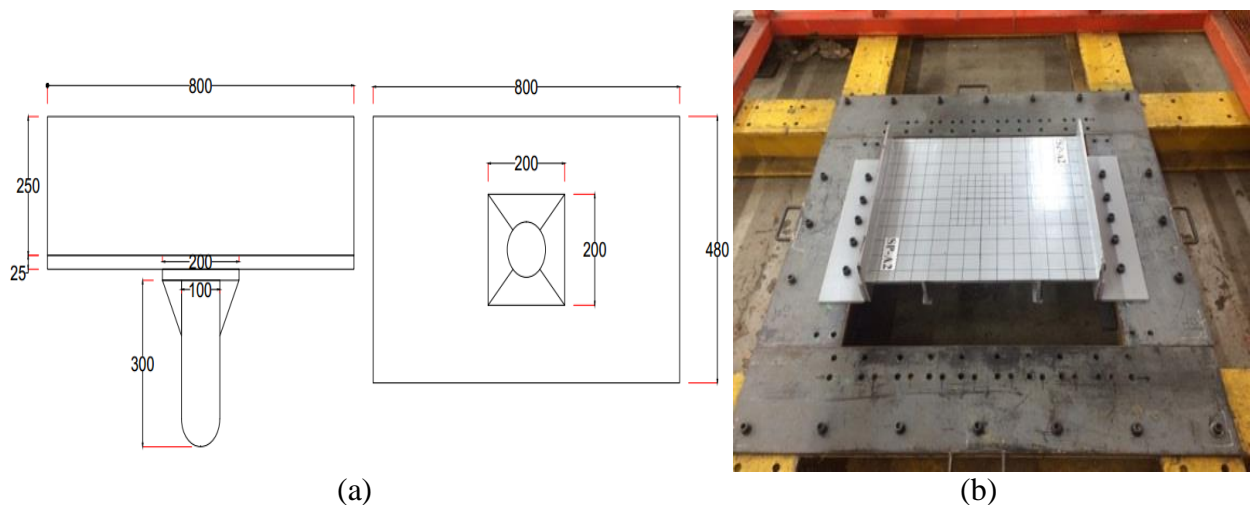


Fig. 2.6 Lateral collision test (a) striker-head shape (b) boundary conditions

The experiment is commenced with damage generation of a stiffened plate, a prototype of ship structures, collided by a hemispherical indenter. This machine has been successfully employed in impact tests for the double-hull structures of a small-scale tanker [17], as well as the beam structures [18,19], ring-stiffened cylinders [20], and unstiffened tubular structures [21, 22]. The detail specification of the spherical indenter is 400 kg and 100 mm diameter (Fig. 2.6(a)). The indenter drops from a known variable height using magnetic holder and tension supports (Fig. 2.7). Experimental study on four collision test models is set up with two different velocities, 3.4 and 4.4 m/s respectively.

In order to deflect the buckling models of local and overall stiffened panels, the models are made up of one and two half bays in transverse direction and on the other hand with six longitudinal stiffeners.

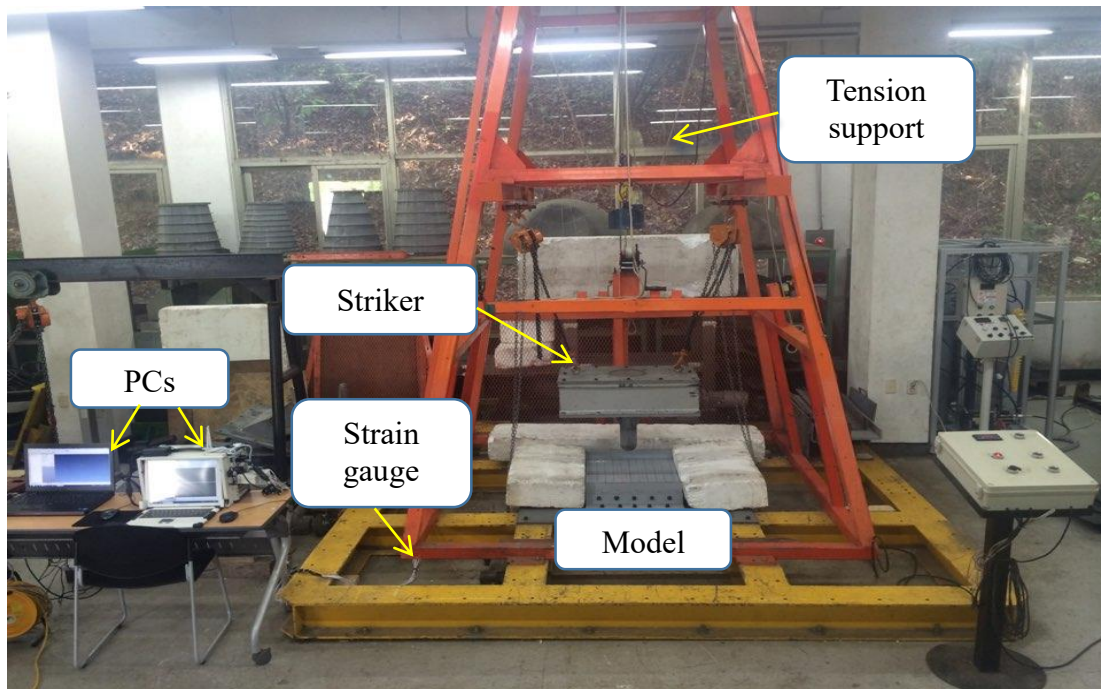


Fig. 2.7 Experimental set-up for lateral collision test

Fixed and free boundary conditions are implemented in this study. End plates are connected with joining angles in order to provide the rigid boundary conditions at both ends in Fig. 2.6 (b). Our main purpose of lateral collision test is to engender the extent of damage without causing any fracture on four models. The outline of collision test set up is shown in Fig. 2.7.

Table 2.5 Summary of test variables

Model	$\beta$	$\lambda_c$	$\lambda_t$	Drop height	Damage status
				(mm)	
SP-A1	1.3	0.34	0.37	-	Intact
SP-A2				1000	Damage
SP-A3				600	Damage
SP-B1		0.24	0.28	-	Intact
SP-B2				1000	Damage
SP-B3				600	Damage

In lateral collision test, the main target of impact point is the mid-point between stiffeners. If all the supports on the magnetic hold are in tension, the impact point is in the centre of the plate in Fig. 2.8 (a). However, the free edges of the stiffeners on each side of the model are different: 20 and 30 mm respectively. Therefore, the impact location is arranged as shown in Fig. 2.8 (b) in order to collide the striker at the mid-point between stiffeners.

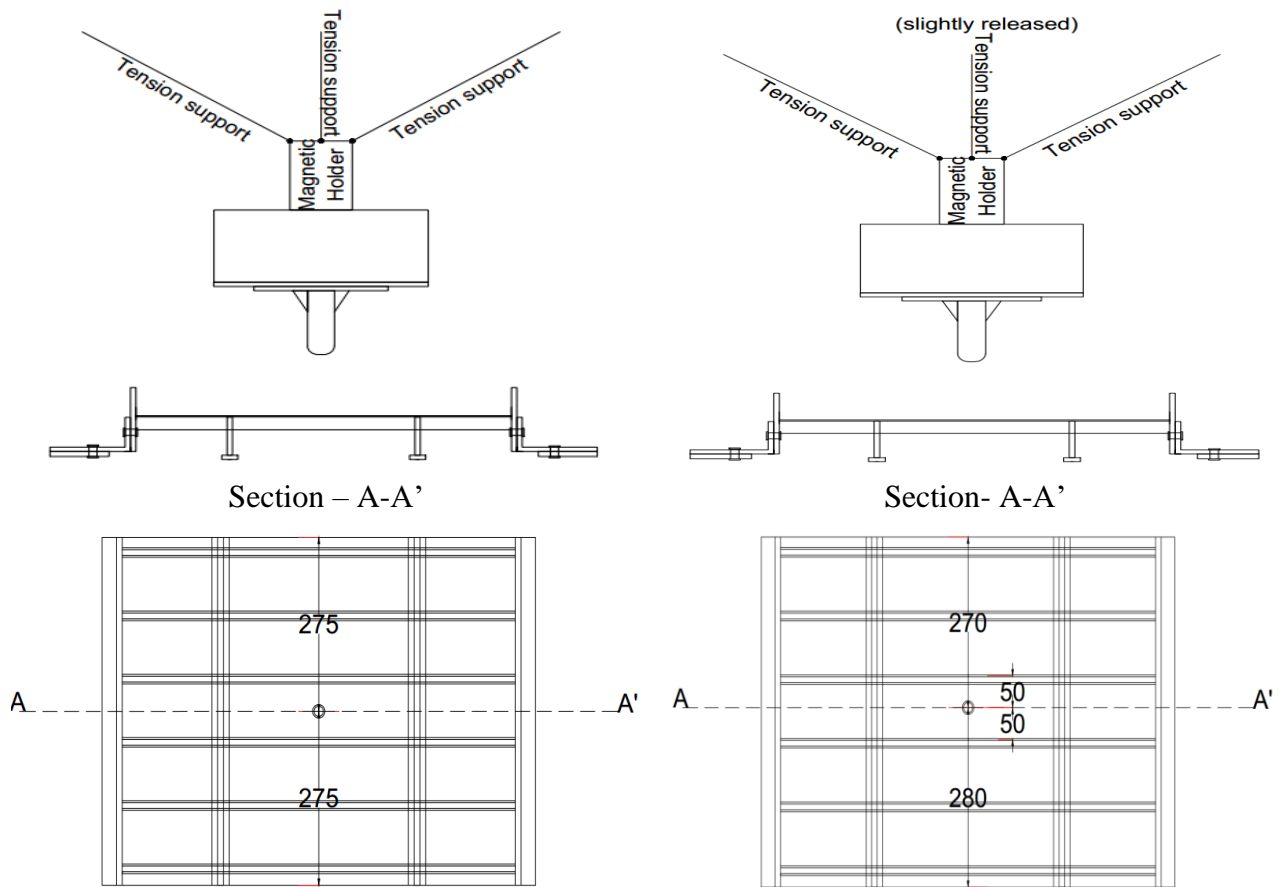


Fig. 2.8 Position of impact point and arrangement of striker (a) all the supports are in tension (b) the support on one side is slightly released.

There are five biaxial strain gauge-attachments on each model in order to capture the dynamic response of the plate and stiffeners. One strain gauge near the impact point, two strain gauges on the stiffeners and two strain gauge on the transverse girders are fitted as shown in Fig. 2.9.

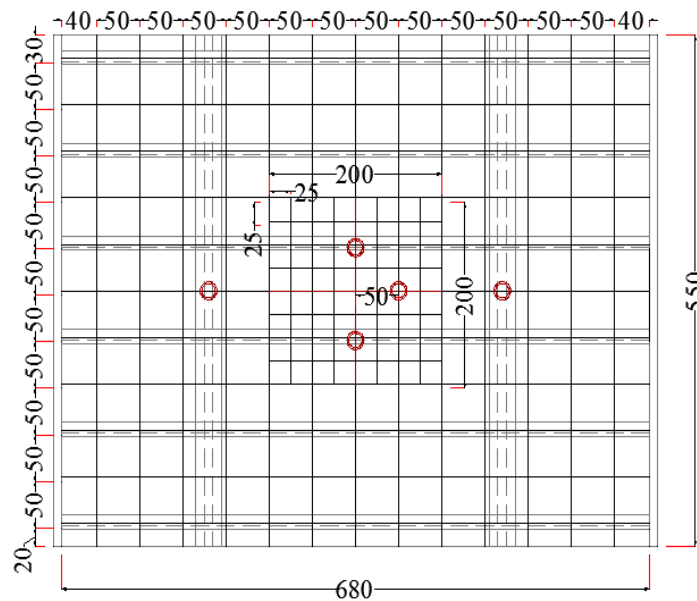


Fig. 2.9 Strain gauge arrangement for lateral collision test



## 2.3 Lateral collision test results

Different local dent depths of the stiffened plate with the presence of initial global imperfection can be seen from Fig. 2.12 to Fig. 2.15. The simulation of collision test is carried out by varying the impact velocities.

In *SP-A* series, the maximum depth of dent that is twenty times of the plate thickness occurred in *SP-A1*. According to the variation in drop height and their structure's stiffness, the depth of dent of each model varies (Fig. 2.11).

In *SP-A2* and *SP-B2* models, a significant difference between depth of dent before and after releasing joining angles indicated that the net conservation of energy of the two bodies after the encounter is large enough to bounce back the structure. The final extent of damage after releasing the joining angle is in the range of 4-18 percent larger than the original dent of depth.

The extent of damage of plate before and after releasing the joining angles are presented in Table. 2.6. Some dent damages were imposed on different location according to the rotation angle of the striker.

Rotation of the striker made the position of impact point slightly differ from the mid-point between the stiffeners (Fig. 2.10). A considerable reduction occurs along the length between the impact point and the transverse girder.

The impact point near the stiffeners possesses less permanent deflection compared with others. The deflection near the transverse stiffeners shifted slightly from the position of original point since highly membrane tension or compression near the impact region and transverse girders acting as a simply support all over the structures.

Table 2.6 Test results

Model	$\theta$	Impact point		Permanent deflection at impact point	
		$x$	$y$	Before	After
	( $^{\circ}$ )	mm	mm	mm	mm
<i>SP-A2</i>	3	25	15	54.3	59.21
<i>SP-A3</i>	7	15	0	37.6	40.41
<i>SP-B2</i>	6	20	-10	36.0	40.68
<i>SP-B3</i>	8	10	-12	29.3	32.29

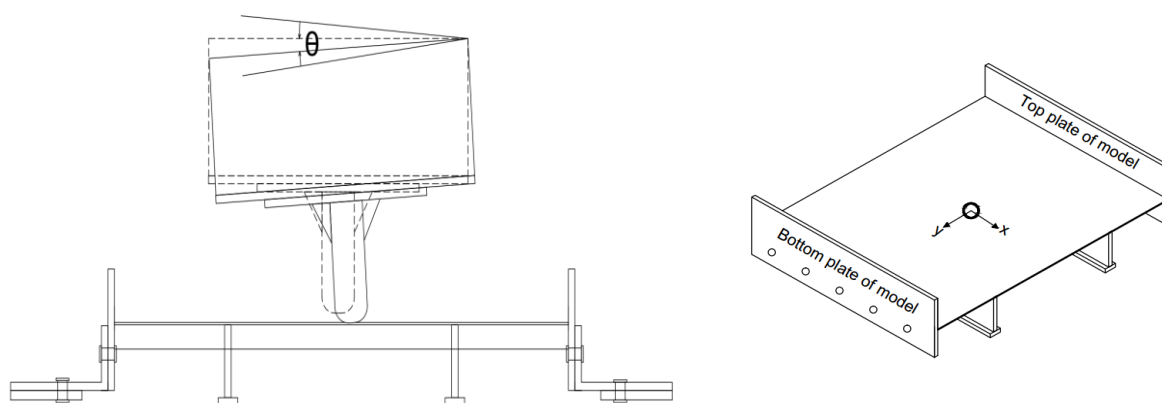


Fig. 2.10 The location of the impact point

Initial shape imperfection has the overwhelming effect on the buckling shape of damaged stiffened plate. It is obvious in failure of *SP-A2* which has the similar half sinusoidal wave of initial shape imperfection and depth of dent between stiffeners.

The stiffened plates with lesser scantling shape attained the global deformation pattern as can be seen in Fig. 2.12. It is indicated that the rigidity of the scantlings is not strong enough against the lateral impact velocity.

In contradiction to *SP-A2* and *SP-A3*, only local elastic and plastic deformation occurs in *SP-B2* and *SP-B3*. A significant increment and reduction of depth of dent in *SP-B2* indicated the bending moment at the end plates when the joining angles are released.

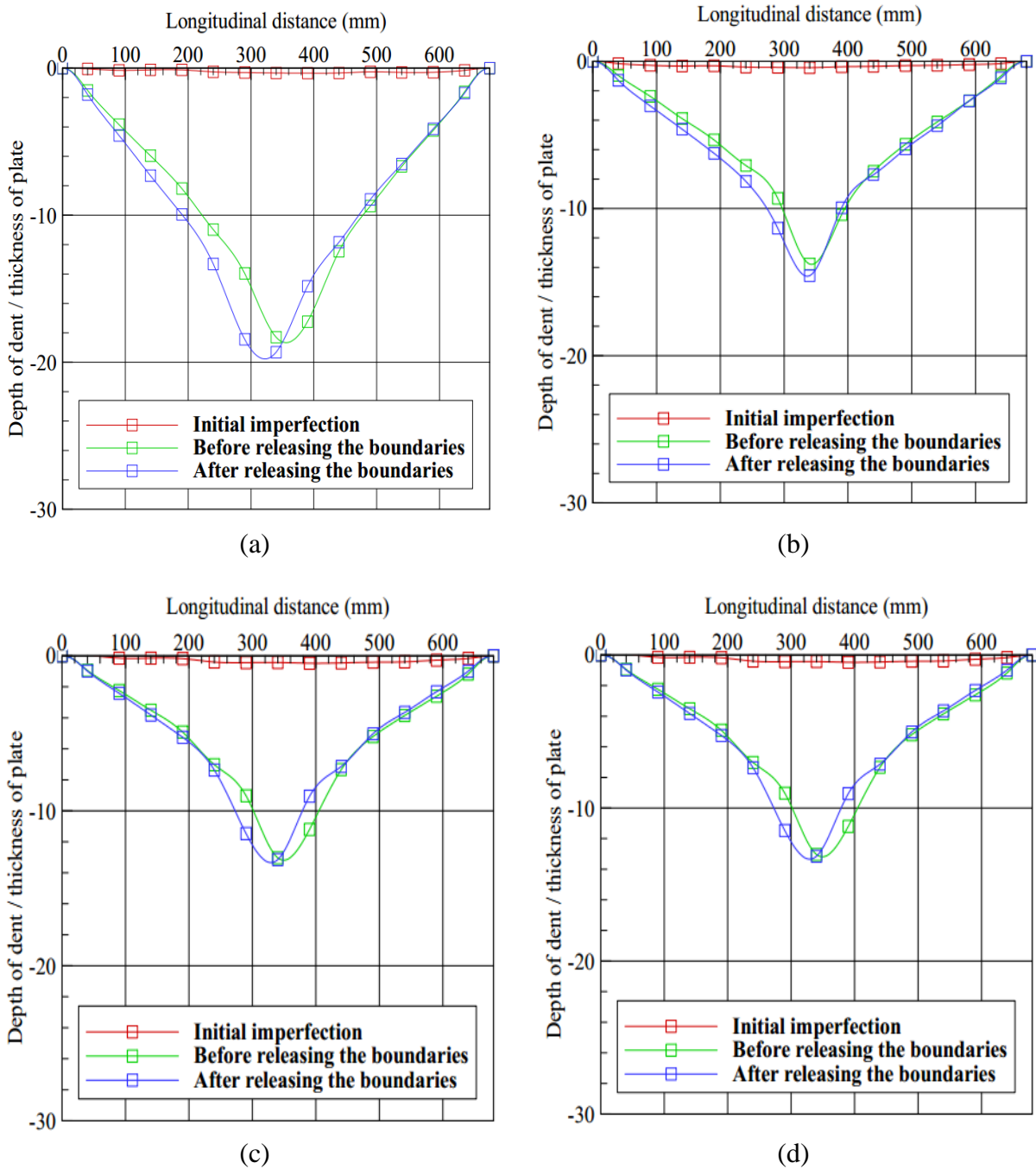


Fig. 2.11 Comparison of depth of dent (a) *SP-A2* (b) *SP-A3* (c) *SP-B2* (d) *SP-B3*

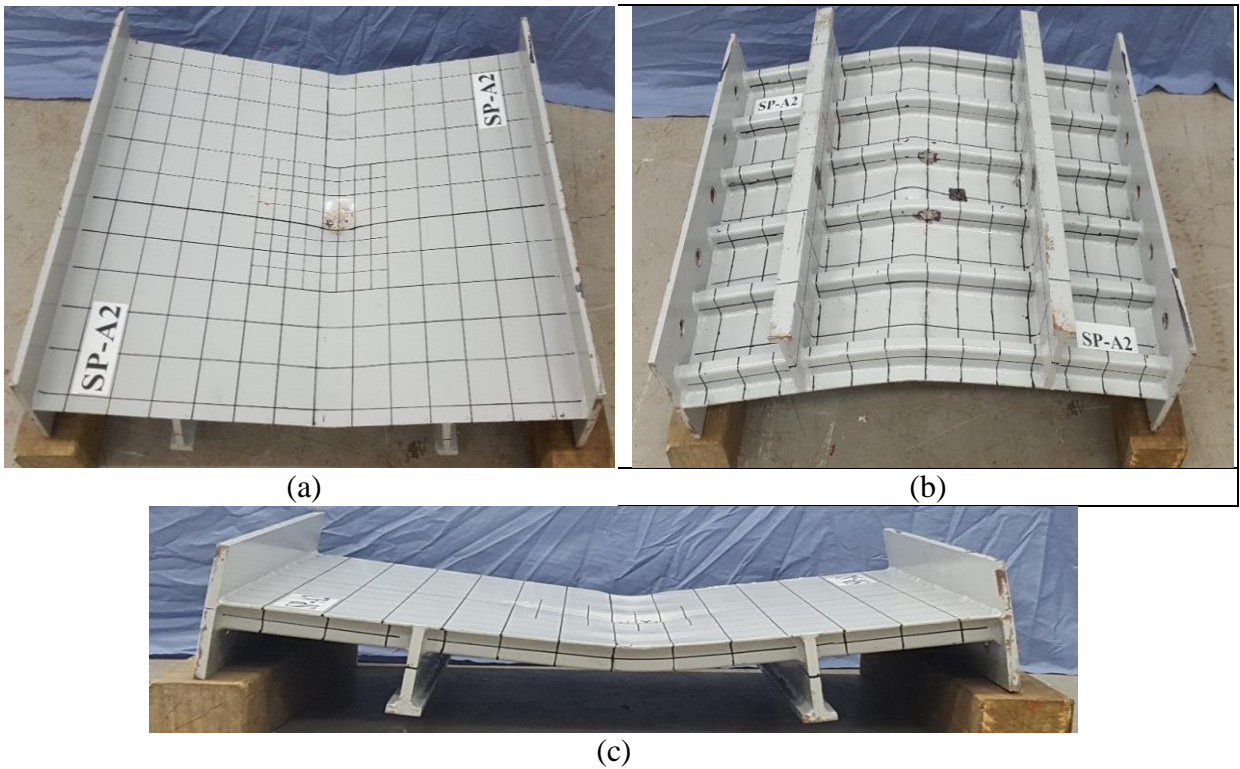


Fig. 2.12 Model *SP-A2* (a) Plate side (b) Stiffener side (c) Lateral view of deformation

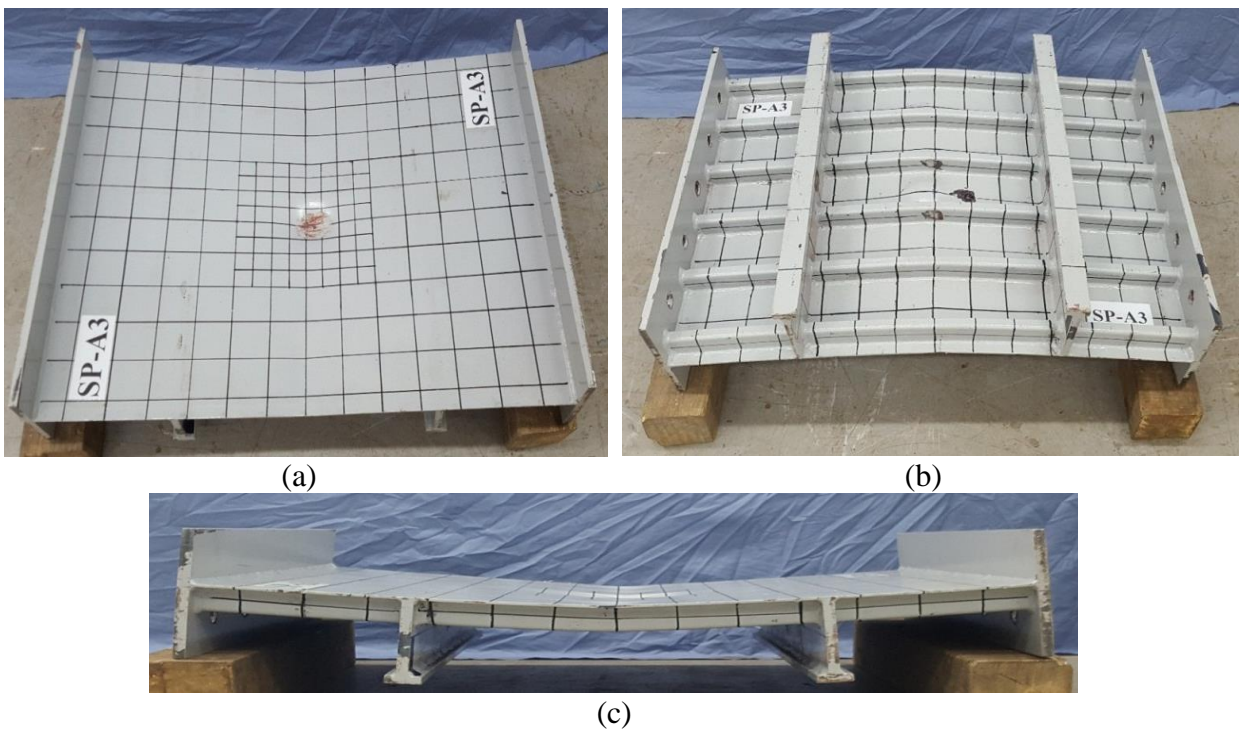
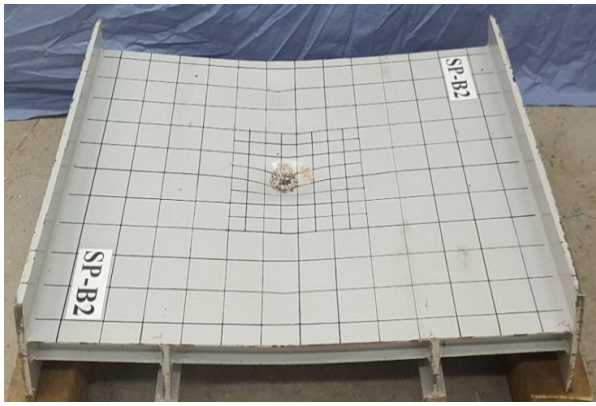
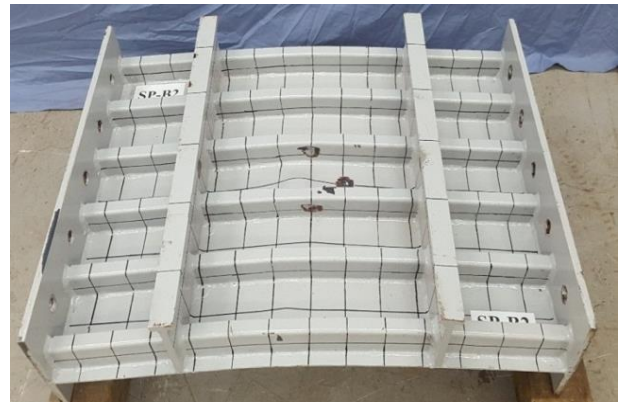


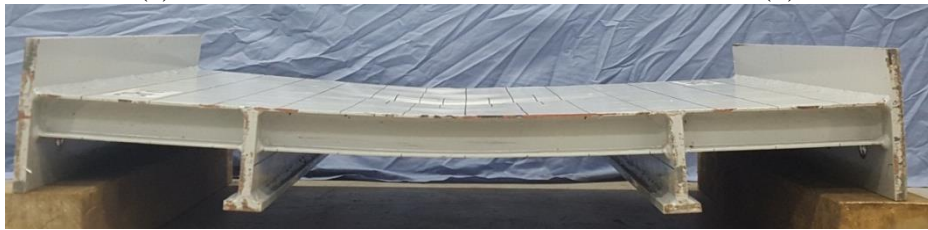
Fig. 2.13 Model *SP-A3* (a) Plate side (b) Stiffener side (c) Lateral view of deformation



(a)

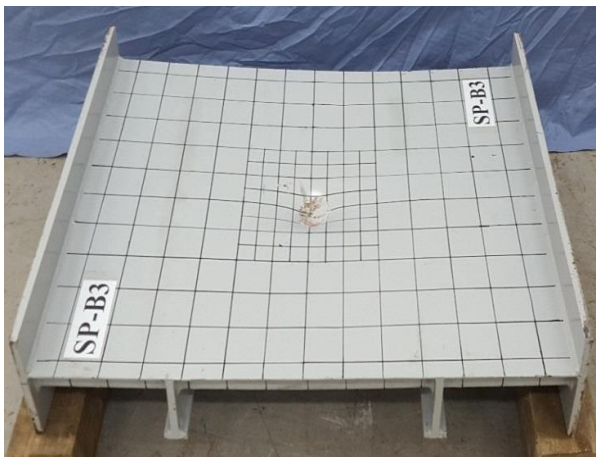


(b)

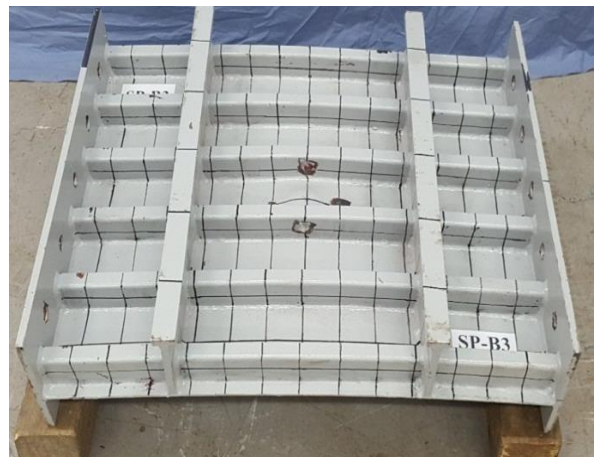


(c)

Fig. 2.14 Model *SP-B2* (a) Plate side (b) Stiffener side (c) Lateral view of deformation



(a)



(b)



(c)

Fig. 2.15 Model *SP-B3* (a) Plate side (b) Stiffener side (c) Lateral view of deformation

# Chapter 3 Residual strength tests of damaged stiffened plates under axial compression

## 3.1 Geometric measurement of damaged stiffened plates

Residual strength is the load or force that a damaged object or material can still carry without failing. The strength of a structure can be significantly affected by the presence of damage and it is usually substantially lower than the strength of the undamaged structures. To prevent the catastrophic failure, one must evaluate the load carrying capacity that will exist in the potentially damaged structures throughout its expected service life. The load carrying capacity of a damaged structure is the residual strength of that structure.

The deflection of damaged stiffened plates are measured before and after releasing boundaries in order to detect changing in depth of depth. The measured data with the boundaries conditions represent for the state of lateral collision situation. Releasing the boundaries changes around 10 percent increment in the depth of dent that will be applied in residual strength tests. The detail measurement data can be seen in Appendix B and C.

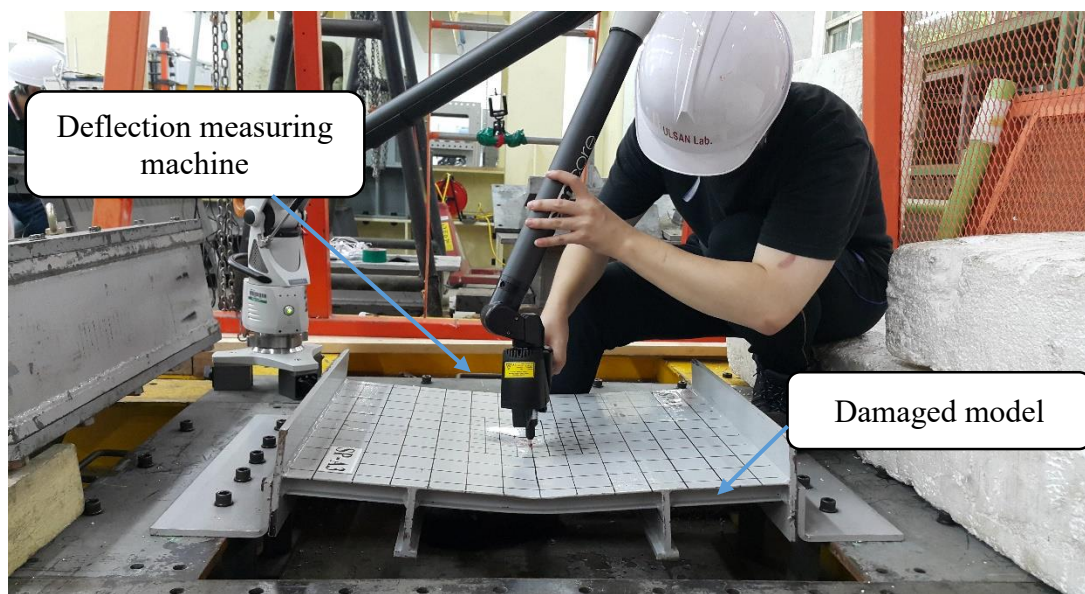


Fig. 3.1 Measurement of damaged stiffened plate

## 3.2 Set up of the experiment

In residual strength test, six models are conducted to detect the ultimate strength of stiffened plate structures under uniform axial compression with varying the configuration (eg. Location and orientation of damages) including the intact structures without having damages.

After lateral collision test, the intact and damaged models are prepared for the uniform axial compression test (Fig. 3.2). The round bars are attached at the both ends together with the end plates in order to uniformly distribute the load and appropriate boundary conditions at the ends.

The Teflon plates are used to reduce undesired friction between the round bars and the bearing plates as shown in Fig. 3.3.

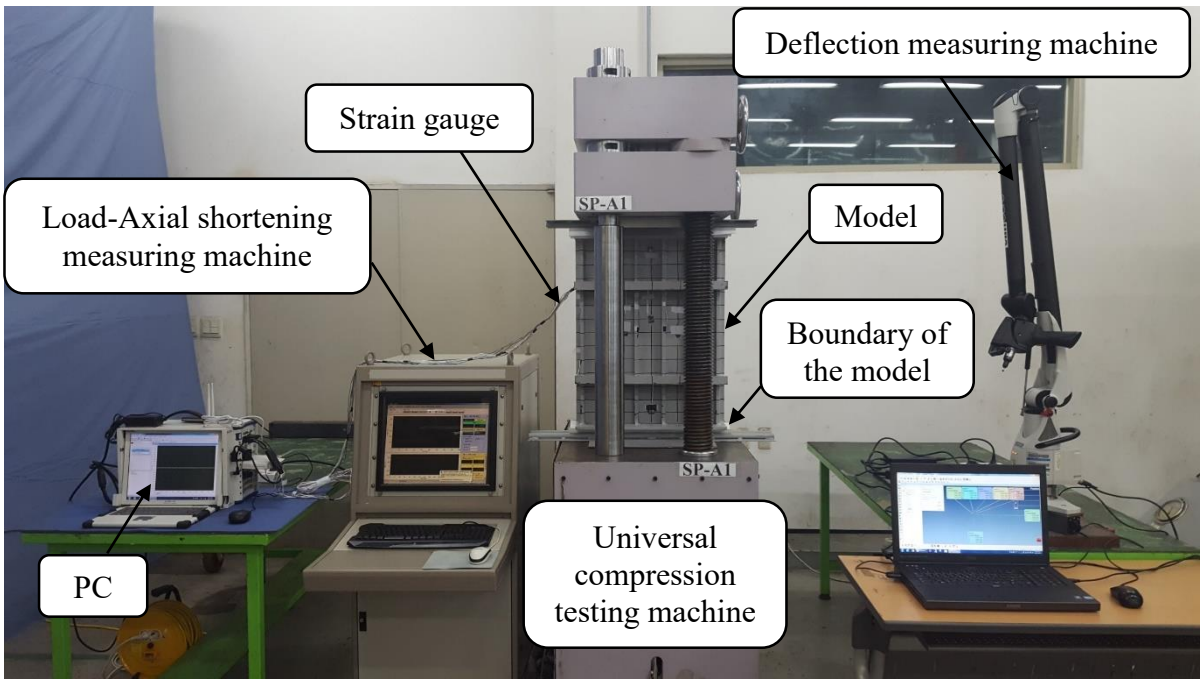


Fig. 3.2 Ultimate strength test set-up

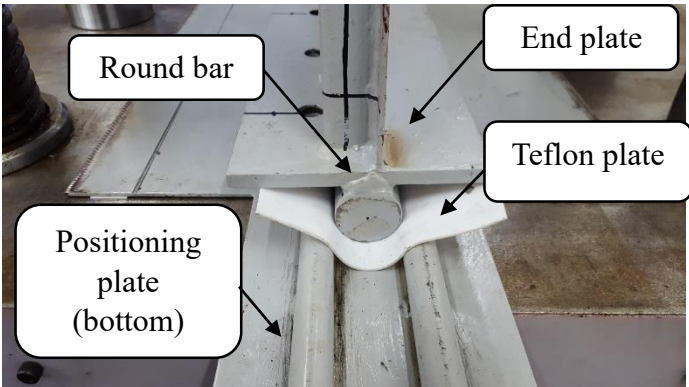


Fig. 3.3 Arrangement of boundary conditions

Table 3.1 Requirements for axial compression test

Classification	Capacity	Remark
Test Machine	100 ton	Bending, compression, tensile tests
Positioning plate (top)	760x510 mm	10 mm plate welded together with 20 mm diameter round bar
Positioning plate (bottom)	900x510 mm	10 mm plate welded together with 20 mm diameter round bar
Computer		AD convertor
Measuring machine		Point collection system
Strain gauge (biaxial)		Near the mid-point of the plate
Strain gauges (uniaxial)		On the stiffeners and plate around the mid-length region

There are seven strain gauges (Fig. 3.4) attached on each model in order to capture the strain histories throughout the test. Five uniaxial strain gauges and a biaxial strain gauge near the impact point is adhered to the plate. The others are intended for the stiffeners. During the tests, controlling computer records axial loading and shortening in every each increment.

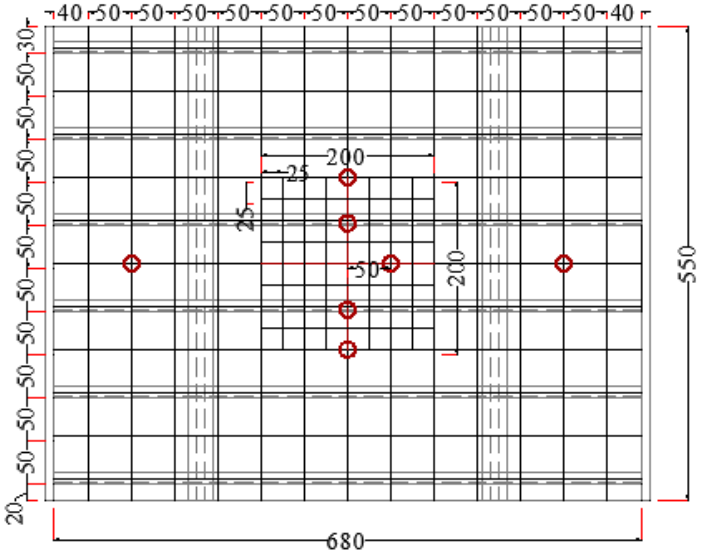


Fig. 3.4 Strain gauge arrangement for axial compression test

The models are intended to load uniformly throughout the neutral axis of the models (Fig. 3.2), an axis in the cross section of a beam. If the loading is disturbed evenly along the neutral axis, the models will undergo the pure uniform axial loading and shear situation can be neglected. The calculation of neutral axis of the cross section of a beam is presented below.

$$\text{Neutral axis of a beam} = (\text{Total area moment of cross section}) / (\text{Total area}) \tag{5}$$

The calculated results for neutral axis of Model SP-A and SP-B series are 9 mm and 13 mm respectively. In order to distribute the load evenly on the models, the round bar is intended to attach at the neutral axis that is measured from the outer edge of the plate shown in Fig. 3.5. Based upon the measurement data of the models before performing the test, there is an eccentricity between the centre of the round bar and the neutral axis.

Table 3.2 Eccentricity of the models (mm)

Model	Measured	Centroid location	Eccentricity
<i>SP-A1</i>	9	9	0
<i>SP-A2</i>	9	9	0
<i>SP-A3</i>	8	9	1
<i>SP-B1</i>	18	13	-5
<i>SP-B2</i>	17	13	-4
<i>SP-B3</i>	18	13	-5

Note:  
 Measured = average values of the measured data between the centre of the round bars and the outer surface of the plate noted on four points in Fig. 3.5 (a)

Centroid location = distance from the outer surface of the plate to the centroid calculated by using Eq. (5)

Eccentricity = Calculated – Measured

Positive value of the eccentricity in Table 3.2 is intended to represent the loading axis that is the centre of the round bars towards the plated edge and negative values for the loading axis towards the stiffener edges.

The lateral deflection of the plate and stiffeners are collected by using the laser machine in order to handle the response of the plate and stiffeners. The loading along the round bar is recorded by the computer connected to the axial machine.

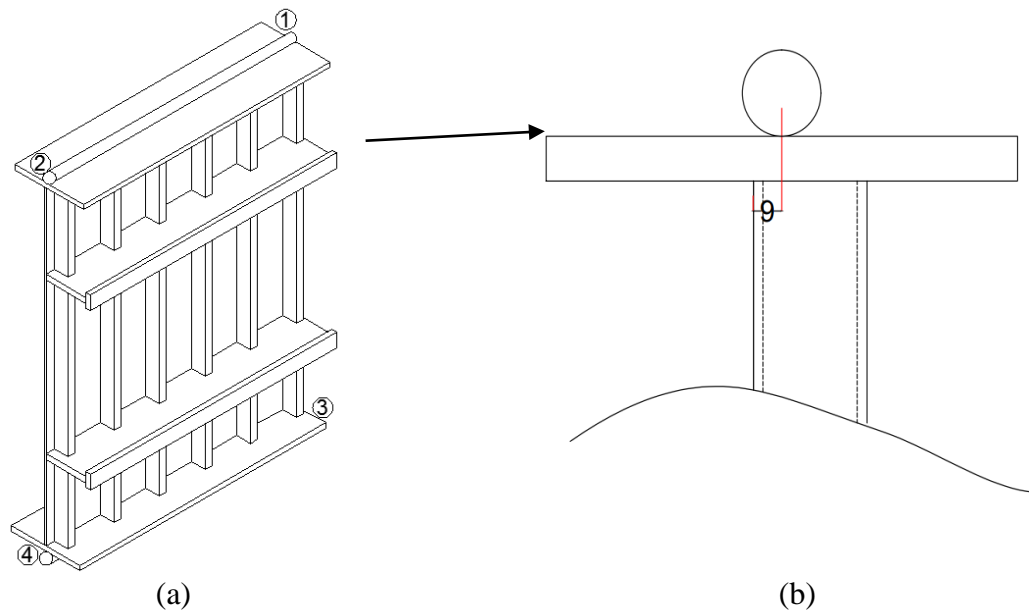


Fig. 3.5 Position of measurement points

### 3.3 Residual strength test results

According to the experimental results, the intact models have the greatest resistance to the uniform axial compression (Fig. 3.6(a)). There is a great difference of residual strength between the intact models and damaged models since their damaged generation differs discussed in Chapter 2. The models with higher depth of dent attain a significant reduction under uniaxial compression.

Contribution of the stiffeners is really important in the ultimate strength of stiffened plate structures. It can be seen clearly between *SP-A2* and *SP-B2*. Although the structures with different scantlings received the same kinetic energy, their reduction factors stand apart each other. The residual strength of damaged plates with lesser impact velocity is greater than the one with high impact velocity.

The global deformation of plate also effect on the ultimate strength of one and two half bays stiffened plates. The distortion of plate against lateral collision varies according to their impact velocity and location of dent.

The models with less stiffness achieve the overall distortion of the plate throughout the transverse section as can be seen in *SP-A2*. Their residual ultimate strength decreases approximately 80 percent of the intact structure that can be seen in Table-3.3.



There is a great difference in ultimate strength of *SP-B2* and *SP-B3*. It seems to be that *SP-B3* with only local plastic deformation can withstand the uniform axial compression than *SP-B2* with slightly approached to the global deformation pattern.

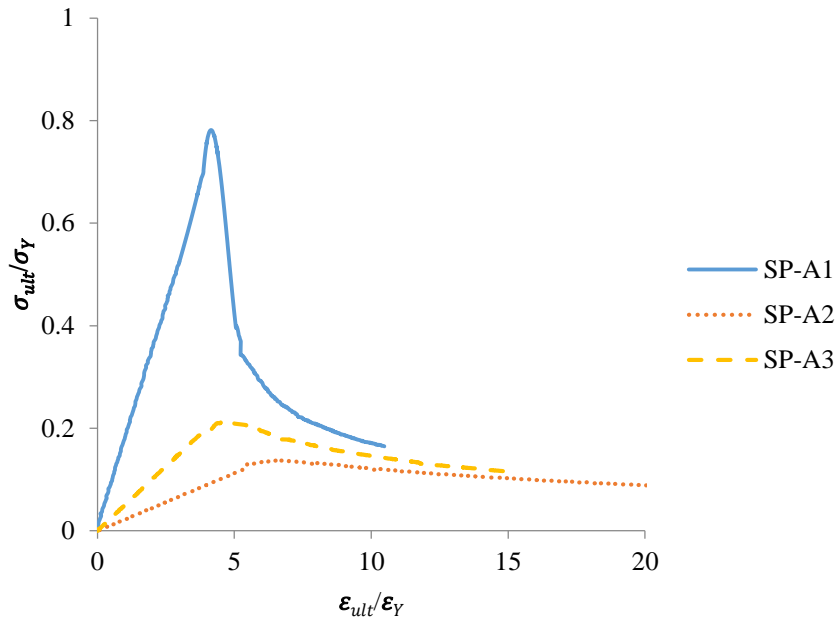
The ultimate strength of intact model *SP-B1* does not show any significant difference with *SP-B3* that is the damaged model generated by low impact velocity. Although *SP-B* series have larger stiffness, their residual strength in higher and lower impact velocities is approximately 30 percent different in each model which is only 10 percent difference in *SP-A* series.

*SP-B1* has a lower resistance against the uniform axial compression than the intact model *SP-A1* even though it has the greater stiffness profile and also the deformation shape on the stiffeners' flanges can be found during the experiment.

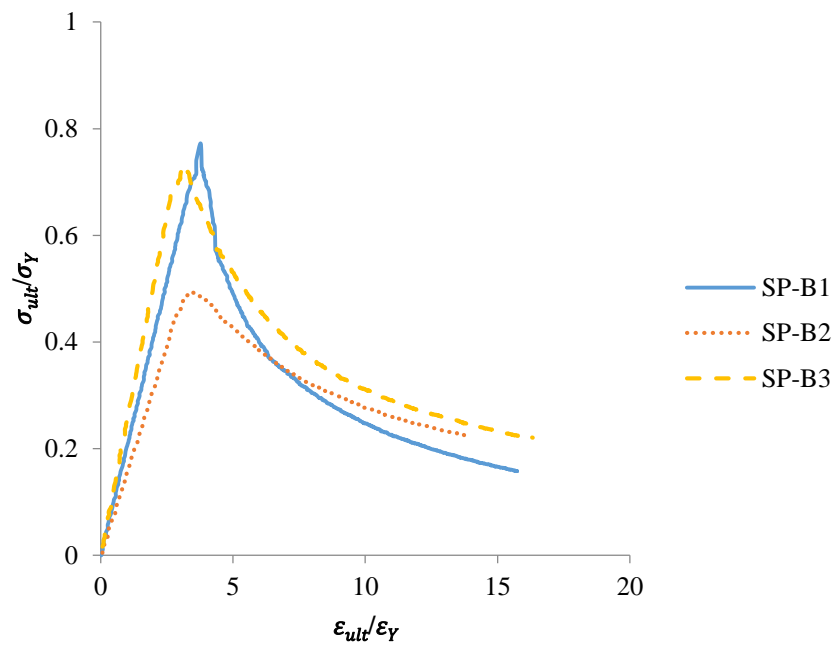
Table 3.3 Ultimate strength and their reduction factor

Model	Failure of structure	Ultimate state		$\sigma_T$ (MPa)	Reduction factor (%)
		$F_{max}$ ( kN )	Axial shortening (mm)		
<i>SP-A1</i>	Stiffener induced	595	3.99	252.3	-
<i>SP-A2</i>	Stiffener induced	103	6.75	43.7	82.58
<i>SP-A3</i>	Stiffener induced	160	4.82	67.8	73.16
<i>SP-B1</i>	Plate induced	580	3.63	221.2	-
<i>SP-B2</i>	Stiffener induced	370	3.21	141.1	36.09
<i>SP-B3</i>	Stiffener induced	549	2.93	209.4	5.21

Note:Reduction factor = (Intact-Damage)  $\times$  100/Intact

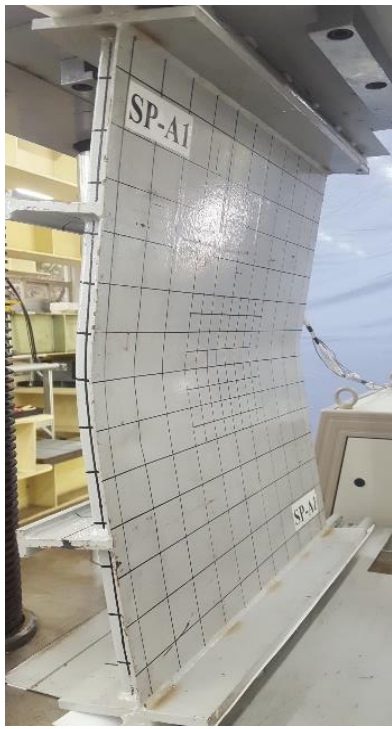


(a)



(b)

Fig. 3.6 Load axial shortening curve (a) *SP-A* series (b) *SP-B* series

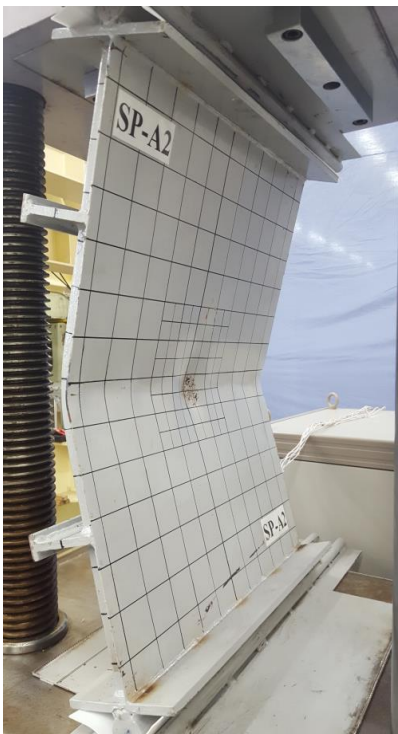


(a)



(b)

Fig. 3.7 Collapse shape of Model *SP-A1* (a) Plate side (b) Stiffener side



(a)



(b)

Fig. 3.8 Collapse shape of Model *SP-A2* (a) Plate side (b) Stiffener side



(a)



(b)

Fig. 3.9 Collapse shape of Model *SP-A3* (a) Plate side (b) Stiffener side



(a)



(b)

Fig. 3.10 Collapse shape of Model *SP-B1* (a) Plate side (b) Stiffener side

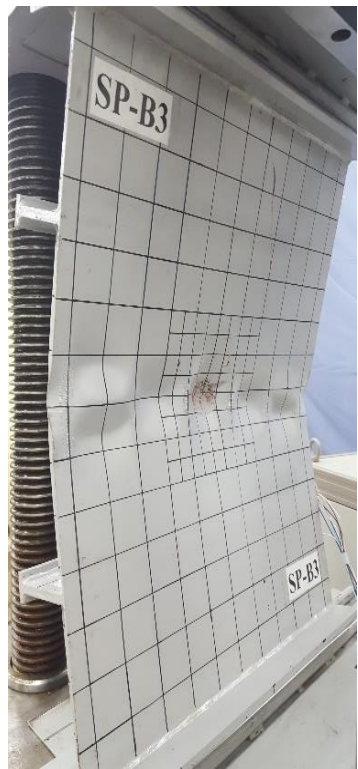


(a)



(b)

Fig. 3.11 . Collapse shape of Model *SP-B2* (a) Plate side (b) Stiffener side



(a)



(b)

Fig. 3.12 Collapse shape of Model *SP-B3* (a) Plate side (b) Stiffener side

# Chapter 4 Numerical analysis of lateral collision tests

## 4.1 Lateral collision simulation

### 4.1.1 Assembly of finite element model

Finite element method (FEM) has been developed to simulate the various structural elements with several aspects. Finite element method is commonly used for the prediction of ultimate strength of plate and stiffened plates with the nonlinearity of geometry and material properties. For the case of moving boundary problems, crack growth with arbitrary and complicated paths and phase transformation problem, mesh free method is more reliable than FEM. For larger structural units, ISUM takes more credits according to their accuracy in prediction.

The 3D finite element (FE) simulation is carried out by using the commercial package of Abaqus/Explicit [24] which is relevant for dynamic simulation with large deformation. The FE model consists of the testing model, striker and the joining angle. The size of all models was the same as in the experiments. The shell and stiffeners are modelled by four node shell element (S4R) with five integration points throughout the thickness.

The edges are constrained with the joining angles that are fixed with the supports and the others with a free boundary condition in order to be realistic as possible with the experiment. It is necessary to represent the real boundary conditions instead of the ideal theoretical ones. Therefore, boundary condition similar with experimental restraint is implemented in the analysis.

The striking mass and the indenter is assembled as shown in Fig. 4.1. Rigid hemisphere head shape is modelled using shell element and defining the appropriate offset distance to the target. The initial velocity is assigned in the prescribed field with the free vertical translation of the rigid body. The rotation of the striker is also considered in order to resemble the actual experiment.

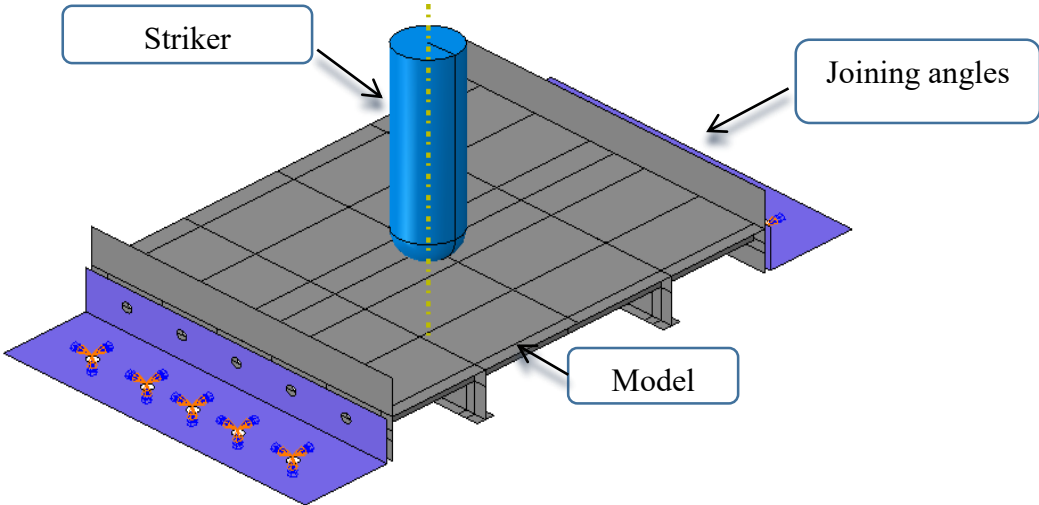


Fig. 4.1 Assembly of model for lateral collision test

### 4.1.2 Material definition

An engineering stress-strain curve does not represent the true indication of the metal. It should be transformed the true stress-strain curve in order to attain the basic characteristic flow of the material. Since the models are collided with striker, they are highly affected by large strain and high strain rates. Therefore, elastic plastic material law with kinematic isotropic hardening was chosen. A fracture criterion is neglected since our study is intended to generate the dent without any fracture.

In this study, two kind of material properties are applied. The one with the material properties which were defined using the equations proposed by Cho et al. [25] and the other with Cowper Symond equation.

‘*Material Properties-1*’ represents Cowper Symond constitutive models with material constant for mild steel ( $D = 40.4 \text{ s}^{-1}$ ,  $q = 5$ )

$$\sigma_d = \left[ 1 + \left( \frac{\dot{\varepsilon}}{D} \right)^{\frac{1}{q}} \right] \sigma_o \quad (6)$$

Where  $\sigma_d$ ,  $\sigma_o$ ,  $D$  and  $q$  are the dynamic flow stress corresponding to the uniaxial plastic strain rate  $\dot{\varepsilon}$ , associated static plastic flow stress and constants for a specific material respectively.

The procedure from Eq. (7)-(18) represents the calculation of the material properties proposed by Cho et al [25] that will later be referred with the letter ‘*Material Properties-2*’. The Deviations in the yield and ultimate tensile strengths and strains were quite small. Thus, the averages of those values were used when deriving the constitutive equations. Using the engineering strains and stresses obtained from the quasi-static tensile tests (as mentioned in a previous section), the corresponding true values were calculated using Eqs. (7) and (8).

$$\sigma_{tr} = \sigma(\varepsilon + 1) \quad (7)$$

$$\varepsilon_{tr} = \ln(\varepsilon + 1) \quad (8)$$

where  $\sigma_{tr}$  and  $\varepsilon_{tr}$  are the true stress and true strain, respectively;  $\sigma$  and  $\varepsilon$  are the engineering stress and engineering strain, respectively.

By substituting the stresses and strains obtained from Eqs. (9) ~ (11), the constitutive equation can be constructed considering the yield plateau and strain hardenings.

$$\sigma_{tr} = E \varepsilon_{tr} \quad \text{when } 0 < \varepsilon_{tr} < \varepsilon_{Y,tr} \quad (9)$$

$$\sigma_{tr} = \sigma_{Y,tr} + (\sigma_{HS,tr} - \sigma_{Y,tr}) \frac{\varepsilon_{tr} - \varepsilon_{Y,tr}}{\varepsilon_{HS,tr} - \varepsilon_{Y,tr}} \quad \text{when } \varepsilon_{Y,tr} < \varepsilon_{tr} < \varepsilon_{HS,tr} \quad (10)$$

$$\sigma_{tr} = \sigma_{HS,tr} + K (\varepsilon_{tr} - \varepsilon_{HS,tr})^n \quad \text{when } \varepsilon_{HS,tr} < \varepsilon_{tr} \quad (11)$$

where  $\sigma_{Y,tr}$ ,  $\sigma_{HS,tr}$ , and  $\sigma_{T,tr}$  are the true yield strength, true hardening start stress, and true ultimate tensile strength, respectively;  $\varepsilon_{Y,tr}$ ,  $\varepsilon_{HS,tr}$ , and  $\varepsilon_{T,tr}$  are the true yield strain, true hardening start strain, and true ultimate tensile strain, respectively; and

$$n = (\varepsilon_{T,tr} - \varepsilon_{HS,tr}) \frac{\sigma_{T,tr}}{\sigma_{T,tr} - \sigma_{HS,tr}} \quad (12)$$

$$K = \frac{\sigma_{T,tr} - \sigma_{HS,tr}}{(\varepsilon_{T,tr} - \varepsilon_{HS,tr})^n} \quad (13)$$

In order to consider the effects of strain-hardening on the constitutive relationships, the equations provided in Ref. [25] were used with some modifications. The dynamic values of yield strength, ultimate tensile strength, hardening start strain, and ultimate tensile strain can be obtained using Eqs. (14) ~ (17), which are expressed by the strain rate,  $\dot{\varepsilon}$ . The true plastic strain was then calculated using Eq. (18) in order to apply the numerical model.

$$\frac{\sigma_{YD}}{\sigma_{YS}} = 1 + \left\{ 0.3 \left( \frac{E}{1000\sigma_{YS}} \right)^{0.5} \right\} (\dot{\varepsilon})^{0.25} \quad (14)$$

$$\frac{\sigma_{TD}}{\sigma_{YD}} = 1 + \left\{ 0.16 \left( \frac{\sigma_{TS}}{\sigma_{YD}} \right)^{3.325} \right\} (\dot{\varepsilon})^{0.023} \quad (15)$$

$$\frac{\varepsilon_{HSD}}{\varepsilon_{HSS}} = 1 + \left\{ 0.1 \left( \frac{E}{1000\sigma_{YS}} \right)^{1.73} \right\} (\dot{\varepsilon})^{0.33} \quad (16)$$

$$\frac{\varepsilon_{TD}}{\varepsilon_{YD}} = 1 - \left\{ 0.117 \left( \frac{E}{1000\sigma_{TS}} \right)^{2.352} \left( \frac{\sigma_{TS}}{\sigma_{YS}} \right)^{0.588} \right\} (\dot{\varepsilon})^{0.2} \quad (17)$$

$$\varepsilon_{pl,tr} = \varepsilon_{tr} - \frac{\sigma_{tr}}{E} \quad (18)$$

where  $\sigma_{YD}$  is the dynamic yield strength,  $\sigma_{TD}$  is the dynamic ultimate tensile strength,  $\varepsilon_{HSS}$  is the static hardening start strain,  $\varepsilon_{HSD}$  is the dynamic hardening start strain,  $\varepsilon_{TD}$  is the dynamic ultimate tensile strain, and  $\varepsilon_{pl,tr}$  is the true plastic strain.

The engineering stress and strain must be converted into the corresponding true stress and strain using Eqs. (7) and (13). Equations (9) ~ (13) are used to generate dynamic constitutive relationships. In the impact test, no fracture occurred, meaning that the strain levels did not exceed the strain associated with the ultimate tensile strength. Therefore, no concerns were raised with respect to extending the true stress-plastic strain curve after the initiation of necking, when the impact tests were simulated.

According to the comparison of depth of dent at the impact point in Table 4.1, the results with ‘*Material Properties-1*’ have a great tolerance with the test. Therefore, ‘*Material Properties-1*’ will be used for further investigation.



Table 4.1 Comparison of test results and predictions: Strain rate sensitivity (with *B.C. 'A'*)

Model	Test	Numerical		$X_m$	$X_m$
		<i>M.P. - 1</i>	<i>M.P. - 2</i>	Test/ <i>M.P. - 1</i>	Test/ <i>M.P. - 2</i>
	mm	mm	mm		
<i>SP-A2</i>	54.3	58.0	47.6	1.07	0.88
<i>SP-A3</i>	37.6	38.2	31.4	1.02	0.84
<i>SP-B2</i>	36.0	44.5	38.4	1.24	1.07
<i>SP-B3</i>	29.3	31.2	27.2	1.06	0.93
Mean				1.10	0.93
COV				8.75 %	10.86 %

### 4.1.3 Boundary Condition

Consideration of boundary conditions is also an influential factor for approaching the dynamic analysis. In our study, two types of boundary conditions are specified. The location of bolts screwed between the joining angles and the foundation plates are fixed and the tie constraints are applied between the joining angles and models. This is called *Boundary Condition 'A'* that can be seen in Fig.4.2.

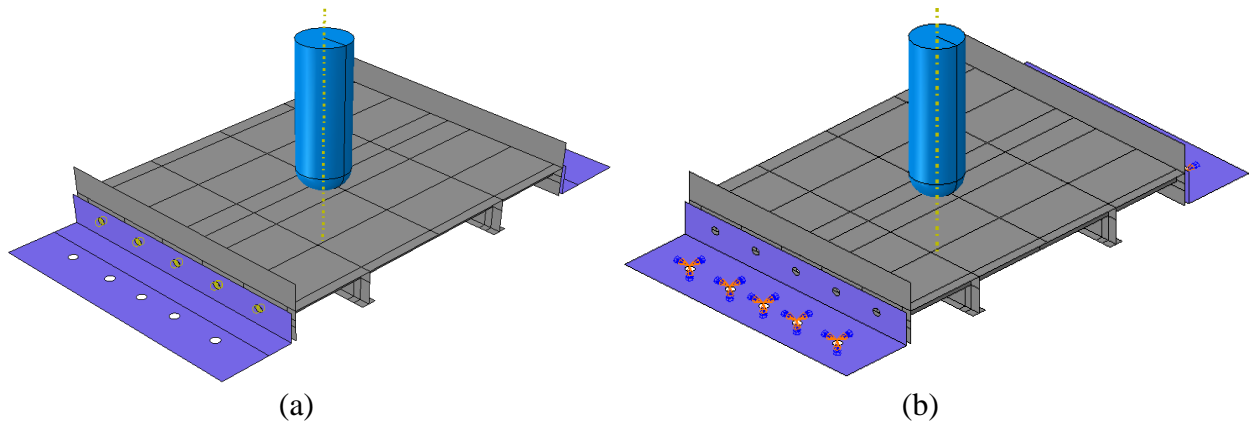


Fig. 4.2 *Boundary condition 'A'* (a) Tie constraint (b) Fixed boundary condition

However, one more boundary condition that means the contact area between the joining angles and the foundation plate should be added. *Boundary condition 'B'* refers to this condition in Fig. 4.3 and the results of depth of dent at the impact point using this boundary condition (Table 4.2) pointed out the fact that it has a great tolerance with the test. In the analysis of boundary conditions' influence, the strain rate sensitivity using '*Material Properties-1*' is applied.

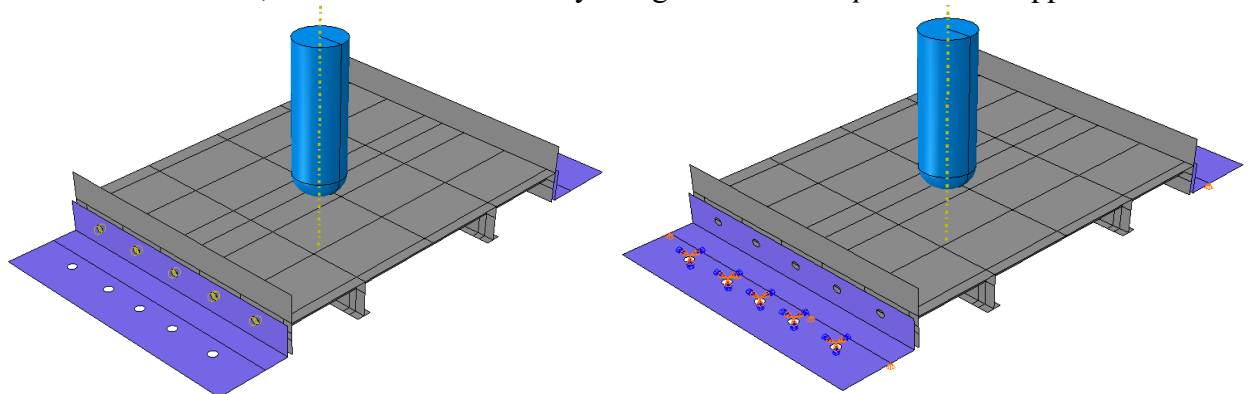


Fig. 4.3 *Boundary condition 'B'* (a) Tie constraint (b) Fixed boundary condition

Table 4.2 Comparison of test results and predictions: Boundary conditions (with *M.P. - 1*)

Model	Test	Numerical		$X_m$	$X_m$
		<i>B.C. 'A'</i>	<i>B.C. 'B'</i>	Test/ <i>B.C. 'A'</i>	Test/ <i>B.C. 'B'</i>
mm	mm	mm			
<i>SP-A2</i>	54.3	58.0	53.8	1.07	0.99
<i>SP-A3</i>	37.6	38.2	37.2	1.02	0.99
<i>SP-B2</i>	36.0	44.5	42.7	1.24	1.19
<i>SP-B3</i>	29.3	31.2	30.2	1.07	1.03
Mean				1.10	1.05
COV				8.78%	8.89%

#### 4.1.4 Convergence study

In a finite element modelling, a finer mesh typically produces a more accurate solution. However, the finer the mesh is, the longer the computation time. A convergence study is useful to solve this problem. A convergence test is performed in order to get the most appropriate mesh refinement for this study.

The evaluation of mesh size usually starts from the same size from the plate thickness and arranged until 3 or 4 times of the plate thickness. The mesh size of plate and stiffeners is 6x6 mm which is evaluated based on the convergence test (Fig. 4.4). This mesh size is actually twice of the plate thickness and its mesh density and the required CPU time are convenient with the present analysis.

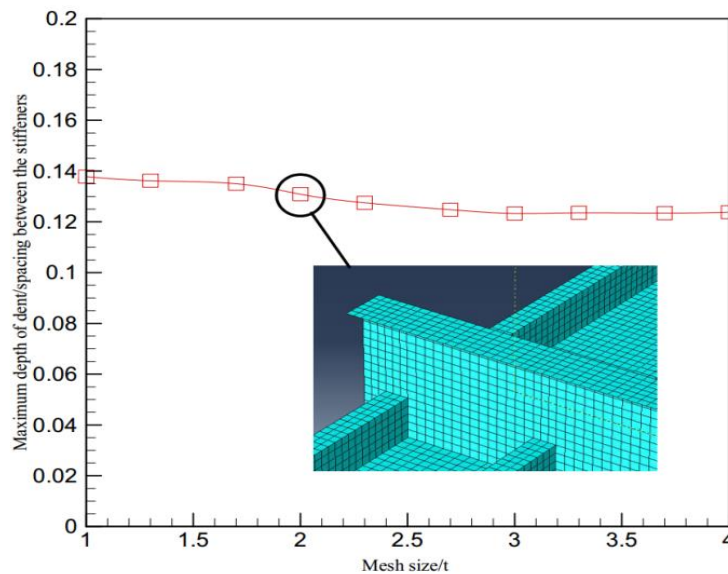


Fig. 4.4 Convergence study on finite element models

#### 4.1.5 Comparison of predictions and tests

The comparison of finite element analysis and test results are mentioned in Table 4.3. Two kinds of strain rate sensitivity; '*Material Properties-1*' and '*Material Properties-2*' are considered in this analysis. It is seemed to be that '*Material Properties-2*' is somewhat underestimated compared with the test results meanwhile the variance of models with '*Material properties-1*' is approximately nine percent.

Table 4.3 Comparison of depth of dent at the impact point

Model	Test	Numerical	$X_m$
	mm	mm	Test/ Numerical
<i>SP-A2</i>	54.3	53.8	0.99
<i>SP-A3</i>	37.6	37.2	0.99
<i>SP-B2</i>	36.0	42.7	1.19
<i>SP-B3</i>	29.3	30.2	1.03
Mean			1.05
COV			8.89%

Two boundary conditions are specified in this analysis. Although the comparison of the prediction and tests using the different boundary conditions does not have a great significant, our intention is to simulate the analysis as similar as the tests.

However, the final response of plate is in similar deformation pattern with the tests as can be seen in Fig. 4.5-4.8. The first encounter of plate and striker initiate the deformation around the radius of the striker. Their stress impulse is spreading out along the plate between the stiffeners and the stiffeners experience lateral outward deflection that is not significant in experiment. The simulation of lateral collision resulted the sinusoidal deformation pattern between stiffeners and fixed boundaries. However, the sinusoidal wave form of extent of damage is appeared between the stiffeners along the free end of the boundary conditions in our experiment.

The stress concentration along the end plate and the holes meant for the bolts are in the highest state when the rigid striker hit the specimen. After removing the striker, the stress dissipated around the holes that may be transformed the rotation of the end plates.

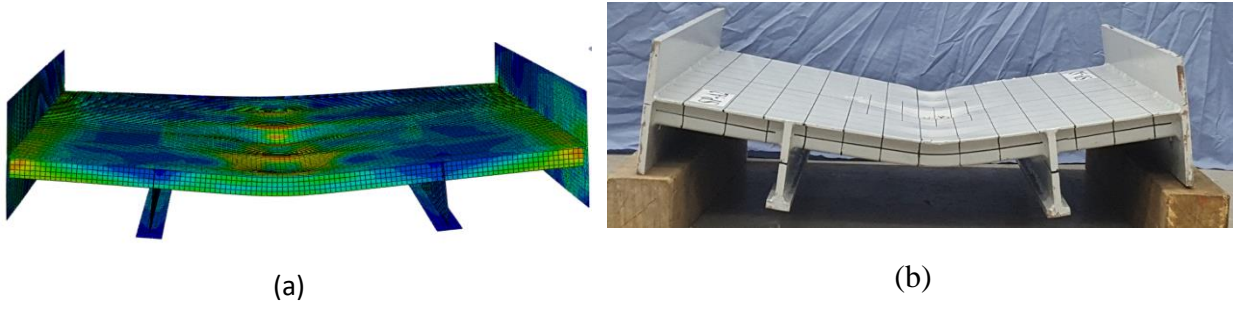


Fig. 4.5 Deformation pattern of *SP- A2* (a) Numerical analysis (b) Experiment

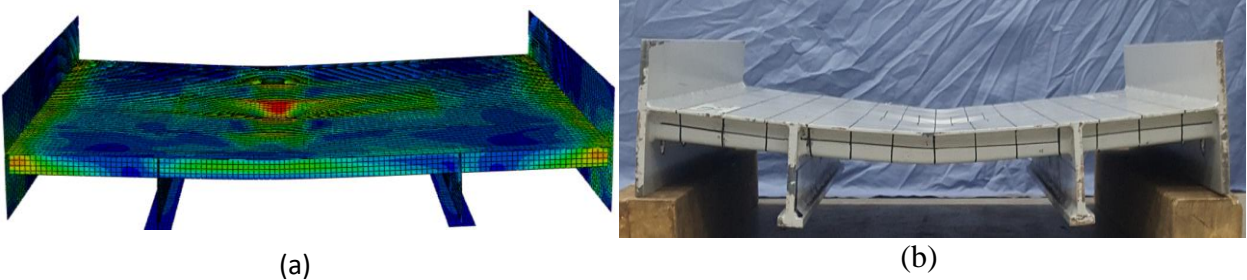


Fig. 4.6 Deformation pattern of *SP- A3* (a) Numerical analysis (b) Experiment

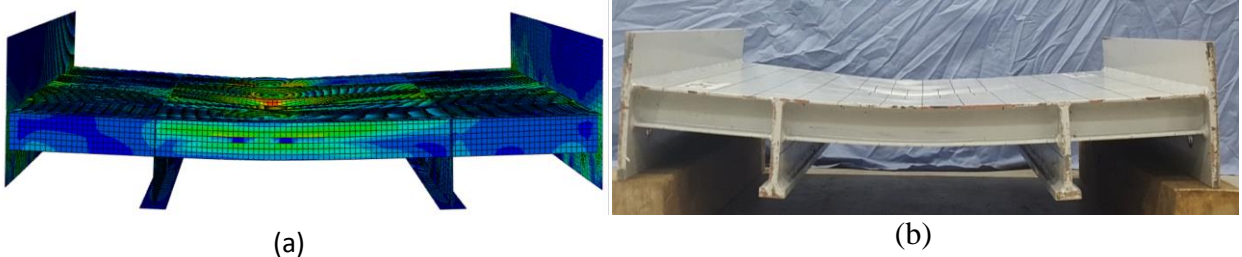


Fig. 4.7 Deformation pattern of *SP- B2* (a) Numerical analysis (b) Experiment

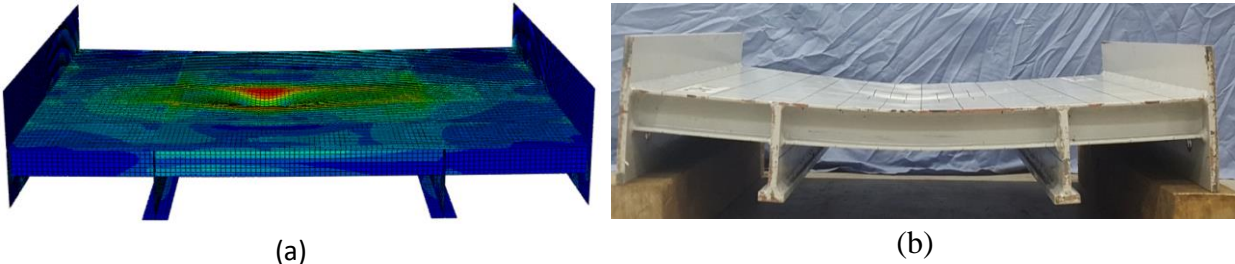


Fig. 4.8 Deformation pattern of *SP- B3* (a) Numerical analysis (b) Experiment

## 4.2 Intermediate step for releasing boundaries

As we mentioned in Chapter 2, the depth of dent before and after releasing boundary conditions shows a great significant. The effect of this one should be added into the numerical analysis. The models after releasing boundary conditions is used for residual strength analysis.

Table 4.4 Comparison of depth of dent at the impact point after releasing boundary conditions

Model	Test	Numerical	$X_m$
	mm	mm	Test/ Numerical
<i>SP-A2</i>	59.21	57.42	1.03
<i>SP-A3</i>	40.41	40.43	1.00
<i>SP-B2</i>	40.68	36.08	1.13
<i>SP-B3</i>	32.29	29.36	1.10
Mean			1.06
COV			5.57%

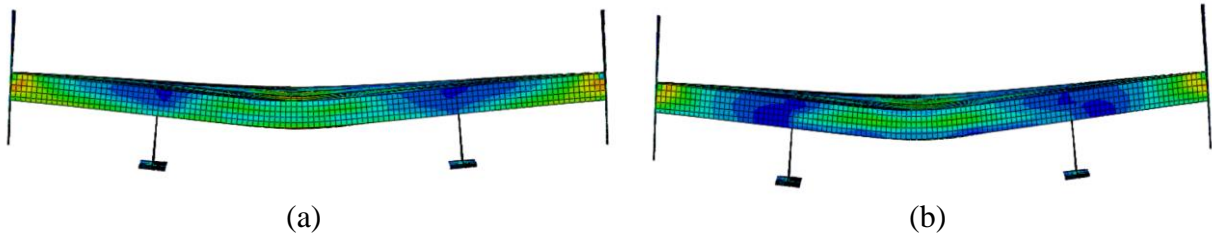


Fig. 4.9 Deformation of Model-*SP-A2* (a) before releasing boundary conditions (b) after releasing boundary conditions

# Chapter 5 Residual strength analysis of damaged stiffened plates

## 5.1 Residual strength simulation

### 5.1.1 Assembly of finite element model

The ultimate strength simulation is carried out based upon the structures against the lateral collision test. Before the ultimate strength simulation, the spring-back effect should be considered into the analysis. Since the test specimens in lateral collision tests has large deflections and plastic deformations, finite element analyses had to be performed using software offering combined geometric and material non-linear capabilities.

The initial shape imperfection is really sensitive on the ultimate strength of the structures. The average value of the initial imperfection measured before the test will be applied as the amplitude of the initial deformation. . For the analysis of non-linear problems, the displacement-controlled method (DCM) has a more extensive application scope and more powerful abilities than the load-controlled method (LCM) [26]. However, the correlation between the load-controlled method and displacement control method cannot be neglected.

The primary aim of the collision analysis step is to obtain a distorted geometry together with the initial residual stresses of element. After analysing the releasing the boundary conditions, the deformed geometry and residual strength have to add as an input into axial compression analysis. The assembly of the models applied in the analysis is shown in Fig. 5.1.

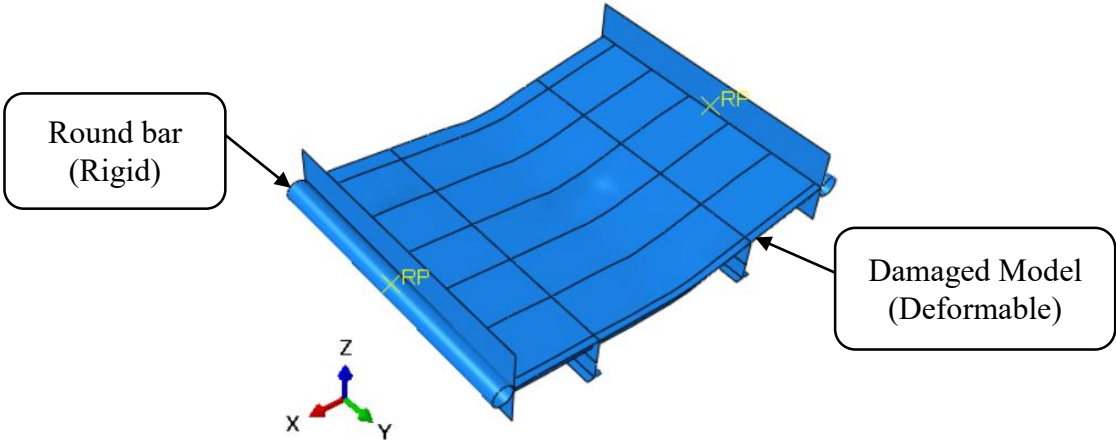


Fig. 5.1 Assembly model for residual strength analysis (SP-A2)

### 5.1.2 Material definition

In the residual strength analysis of the damaged stiffened plate, the modified Riks method, commonly used in an unstable phase of response. However, displacement-controlled method is used according to its convenience and common usage. Large deformation and plasticity were taken into account from the collision analysis after releasing boundary condition. The material was assumed to be linear elastic perfectly plastic, neglecting the strain hardening although the collision

impact some parts of the model could have entered into the strain hardening regime. When the Bauschinger effect is taken into account, the yield strengths of the elements experienced strain hardening could be higher than that of the original plate. In the ultimate strength analysis of the damaged model the change of the stress-strain curves should be modified before performing starting the simulation. However, in this study the curves of the corresponding elements were not modified.

### 5.1.3 Boundary conditions

The round bars are assumed as the control points for axial compression analysis. The boundary conditions on one of the round bars is fixed in all directions except the rotation of the end plate and axial shortening. Moreover, the others is allowed only the rotation of the end plate as shown in Fig. 5.2. In this simulation, the interaction between the end plates and the round bars is also considered.

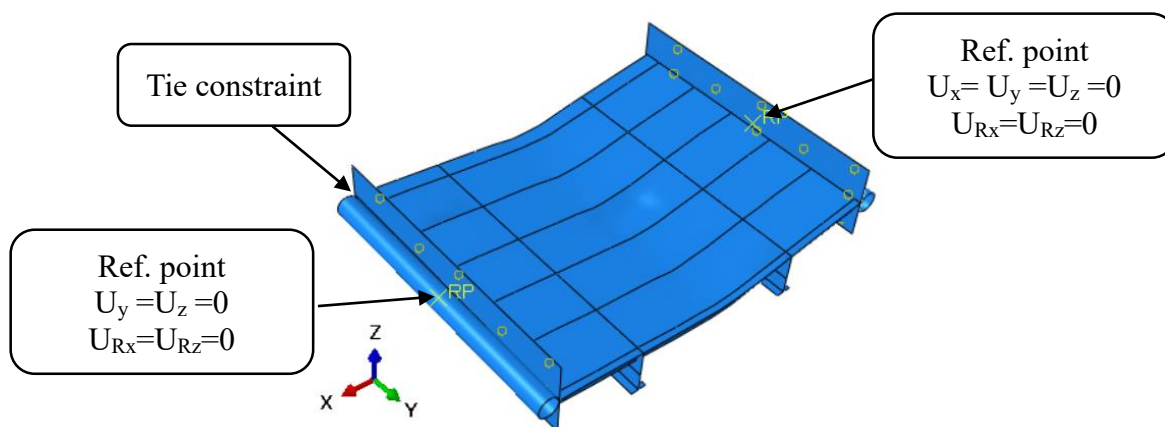


Fig. 5.2 Boundary conditions for residual strength analysis (SP-A2)

### 5.1.4 Comparison of predictions and tests

In plate panels, the longitudinal stiffeners have the main function of supplying the necessary support to the plate. Therefore, the stiffeners should have the adequate rigidity and the slenderness parameter becomes important. The slenderness parameter is designed according to considering the ultimate strength closer to the yield strength as much as possible.

Failure of plate is divided into four groups: plate induced failure, column-like failure, tripping of stiffeners and overall grillage failure. Plate induced failure occurs when the plates are stocky and has a critical elastic stress lower than yield stress. Column buckling occurs towards plate or stiffeners according to the initial shape of column and type of loadings i.e eccentrically applied or not. In a continuous panels, it is usual that the failure is towards the plate in one span and towards the stiffeners in the adjacent spans.

The tripping of stiffener is associated with a very quick shed of load carrying capacity of the column. Lateral-torsional instability may occur alone by twisting of the stiffeners about its line of attachment to the plating, developing a partial or full hinge at the intersection or induced by flexural buckling especially if the deflected shape of the column is towards the plate. In that case, the stiffeners will be subjected to a higher stress than the average column stress [29].

The welding residual stress due to fabrication remains in the stiffened plates. This kind of stress can decrease the ultimate strength of the plates. The effect of welding residual strength have been assigned in this study. The tension block will be formed within the welding line along the stiffeners meanwhile the other part with the compression residual stress will occur to satisfy the self-equilibrium condition. The contribution of welding along the attachment of stiffeners and transverse girders to the plates are predicted using Eq. 19 proposed by Hughes (1983). The width of tension block is determined by Eq. 20 proposed by the Ultimate longitudinal strength Committee of ISSC 2000.

$$\sigma_r = \frac{2\eta}{\frac{s}{t}-2\eta} \sigma_Y \quad (19)$$

$$\eta = \left\{ \frac{t_w}{2} + \frac{0.26\Delta Q}{t_w+2t_p} \right\} / t_p \quad (20)$$

$$\Delta Q = 78.8l^2 \quad (21)$$

$$\text{Where } l = \begin{cases} 0.7 \times t_w \text{ (mm)} & (\text{when } 0.7 \times t_w < 7 \text{ mm}) \\ 7 \text{ (mm)} & (\text{when } 0.7 \times t_w \geq 7 \text{ mm}) \end{cases} \quad (22)$$

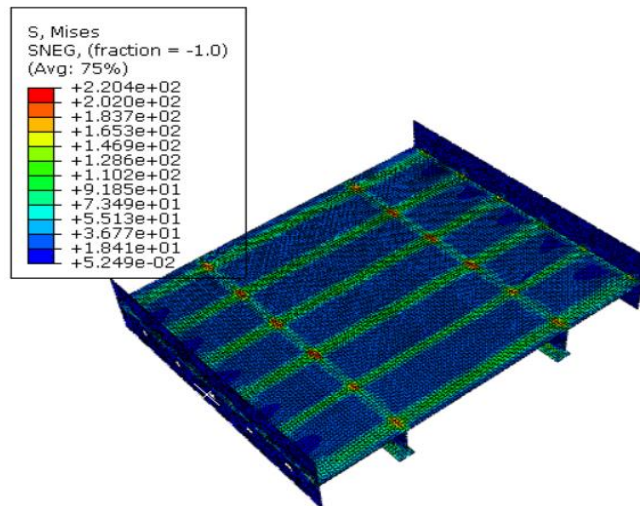


Fig. 5.3 Distribution of welding residual strength with initial imperfection (SP-BI)



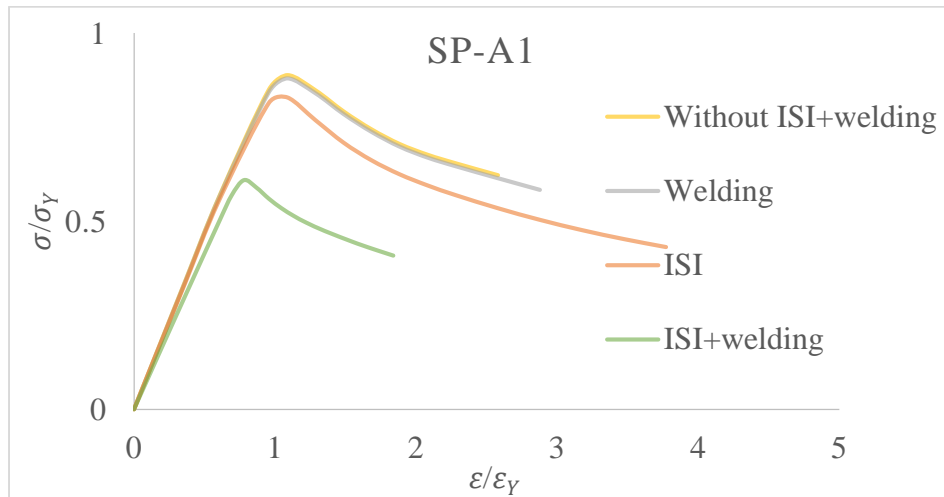


Fig. 5.4 Stress-strain curves (*SP-A1*)

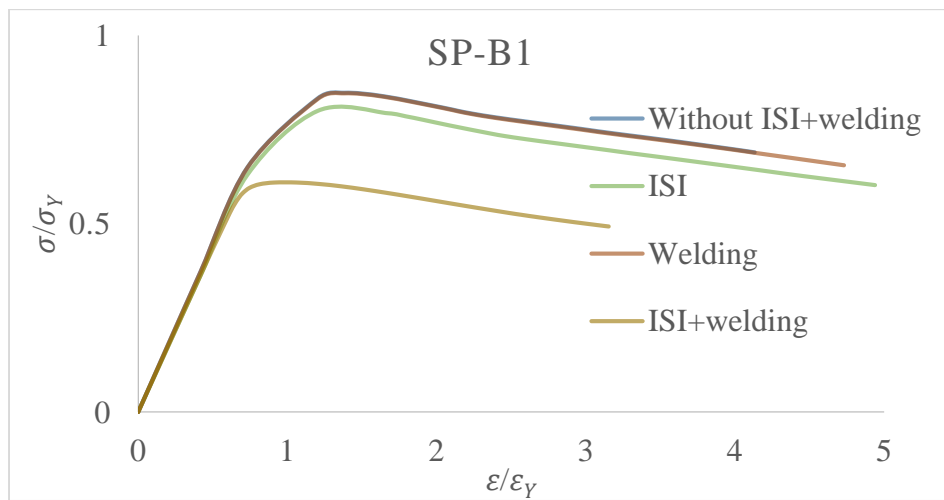


Fig. 5.5 Stress-strain curves (*SP-B1*)

As mentioned earlier (Chapter 2), the initial shape imperfection are measured in order to consider the reduction factor on the stiffened plate. The initial shape imperfection have a great influence on the ultimate strength in contradiction to the welding residual strength as can be seen in Fig. 5.4 and 5.5. Approximately 1 percentage reduction is shown when considered the welding residual strength from the ultimate strength without considering imperfection and welding effect meanwhile around 5 percent reduction with initial imperfection.

The final state is considered not only imperfection and welding but also material properties as a perfectly plastics. The collapse load is overestimated in intact cases and 10 percentage difference from the tests can be seen within damaged conditions. The average of  $X_m$  for residual strength of all models is approximately 1 and their COV is around 12 percent.

The final collapse shapes are similar with the experiments except *SP-A1*. The damaged cases are already buckled towards stiffeners and their final shapes are inevitable to follow in this directions. However, the collapse shapes for intact models are different according to the load application points.

The axial shortening for the prediction is much smaller than the tests. There are many uncertainties in order to improve the results of axial shortening curves.

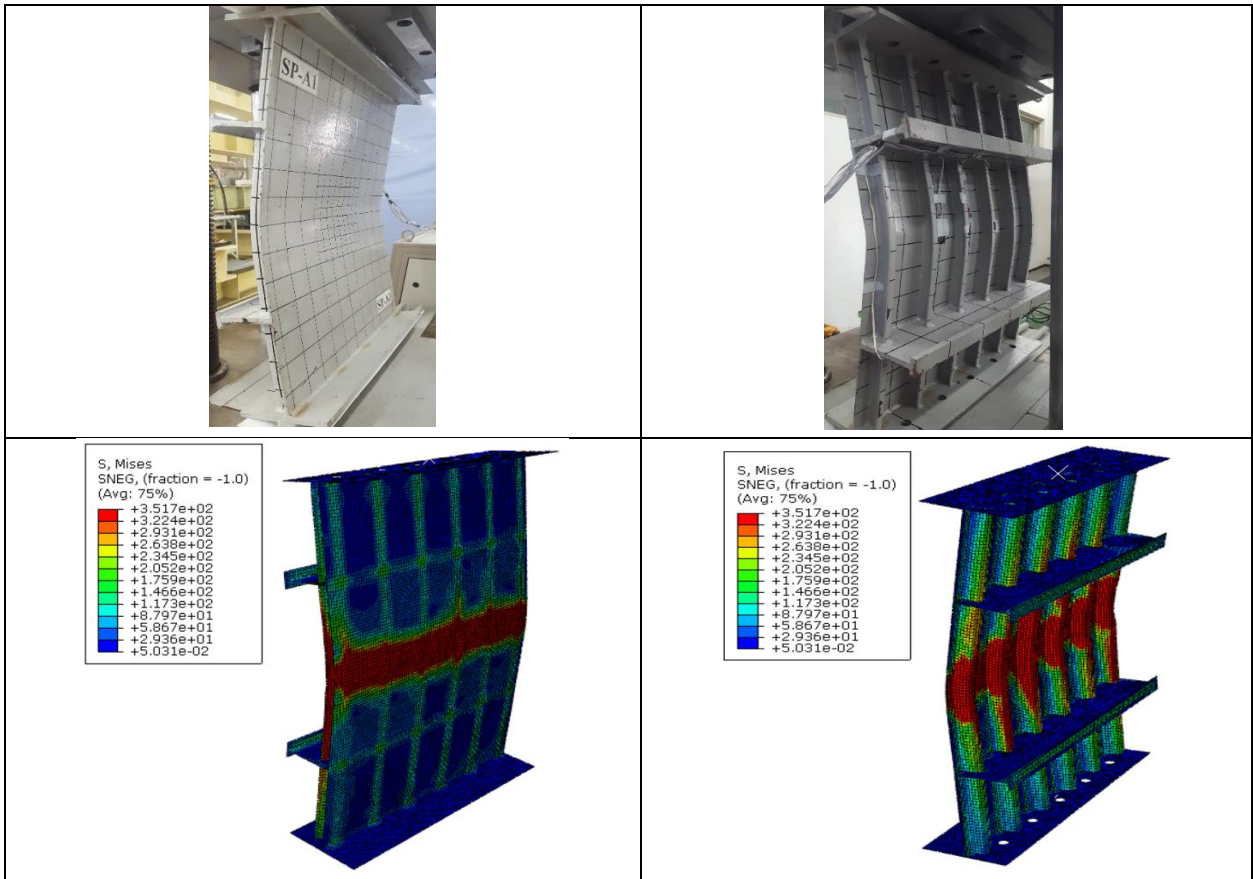


Fig. 5.6 Stress distribution across the whole model under uniform axial compression (*SP-A1*)

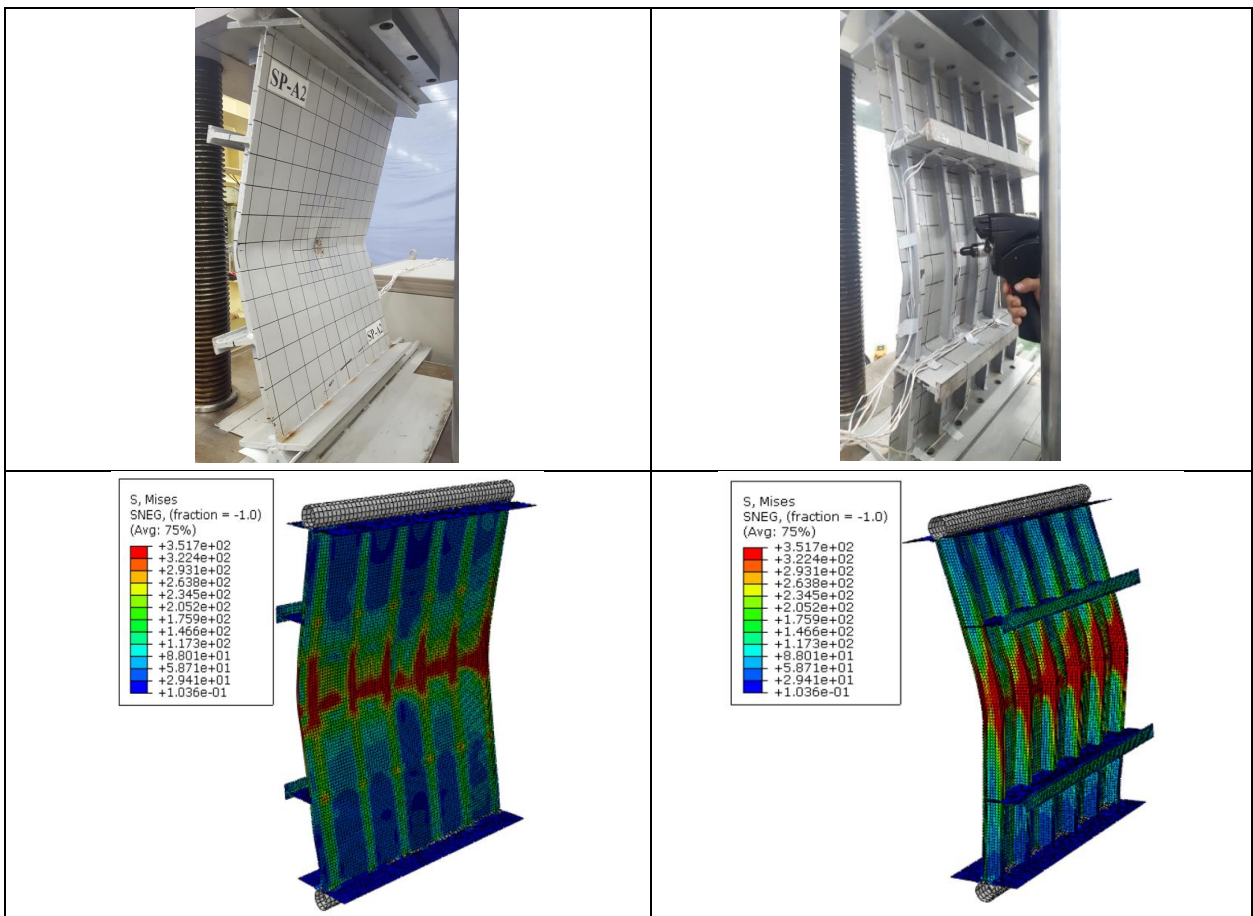


Fig. 5.7 Stress distribution across the whole model under uniform axial compression (*SP-A2*)

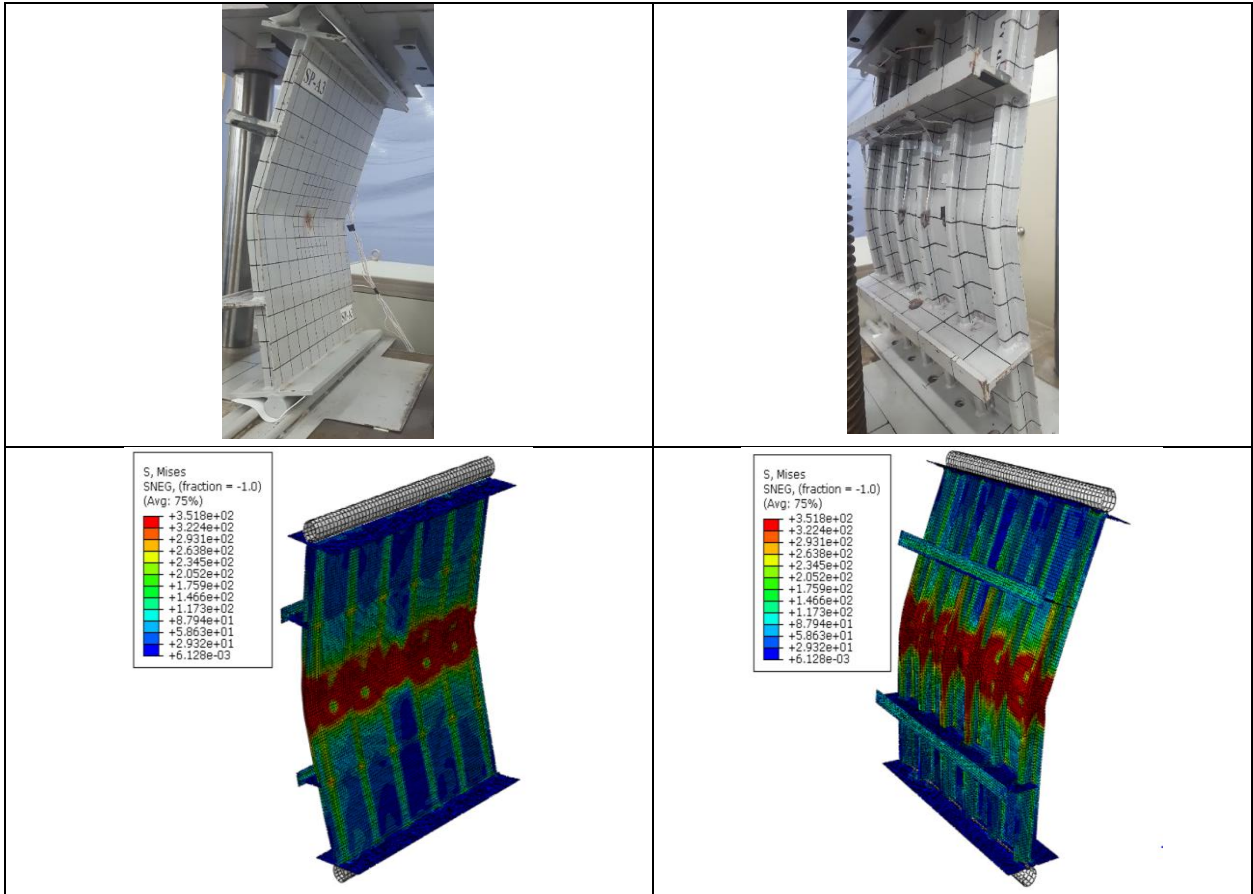


Fig. 5.8 Stress distribution across the whole model under uniform axial compression (*SP-A3*)

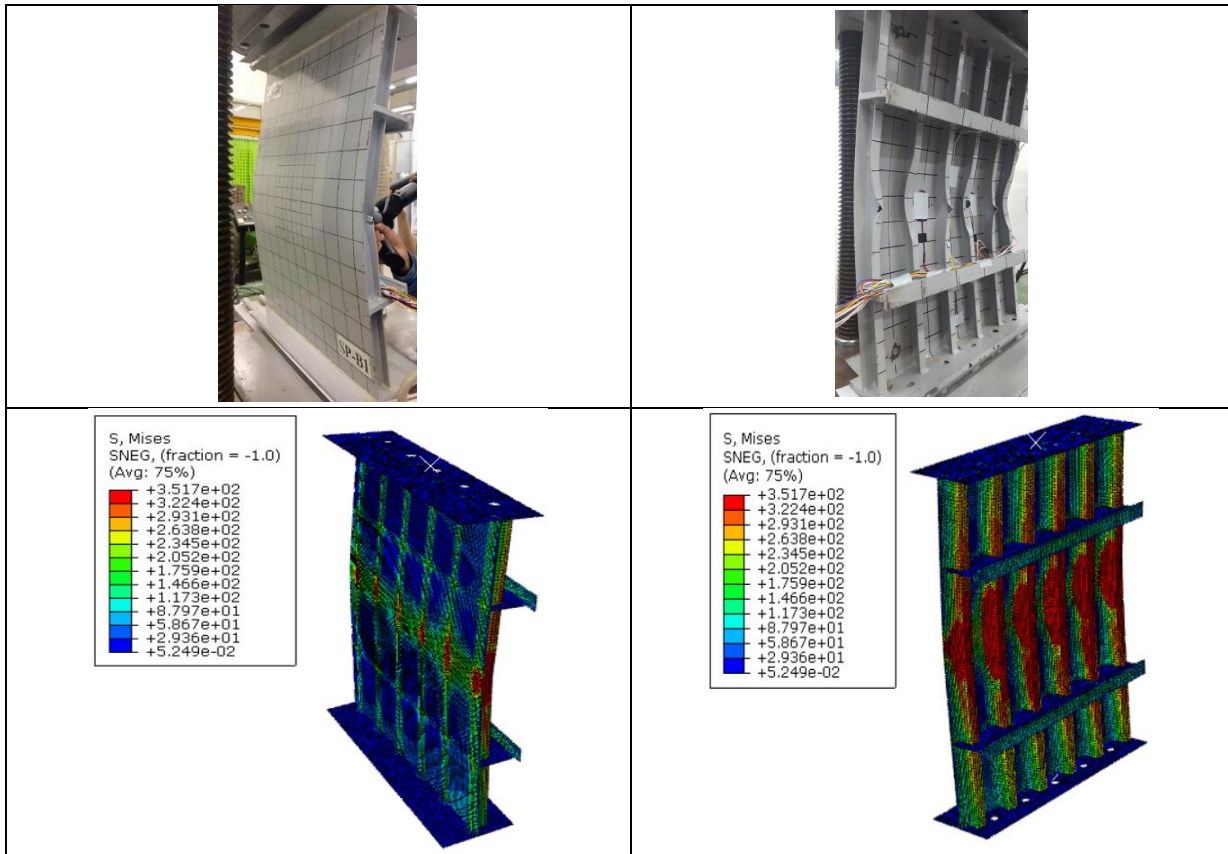


Fig. 5.9 Stress distribution across the whole model under uniform axial compression (*SP-B1*)

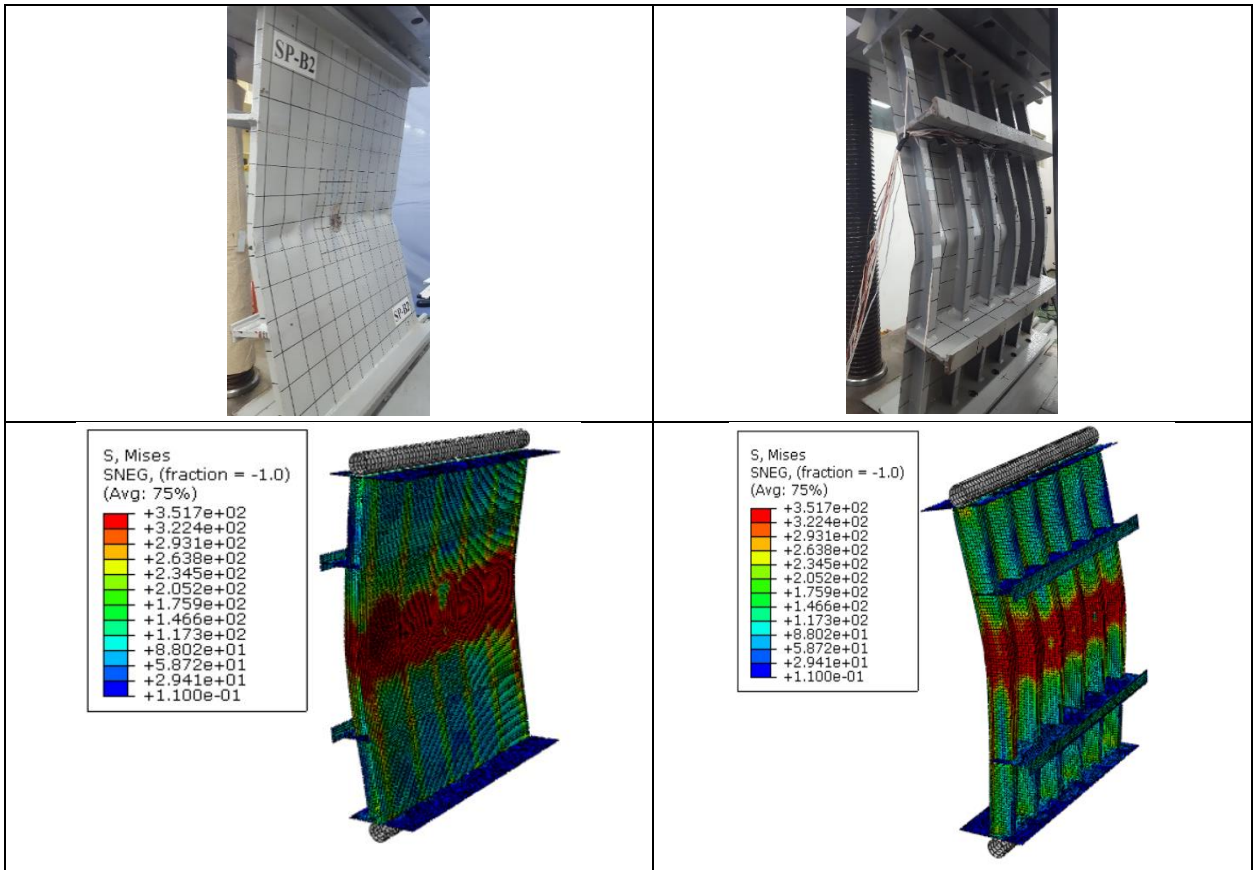


Fig. 5.10 Stress distribution across the whole model under uniform axial compression (*SP-B2*)

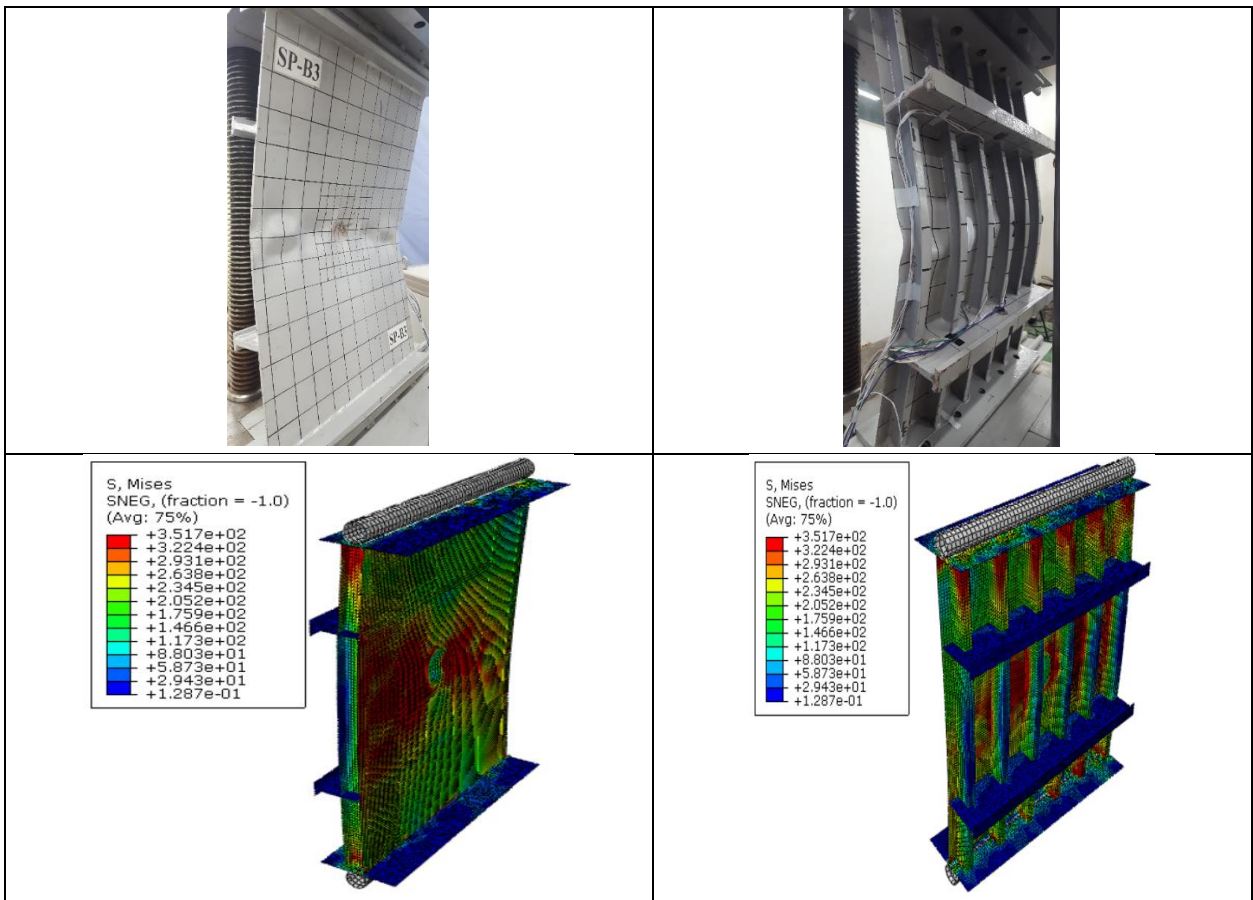


Fig. 5.11 Stress distribution across the whole model under uniform axial compression (*SP-B3*)

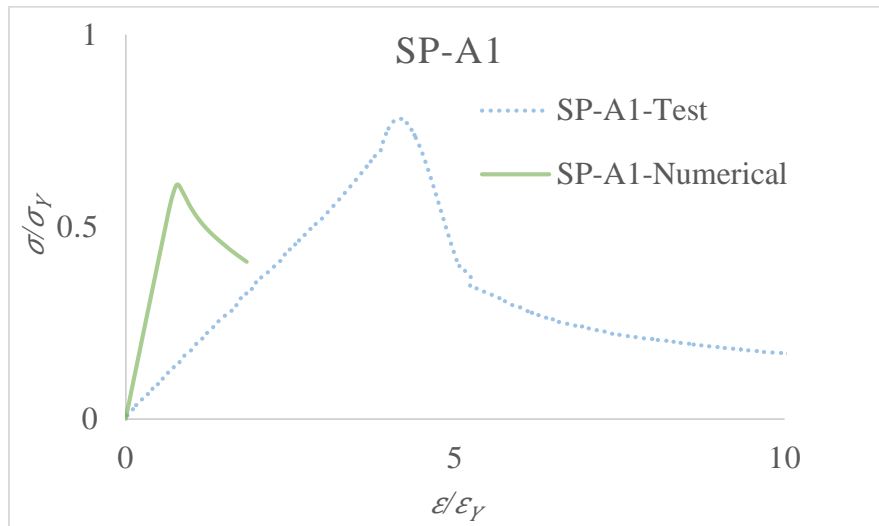


Fig. 5.12 Comparison of stress-strain curves (*SP-A1*)

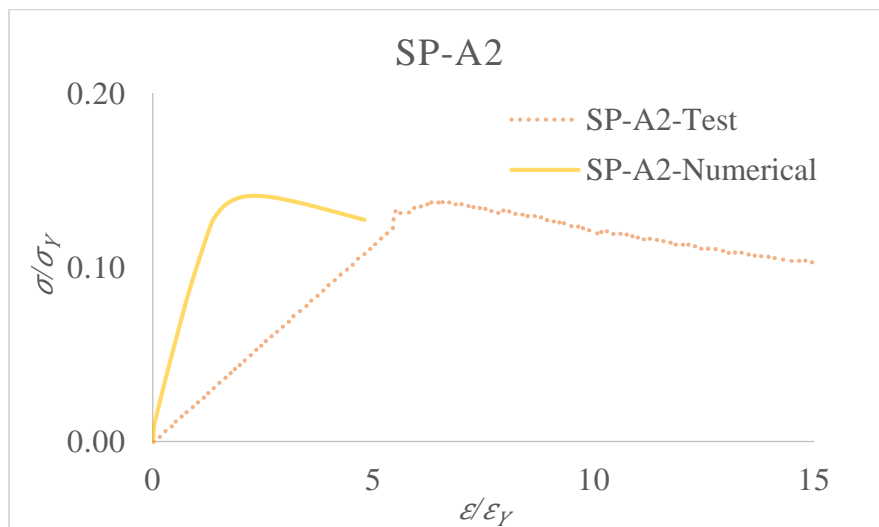


Fig. 5.13 Comparison of stress-strain curves (*SP-A2*)

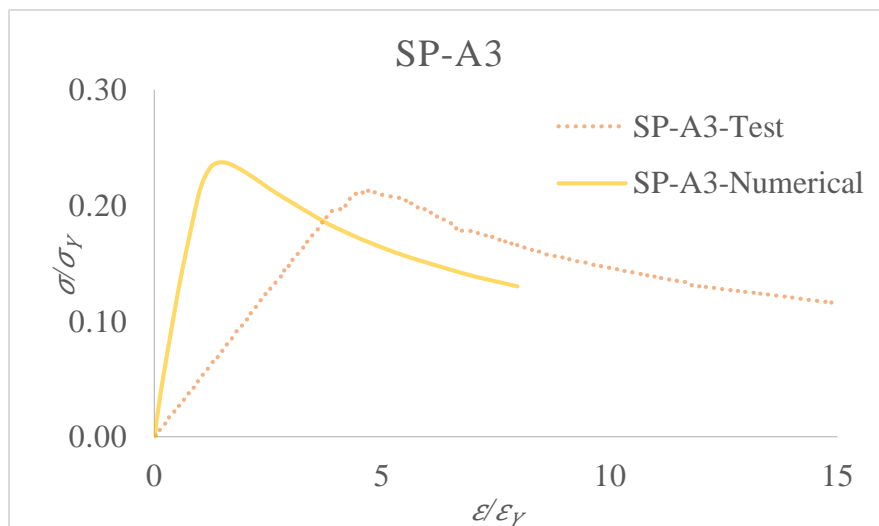


Fig. 5.14 Comparison of stress-strain curves (*SP-A3*)

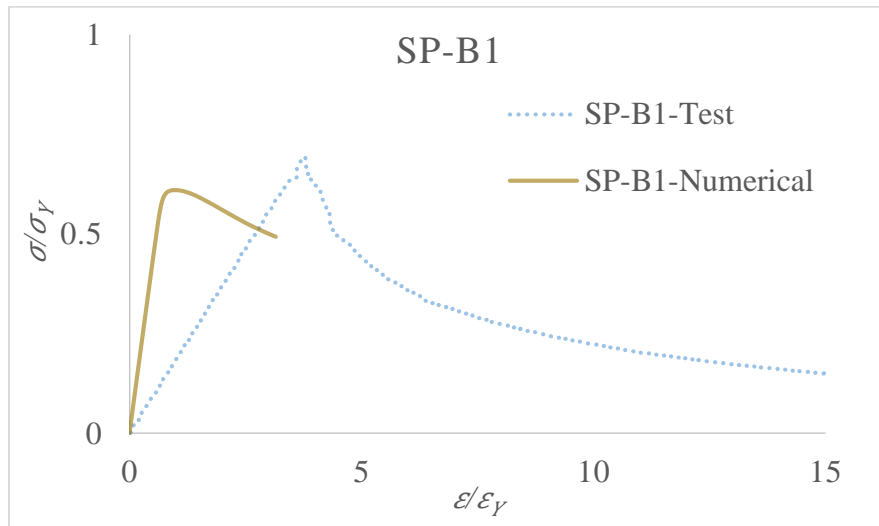


Fig. 5.15 Comparisons of stress-strain curves (*SP-B1*)

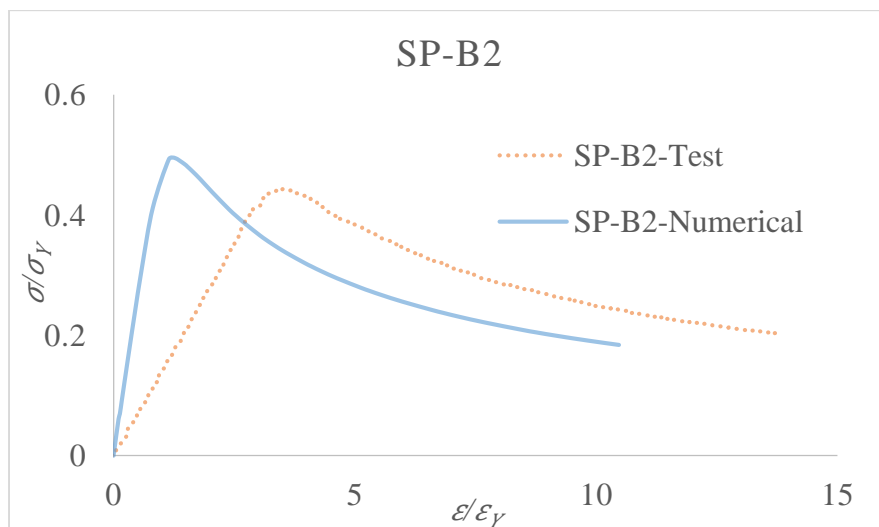


Fig. 5.16 Comparison of stress-strain curves (*SP-B2*)

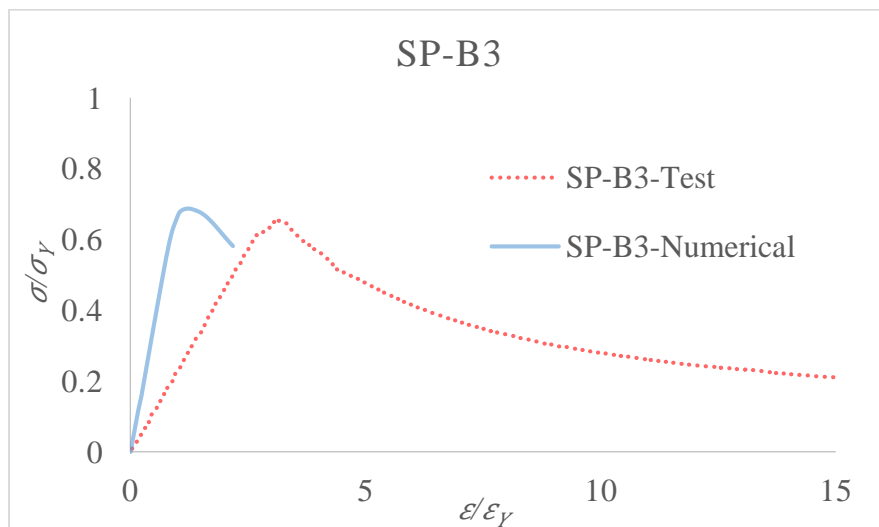


Fig. 5.17 Comparison of stress-strain curves (*SP-B3*)

Table 5.1 Comparison of residual strength test and numerical analysis results

Model	Tests			Predictions			$X_m$
	Max			Max			
	Axial shortening	Force	$\sigma_T$	Axial shortening	Force	$\sigma_T$	Exp./Pred.
	mm	kN	MPa	mm	kN	MPa	
<i>SP-A1</i>	3.99	595	252.3	0.74	508.7	215.7	1.17
<i>SP-A2</i>	6.75	103	43.7	2.02	105.6	44.8	0.98
<i>SP-A3</i>	4.82	160	67.8	1.51	177.7	75.4	0.90
<i>SP-B1</i>	3.63	580	221.2	0.87	508.6	193.9	1.14
<i>SP-B2</i>	3.21	370	141.1	1.22	413.1	157.5	0.90
<i>SP-B3</i>	2.93	549	209.4	1.23	573.1	218.5	0.96
Average							1.01
COV (%)							11.88

# Chapter 6 Discussion

## 6.1 Introduction

Residual stresses are stresses that remain in a solid material after the original cause of the stresses has been removed. Residual stresses can occur through a variety of mechanisms including inelastic (plastic) deformation, temperature gradients (during thermal cycle) or structural changes (phase transformation).

The stiffened plate of marine structures may be subjected to axial load, transverse load, lateral pressure and shear force or the combination of this various loadings. Collision scenario is inevitable once in a life time. The evaluation of residual strength becomes vital in service life.

Experimental study results on stiffened plate under combined loading are very difficult to find in the open literature. However, the study of ultimate strength of stiffened plate under each loading condition has been paid attention by many researchers. Our study is also focused on the residual strength of stiffened plate under axial compression.

In order to derive any ultimate strength design formulation for stiffened plate subjected to axial compression, it is necessary to understand their ductile failure modes. There are various failure modes for stiffened plates as follows.

- Plate induced failure
- Column like failure
- Tripping of stiffeners
- Overall grillage failure

Plate induced and column-like failure are sometimes incorporated in the same group because the buckled shape of the panel is similar and is normally towards the stiffener. In plate induced failure, the stiffener is able to withstand the stress near yield, however, the plate can only withstand its ultimate strength.

The tripping failure mode is always associated with a very quick shed of load carrying capacity of the column. Lateral collision instability may occur by twisting of the stiffener about its line of attachment to the plating. Tripping involves a rotation of the stiffener about a hinge which is usually considered to be located on the connection of the stiffener to the plating, and vertical flexure in the principal direction of the stiffener.

## 6.2 Comparison of numerical predictions with test results

In numerical analysis, three kinds of distortions: initial imperfection of the plate element, lateral and transverse deflection of not only stiffeners but also girders are considered. The initial imperfection of the plate element decreases the ultimate strength of the plate and consequently the strength of the panels.

Lateral and transverse deflections of the stiffeners can cause the bending stress along the span of the stiffeners with stiffener tripping. For girders, there is no significant change in stress distribution. The prediction reaches the collapse strength when the strength is approximately 18



percent greater than the test results for intact cases that comes along with the shortest axial shortening.

For damaged *SP-A2*, although the collapse load is almost the same, however, the axial shortening is three times larger than the test. The final collapse shape is the same with the test when the initial shape imperfection, residual strength and eccentricity are considered. Both test and prediction models for *SP-A3* accompany with the tension at the flange of the stiffener at the mid-bay.

*SP-B1* buckled towards plate when their ultimate strength approaches because the plate is in compression when the load starts exposed to the models. The stiffener web faces greater compression situation when the models starts to collapse. The flange is in tension when the web is in compression and their adjacent stiffeners suffers alternative way in tension and compression. This may be due to the eccentricity and the connectivity of plate, stiffeners and transverse girders. However, the numerical method is very conservative with the collapse shape.

Plate induced failure incorporated with column buckling mode can be seen in both numerical and test for *SP-B2*. In *SP-B3*, the plate near the free edge are in compression and the other parts are in tension. This may be due to the arrangement of the models (tightness of the round bar into the top and bottom bearing plates). The collapse shape of prediction method is not as significant as the test because there are many uncertainties during installing the models and this can't be simulated into the analysis.

The axial shortening of the predictions are two or three time smaller than the experiment although their collapse load is similar. In the analysis, the load is directly applied to the round bar. However, the load is firstly applied to the bottom bearing plate and it is transmitted to the Teflon plate. Finally, it reaches to the round bar. This steps should be added into numerical analysis in order to investigate the changes in axial shortening cases. Mesh size may be one of the factors in order to improve the axial shortening.

### **6.3 Comparison with design formulations**

There are many formulations proposed for the prediction of ultimate strength under different loadings. DNV [30] rules proposed the ultimate formulation dealing with the yield strength and column buckling. That means it depends on the slenderness parameter of the stiffeners. The effective width of the plate is also considered based upon the slenderness parameter of the plate. A simplified equation specified by DNV rules is very conservative and produces great coefficient of variance.

An alternative way for ultimate strength calculation is proposed by IACS, Common structural rules for bulk carriers and oil tankers [31]. The interaction between axial load, bending stress at the stiffeners and torsional stresses are also considered in this calculation. Types of stiffeners and lateral pressure are the factors for bending stress and only axial load applying on the effective width of plates are used. Failure modes should be predefined for torsional stresses. Nevertheless, CSR-H is very complicated and their variation is accurate based on different situations.

The method of [32] and [33] is based upon the interaction between column buckling, torsional buckling, overall buckling and yielding. The basic method is Merchant-Rankine formula and their reduction knock-down factor is the main character for considering the accuracy of the prediction methods.

Table 6.1 Comparison of various existing design formulae

Prediction Method	Average	COV (%)
CSR-H	0.94	25.65
DNV	0.81	38.68
Offshore Structure [32]	0.90	47.35
Hyun-Su Kim [33]	0.95	57.09

According to Table 6.1, CSR-H has the highest reliability compared with the test results. This may be because of the variation of the equation followed with the type of stiffeners, loading condition and consideration of interaction between different loadings. A simplified equation attains higher coefficient of variance.

This comparison is made based upon the collection of 67 models from various references. The calculation procedure and the data are mentioned in Appendix- I and J.

# Chapter 7 Conclusions and recommendations for future works

## 7.1 Conclusions

In this thesis, six models of a stiffened plate with one full bay and two half bays were performed. The effects of the impact point location can vary the maximum depth of a dent and the deformation patterns between the stiffeners and impact location. The shape of the local plastic deformation is similar with the shape of the striker. The maximum extent of the damage appears around the tip of the striker.

A considerable reduction occurs along the length between the impact point and the transverse girder. The impact point near the stiffeners possesses less permanent deflection compared with the others. The deflection near the transverse stiffeners shifted slightly from the position of the original point owing to a high membrane tension or compression near the impact region, as well as the transverse girders acting as a simple support across the structures.

The distortion of the plate only spread out between the stiffeners. This is obvious in the failure of *SP-A2*, which has a similar half sinusoidal wave in the initial shape imperfection and the depth of denting between the stiffeners. However, the distortion after releasing the boundaries shows a different shape at the free edge of the stiffener. The stiffened plates with a higher impact velocity and lesser scantling shape attained a global deformation.

This indicates that the rigidity of the scantlings is insufficient against the lateral impact velocity. In contrast to *SP-A2* and *SP-A3*, only local elastic and plastic deformations occur in *SP-B2* and *SP-B3*. A significant increase and reduction in the depth of the denting in *SP-B2* indicates the occurrence of a bending moment at the end plate when the joining angle is released.

Contribution of the stiffeners is really important in the ultimate strength of stiffened plate structures. It can be seen clearly between *SP-A2* and *SP-B2*. Although the structures with different scantlings received the same kinetic energy, their reduction factors stand apart each other. The lower the kinetic energy is, the higher the ultimate strength attains with larger stiffeners parts. Moreover, only a slight reduction in ultimate strength can occur between the intact model and the damaged model with low impact velocity with a large scantlings.

The global deformation of plate also effect on the ultimate strength of one and two half bays stiffened plates. The distortion of plate against lateral collision varies according to their impact velocity and location of dent.

The final dent of depth influences on the ultimate strength of stiffened plate under uniform axial compression. It seems to be that *SP-B3* with only local plastic deformation can withstand the uniform axial compression than *SP-B2* with slightly approached to the global deformation pattern. The failure modes of two intact models under axial compression are different: one with plate-induced failure and the others with stiffener failure. This may be due to the resistance of scantlings to shear stress caused by the distance between neutral axis of the plate and the loading direction.

In numerical analysis, the simulation was performed based upon the experiment. However, there are many uncertainties throughout the analysis. The discrepancies were partially attributed to the uncertainties in the tests such as initial shape imperfection, welding residual strength, rotation of strikers, eccentricity and impact location.

## 7.2 Recommendations for future works

The aim of our study is to investigate damage the collision resistance of undamaged stiffened plates and the residual strength of damaged stiffened plates under axial compression. Lateral collision tests were performed on two different groups of stiffened plates by using rigid hemisphere striker. The significant difference in depth of dent occurs based upon the difference in contribution of stiffeners.

The extent of damage of the plate due to lateral collision has a great influence on the ultimate strength of the plate. The location of loading applied to the model is one of the factors in consideration of the final collapse shapes. The intact model (model *SP-BI*) was eccentrically loaded toward stiffener and the collapse mode induced by stiffener tripping which endures the axial compression lesser than the other intact model (model *SP-AI*).

The numerical predictions presented for damage extent in stiffened plates showed good agreement with the test results. Uncertainty in experiment should consider in the numerical analysis based upon the results of this investigation. According to the analysis results of six experiment data on stiffened steel plates subjected to uniform axial compression, the accuracy of the collapse load obtained through FEM simulation need to be developed. Therefore, parametric study is a future work to investigate.

# References

- [1] Paik J.K., Residual ultimate strength of steel plates with longitudinal cracks under axial compression-experiments, 2008, *Ocean Engineering* 35 (2008) 1775-1783.
- [2] Paik J.K., Residual ultimate strength of structural members with multiple crack damage, 2009, *Thin walled structures* 47 (2009) 1439-1446.
- [3] Li Z.G., Influence of dent on residual ultimate strength of 2024-T3 aluminum alloy plate under axial compression, *Trans. Nonferrous Met. Soc. China* 24 (2014) 3084-3094.
- [4] Paik J.K., Lee J.M. & Lee D.H., Ultimate strength of dented steel plates under compressive loads, *Int. J. Mech. Sci.* 45 (2003) 433-448.
- [5] Gruben G., Solverness S., Berstad T., Morin D., Hopperstad O.S. & Langseth M., Low velocity impact behavior and failure of stiffened steel plates, *Marine Struct.* (2017).
- [6] Gruben G., Langseth M., Fagerholt E. & Hopperstad O.S., Low velocity impact on high-strength steel sheets: An experimental and numerical study, *Int. J. Impact Eng.* 88, (2016) 153-171.
- [7] Yuen S.C.K. & Nurick G.N., Experimental and numerical studies on the response of quadrangular stiffened plates: Part I: subjected to uniform blast load, 31 (1) (2005) 55-83.
- [8] Wang Ge., Ohtsubo H. & Arita K., Large deflection of a rigid-plastic circular plate pressed by a sphere, *Transaction of ASME*, 65 (1998).
- [9] Amante D.D.M., Chujutalli J.A. & Estefen S.F., Experimental and numerical analyses of dented stiffened panels, *J. Offshore Mech. Arti. Eng* 137(3) (2015).
- [10] Liu B., Villavicencio R. & Guedes Soares C., Experimental and numerical plastic response and failure of laterally impacted rectangular plates, *J. Offshore Mech. Arct. Eng* 135(4), 041602 (2013).
- [11] Villavicencio R. & Guedes Soares C., Numerical modelling of laterally impacted plates reinforced by free and end connected stiffeners, *Engineering Struct.* 44 (2012) 46-62.
- [12] Fathallallah E., Qi H., Tong L. & Helal M., Numerical simulation and response of stiffened plates subjected to noncontact underwater explosion, *J. Mar. Sci. Eng* 752586 (2014).
- [13] Hu S.Z. & Jiang L., A finite element simulation of the test procedure of stiffened panels, *Marine Struct.* 11 (1998) 75-99.
- [14] KS. B 0801 (1962) The pieces for tension test for metallic material, Korea industrial standard.
- [15] Ultimate strength, ISSC 2012, Vol. 1.
- [16] DNV classification note 30.1: Buckling strength analysis of bars and frames and spherical shells.
- [17] Cho, S-R., Kim, J.M. & Kim, Y.H., Effect of design parameters of double hull side structures on their collision resistance. In: *Proceedings of 25th Asian-Pacific Technical Exchange and Advisory Meeting on Marine Structures 2011, Incheon, Korea*, 352-360.
- [18] Cho S-R, Truong D.D. & Shin HK. Repeated lateral impacts on steel beams at room and sub-zero temperatures. *Int J ImpactEng* 2014;72:75-84.
- [19] Truong D.D., Shin H.K. & Cho S-R., Response lateral impacts. *Int J Nav Archit Ocean Eng*, accepted for publication 2017.

- [20] Cerik B.C., Shin H.K. & Cho S-R. On the resistance of steel ring-stiffened cylinders subjected to low-velocity mass impact. *Int. J. Impact Eng* 2015;84:108-123.
- [21] Cho S-R, Le D.N.C., Jeong J-H, Frieze P.A. & Shin H.K., Development of simple design-oriented procedure for predicting the collision damage of FPSO caisson protection structures. *Ocean Eng* 2017;142:458-469.
- [22] Cerik B.C., Shin H.K. & Cho S-R, A comparative study on damage assessment of tubular members subjected to mass impact. *Mar. Struct.* 2016;46:1-29.
- [23] Liu B. & Guedes Soares C., Simplified analytical method for evaluating web girder crushing during ship collision and grounding, *Marine Struct.* 42 (2015) 71-94.
- [24] Abaqus analysis user manual (6.14).
- [25] Cho S-R, Choi S.I. & Son S.K., Dynamic material properties of marine steels under impact loadings. In: *Proceedings of the 2015 World Congress on Advances in Structural Engineering and Mechanics, ASEM15*. Incheon, Korea; 2015.
- [26] Zheng H., Liu D.F., Lee C.F. & Tham L.G., Displacement-controlled method and its applications to material non-linearity.
- [27] Dnv-RP C201 Buckling strength of plated structures.
- [28] Common structural rules for bulk carriers and oil tankers, 2015.
- [29] Gordo J.M. & Guedes Soares C., Approximate load shortening curves for stiffened plates under uniaxial compression, Department of Naval Architecture and Ocean Engineering, Technical University of Lisbon.
- [30] Dnv Buckling strength analysis of bars and frames and spherical shells, 2004
- [31] IACS Common structural rules for bulk carrier and oil tankers, 2015
- [32] Study on Floating Offshore Structure, University of Ulsan, 1996
- [33] Cho S-R, Kim H.S., Doh H.M. & Chon Y.K., Ultimate strength formulation for stiffened plates subjected to combined axial compression, transverse compression, shear force and lateral pressure loadings, *Ship and Offshore Structures*, 2013.
- [34] Smith C.S, Compressive strength of welded steel grillages, RINA Spring Meeting, 1975.
- [35] Murray N.W. & Kazar W, The collapse behavior of stiffened steel plates which have high aspect ratios under axial compression, *Stability and Plastic Collapse of Steel Structures*, London, 1983.
- [36] Ghavami K, Ultimate load behavior of stiffened plates subjected to compression load, Civil Engineering Department, Pontificia Universidade Catolica, Rio de Janeiro, Brazil, Presently at Concordia University, Montreal, Canada, 1986-1987.
- [37] Murry N.W., Analysis and design of stiffened plates for collapse load, *The Structure Engineer*, Vol. 53, No.3, March 1975, 153-158.
- [38] Horen M.R. & Narayanan R., Ultimate capacity of longitudinally stiffened plates used in box girders, *Proc. Inst Civ. Engrs*, 61, Part 2, 1976.

## Appendix-A Initial imperfection measurement results (mm)

### SP-A1

X/Y	0	20	70	120	170	195	220	245	270	295	320	345	370	420	470	520	550
0	0.00	0.00	0.00	0.00	0.00	0.00	0.00	0.00	0.00	0.00	0.00	0.00	0.00	0.00	0.00	0.00	0.00
40	3.92	3.66	2.94	2.63	2.18	0.00	1.96	0.00	1.57	0.00	1.39	0.00	1.13	1.11	0.77	0.98	0.98
90	2.81	2.67	1.99	1.85	1.53	0.00	1.36	0.00	1.02	0.00	0.94	0.00	0.69	0.76	0.34	0.68	0.60
140	2.46	2.21	1.75	1.50	1.18	0.00	0.89	0.00	0.65	0.00	0.63	0.00	0.48	0.44	0.18	0.45	0.70
190	2.17	1.93	1.81	1.26	1.08	0.00	0.71	0.00	0.66	0.00	0.45	0.00	0.50	0.30	0.49	0.38	0.70
240	1.31	1.25	0.91	0.84	0.54	0.45	0.39	0.29	0.29	0.23	0.30	0.13	0.10	0.10	0.03	0.29	0.91
265	0.00	0.00	0.00	0.00	0.34	0.27	0.23	0.15	0.17	0.18	0.23	0.07	0.04	0.00	0.00	0.00	0.00
290	0.63	0.62	0.34	0.45	0.22	0.12	0.18	0.10	0.11	0.12	0.12	0.02	0.01	0.03	-0.11	0.13	0.52
315	0.00	0.00	0.00	0.00	0.04	-0.01	0.03	0.01	0.03	0.02	0.09	0.01	0.00	0.00	0.00	0.00	0.00
340	0.09	0.00	-0.11	-0.03	-0.07	-0.14	-0.05	-0.02	0.00	-0.01	0.06	0.07	0.05	0.00	-0.10	0.15	0.37
365	0.00	0.00	0.00	0.00	-0.16	-0.22	-0.16	-0.09	-0.06	-0.09	-0.02	0.04	0.02	0.00	0.00	0.00	0.00
390	-0.20	-0.44	-0.43	-0.30	-0.25	-0.31	-0.19	-0.12	-0.12	-0.12	0.00	0.03	0.07	0.11	0.02	0.24	0.38
415	0.00	0.00	0.00	0.00	-0.31	-0.37	-0.25	-0.15	-0.11	-0.14	-0.08	0.04	0.10	0.00	0.00	0.00	0.00
440	-0.55	-0.62	-0.64	-0.52	-0.40	-0.46	-0.38	-0.26	-0.19	-0.20	-0.10	0.01	0.11	0.19	0.25	0.43	0.63
490	-0.65	-0.76	-0.76	-0.74	-0.62	0.00	-0.41	0.00	-0.22	0.00	-0.07	0.00	0.24	0.37	0.75	0.99	1.32
540	-0.95	-1.30	-0.79	-0.71	-0.65	0.00	-0.48	0.00	-0.23	0.00	-0.06	0.00	0.23	0.39	0.63	0.68	0.98
590	-1.12	-1.68	-1.37	-0.72	-0.64	0.00	-0.50	0.00	-0.31	0.00	0.06	0.00	0.17	0.41	0.40	0.31	0.57
640	-1.58	-1.36	-1.13	-0.55	-0.47	0.00	-0.12	0.00	0.00	0.00	0.25	0.00	0.38	0.74	0.84	0.99	1.28
680	0.00	0.00	0.00	0.00	0.00	0.00	0.00	0.00	0.00	0.00	0.00	0.00	0.00	0.00	0.00	0.00	0.00

### SP-A2

X/Y	0	20	70	120	170	195	220	245	270	295	320	345	370	420	470	520	550
0	0.00	0.00	0.00	0.00	0.00	0.00	0.00	0.00	0.00	0.00	0.00	0.00	0.00	0.00	0.00	0.00	0.00
40	3.27	3.11	2.72	2.43	2.16	0.00	1.72	0.00	1.32	0.00	1.06	0.00	0.80	0.55	0.26	0.03	-0.04
90	3.14	2.76	2.22	1.95	1.56	0.00	1.33	0.00	0.95	0.00	0.79	0.00	0.42	0.33	-0.02	0.06	0.10
140	2.63	2.41	2.06	1.77	1.40	0.00	1.20	0.00	0.94	0.00	0.71	0.00	0.42	0.35	0.21	0.18	0.43
190	2.31	2.06	1.82	1.47	1.26	0.00	0.96	0.00	0.85	0.00	0.68	0.00	0.60	0.44	0.58	0.50	0.70
240	1.63	1.34	1.04	0.83	0.65	0.59	0.51	0.37	0.39	0.43	0.39	0.31	0.36	0.33	0.40	0.48	0.36
265	0.00	0.00	0.00	0.00	0.39	0.41	0.37	0.19	0.28	0.35	0.42	0.25	0.27	0.00	0.00	0.00	0.00
290	0.92	0.68	0.38	0.34	0.16	0.18	0.18	0.05	0.16	0.29	0.42	0.24	0.32	0.52	0.55	1.00	0.76
315	0.00	0.00	0.00	0.00	-0.06	-0.01	0.09	-0.03	0.08	0.23	0.41	0.26	0.32	0.00	0.00	0.00	0.00
340	0.06	0.00	-0.17	-0.15	-0.31	-0.21	-0.09	-0.15	0.00	0.15	0.39	0.27	0.35	0.66	0.78	1.38	1.55
365	0.00	0.00	0.00	0.00	-0.49	-0.33	-0.18	-0.21	-0.05	0.16	0.38	0.26	0.37	0.00	0.00	0.00	0.00
390	-0.43	-0.391	-0.57	-0.51	-0.64	-0.45	-0.20	-0.24	-0.11	0.17	0.45	0.35	0.48	0.99	1.19	2.06	2.14
415	0.00	0.00	0.00	0.00	-0.73	-0.52	-0.26	-0.28	-0.16	0.12	0.46	0.39	0.49	0.00	0.00	0.00	0.00
440	-0.87	-0.85	-1.00	-0.86	-0.89	-0.64	-0.34	-0.34	-0.16	0.11	0.38	0.48	0.64	1.17	1.57	2.40	2.85
490	-1.26	-1.41	-1.23	-1.06	-0.83	0.00	-0.52	0.00	-0.03	0.00	0.40	0.00	1.01	1.62	2.31	3.02	3.59
540	-2.24	-2.26	-1.97	-1.58	-1.11	0.00	-0.65	0.00	-0.22	0.00	0.43	0.00	0.95	1.59	2.25	3.00	3.70
590	-2.43	-2.48	-2.28	-1.58	-1.25	0.00	-0.64	0.00	-0.29	0.00	0.56	0.00	1.04	1.85	2.32	3.23	3.83
640	-2.77	-2.69	-2.48	-1.63	-1.23	0.00	-0.41	0.00	0.00	0.00	0.86	0.00	1.16	1.99	2.47	3.48	4.10
680	0.00	0.00	0.00	0.00	0.00	0.00	0.00	0.00	0.00	0.00	0.00	0.00	0.00	0.00	0.00	0.00	0.00

SP-A3

X/Y	0	20	70	120	170	195	220	245	270	295	320	345	370	420	470	520	550
0	0.00	0.00	0.00	0.00	0.00	0.00	0.00	0.00	0.00	0.00	0.00	0.00	0.00	0.00	0.00	0.00	0.00
40	1.91	1.85	2.08	1.96	1.76	0.00	1.63	0.00	1.62	0.00	1.66	0.00	1.66	1.56	1.34	1.45	1.01
90	0.97	1.16	1.19	1.65	1.43	0.00	1.41	0.00	1.13	0.00	1.28	0.00	1.30	1.36	1.17	1.27	1.32
140	0.92	0.80	0.79	0.71	0.83	0.00	0.96	0.00	0.88	0.00	1.00	0.00	1.16	1.26	1.33	1.35	1.45
190	0.82	0.86	0.93	0.81	0.72	0.00	0.76	0.00	0.80	0.00	0.88	0.00	1.01	1.21	1.39	1.54	1.64
240	0.57	0.69	0.52	0.39	0.24	0.29	0.43	0.33	0.40	0.45	0.47	0.53	0.60	0.86	0.99	1.19	1.12
265	0.00	0.00	0.00	0.00	0.09	0.09	0.25	0.08	0.13	0.37	0.53	0.50	0.53	0.00	0.00	0.00	0.00
290	0.20	0.39	0.27	0.35	0.05	0.11	0.28	0.18	0.20	0.28	0.51	0.48	0.51	0.85	0.84	1.09	1.09
315	0.00	0.00	0.00	0.00	-0.03	-0.01	0.15	0.08	0.11	0.17	0.39	0.39	0.40	0.00	0.00	0.00	0.00
340	-0.33	0.00	-0.02	0.09	-0.08	-0.09	0.05	0.04	0.00	0.08	0.31	0.38	0.45	0.79	0.80	0.98	0.88
365	0.00	0.00	0.00	0.00	-0.19	-0.14	0.03	0.00	0.02	0.11	0.37	0.44	0.45	0.00	0.00	0.00	0.00
390	-0.74	-0.29	-0.31	-0.15	-0.23	-0.17	0.06	-0.01	0.05	0.11	0.42	0.44	0.46	0.79	0.79	0.84	0.86
415	0.00	0.00	0.00	0.00	-0.30	-0.25	0.01	0.01	-0.01	0.06	0.33	0.37	0.42	0.00	0.00	0.00	0.00
440	-0.95	-0.61	-0.44	-0.29	-0.34	-0.27	-0.13	-0.05	-0.01	0.04	0.27	0.33	0.42	0.73	0.73	0.93	0.97
490	-0.69	-0.70	-0.40	-0.40	-0.28	0.00	-0.15	0.00	-0.01	0.00	0.24	0.00	0.38	0.73	0.90	0.98	1.26
540	-0.54	-0.70	-0.68	-0.48	-0.33	0.00	-0.17	0.00	-0.08	0.00	0.15	0.00	0.34	0.63	0.75	1.12	1.49
590	-0.55	-0.50	-0.64	-0.28	-0.26	0.00	-0.03	0.00	-0.06	0.00	0.26	0.00	0.28	0.66	0.82	0.99	0.94
640	-0.40	-0.28	-0.36	-0.04	-0.18	0.00	0.13	0.00	0.00	0.00	0.39	0.00	0.34	0.70	0.61	0.84	0.97
680	0.00	0.00	0.00	0.00	0.00	0.00	0.00	0.00	0.00	0.00	0.00	0.00	0.00	0.00	0.00	0.00	0.00

SP-B1

X/Y	0	20	70	120	170	195	220	245	270	295	320	345	370	420	470	520	550
0	0.00	0.00	0.00	0.00	0.00	0.00	0.00	0.00	0.00	0.00	0.00	0.00	0.00	0.00	0.00	0.00	0.00
40	4.09	3.95	3.56	3.49	3.01	0.00	2.87	0.00	2.53	0.00	2.56	0.00	2.29	2.37	1.85	1.84	1.59
90	3.30	3.11	2.90	2.90	2.54	0.00	2.48	0.00	2.16	0.00	2.09	0.00	1.90	1.94	1.63	1.58	1.56
140	2.50	2.40	2.19	2.26	1.99	0.00	1.93	0.00	1.69	0.00	1.71	0.00	1.62	1.64	1.57	1.45	1.43
190	1.89	1.88	1.66	1.42	1.24	0.00	1.17	0.00	1.26	0.00	1.18	0.00	1.17	1.28	1.28	1.22	1.60
240	1.02	1.06	0.66	0.74	0.67	0.59	0.62	0.61	0.69	0.75	0.84	0.79	0.87	0.97	1.07	1.33	1.63
265	0.00	0.00	0.00	0.00	0.37	0.33	0.35	0.32	0.44	0.55	0.64	0.60	0.65	0.00	0.00	0.00	0.00
290	0.45	0.52	0.09	0.17	0.15	0.10	0.18	0.12	0.31	0.48	0.62	0.56	0.66	0.90	1.10	1.57	2.02
315	0.00	0.00	0.00	0.00	-0.03	-0.02	0.00	-0.06	0.13	0.36	0.50	0.43	0.55	0.00	0.00	0.00	0.00
340	-0.07	0.00	-0.27	-0.10	-0.26	-0.24	-0.19	-0.22	0.00	0.21	0.41	0.38	0.49	0.86	1.10	1.78	2.31
365	0.00	0.00	0.00	0.00	-0.41	-0.38	-0.34	-0.40	-0.19	0.06	0.32	0.30	0.40	0.00	0.00	0.00	0.00
390	-0.42	-0.40	-0.64	-0.53	-0.56	-0.52	-0.47	-0.54	-0.34	-0.08	0.26	0.23	0.37	0.90	1.15	1.95	2.37
415	0.00	0.00	0.00	0.00	-0.71	-0.65	-0.56	-0.61	-0.42	-0.16	0.19	0.23	0.36	0.00	0.00	0.00	0.00
440	-0.67	-0.68	-0.92	-0.73	-0.80	-0.68	-0.50	-0.65	-0.43	-0.21	0.19	0.19	0.42	1.08	1.33	2.18	2.61
490	-1.01	-1.08	-1.13	-0.96	-0.81	0.00	-0.46	0.00	-0.17	0.00	0.24	0.00	0.68	1.12	1.66	2.22	2.80
540	-1.26	-1.40	-1.39	-1.14	-0.94	0.00	-0.59	0.00	-0.19	0.00	0.21	0.00	0.69	1.22	1.76	2.45	3.25
590	-1.21	-1.48	-1.60	-1.15	-1.03	0.00	-0.53	0.00	-0.25	0.00	0.37	0.00	0.77	1.40	1.98	3.00	3.60
640	-1.19	-1.25	-1.49	-0.61	-0.80	0.00	-0.15	0.00	0.00	0.00	0.76	0.00	1.05	1.90	2.26	3.41	3.74
680	0.00	0.00	0.00	0.00	0.00	0.00	0.00	0.00	0.00	0.00	0.00	0.00	0.00	0.00	0.00	0.00	0.00



SP-B2

X/Y	0	20	70	120	170	195	220	245	270	295	320	345	370	420	470	520	550
0	0.00	0.00	0.00	0.00	0.00	0.00	0.00	0.00	0.00	0.00	0.00	0.00	0.00	0.00	0.00	0.00	0.00
40	3.85	3.75	3.02	2.32	1.92	0.00	2.05	0.00	2.07	0.00	1.96	0.00	1.77	1.82	1.64	1.99	1.76
90	3.56	2.74	2.56	1.95	1.76	0.00	1.63	0.00	1.45	0.00	1.64	0.00	1.39	1.43	1.34	1.57	1.39
140	2.19	2.14	1.74	1.63	1.51	0.00	1.37	0.00	1.31	0.00	1.31	0.00	1.27	1.23	1.22	1.33	1.48
190	1.59	1.61	1.53	1.74	1.28	0.00	0.99	0.00	1.09	0.00	1.00	0.00	0.97	0.96	1.16	1.28	1.63
240	0.89	0.92	0.37	0.55	0.37	0.41	0.40	0.34	0.35	0.41	0.61	0.49	0.52	0.76	0.79	1.28	1.47
265	0.00	0.00	0.00	0.00	0.17	0.17	0.27	0.26	0.26	0.36	0.58	0.50	0.49	0.00	0.00	0.00	0.00
290	0.59	0.56	0.14	0.40	0.16	0.06	0.18	0.10	0.11	0.20	0.53	0.40	0.37	0.61	0.68	1.15	1.28
315	0.00	0.00	0.00	0.00	-0.16	-0.18	0.06	-0.01	0.01	0.13	0.43	0.37	0.31	0.00	0.00	0.00	0.00
340	-0.18	0.00	-0.48	-0.31	-0.19	-0.15	0.01	-0.02	0.00	0.07	0.35	0.32	0.29	0.61	0.67	1.28	1.33
365	0.00	0.00	0.00	0.00	-0.37	-0.37	-0.20	-0.20	-0.20	-0.08	0.20	0.17	0.20	0.00	0.00	0.00	0.00
390	-0.56	-0.63	-0.81	-0.57	-0.57	-0.48	-0.30	-0.29	-0.25	-0.13	0.21	0.08	0.08	0.41	0.55	1.01	1.12
415	0.00	0.00	0.00	0.00	-0.52	-0.55	-0.43	-0.39	-0.31	-0.29	0.00	0.00	0.07	0.00	0.00	0.00	0.00
440	-0.73	-0.71	-0.91	-0.69	-0.62	-0.64	-0.51	-0.45	-0.32	-0.26	-0.07	0.05	0.13	0.53	0.74	1.14	1.27
490	-0.99	-1.02	-0.93	-0.94	-0.74	0.00	-0.61	0.00	-0.32	0.00	-0.13	0.00	0.19	0.59	0.98	1.31	1.63
540	-1.08	-1.13	-1.01	-0.81	-0.70	0.00	-0.61	0.00	-0.38	0.00	-0.05	0.00	0.26	0.59	0.81	1.49	2.07
590	-1.01	-1.04	-0.88	-0.50	-0.60	0.00	-0.40	0.00	-0.20	0.00	0.12	0.00	0.31	0.71	0.75	1.09	1.40
640	-1.04	-0.83	-0.88	-0.35	-0.39	0.00	-0.06	0.00	0.00	0.00	0.43	0.00	0.44	0.94	0.67	1.06	1.33
680	0.00	0.00	0.00	0.00	0.00	0.00	0.00	0.00	0.00	0.00	0.00	0.00	0.00	0.00	0.00	0.00	0.00

SP-B3

X/Y	0	20	70	120	170	195	220	245	270	295	320	345	370	420	470	520	550
0	0.00	0.00	0.00	0.00	0.00	0.00	0.00	0.00	0.00	0.00	0.00	0.00	0.00	0.00	0.00	0.00	0.00
40	1.76	1.78	1.60	1.72	1.48	0.00	1.62	0.00	1.63	0.00	1.82	0.00	1.87	2.18	2.17	2.57	2.56
90	1.60	1.39	1.23	1.17	1.14	0.00	1.12	0.00	1.20	0.00	1.36	0.00	1.52	1.78	1.93	2.32	2.32
140	1.10	0.84	0.87	0.72	0.81	0.00	0.79	0.00	0.98	0.00	1.00	0.00	1.32	1.58	1.86	2.05	2.18
190	0.85	0.60	0.61	0.56	0.63	0.00	0.63	0.00	0.89	0.00	0.95	0.00	1.26	1.47	1.79	2.01	2.39
240	0.42	0.45	0.04	0.04	0.01	-0.02	0.20	0.25	0.31	0.33	0.57	0.66	0.68	1.13	1.43	2.11	2.48
265	0.00	0.00	0.00	0.00	-0.30	-0.22	0.01	0.08	0.11	0.19	0.46	0.54	0.52	0.00	0.00	0.00	0.00
290	0.08	0.19	-0.33	-0.44	-0.46	-0.41	-0.11	-0.06	0.01	0.10	0.38	0.52	0.48	0.82	1.31	2.12	2.71
315	0.00	0.00	0.00	0.00	-0.53	-0.42	-0.17	-0.04	0.01	0.12	0.40	0.58	0.53	0.00	0.00	0.00	0.00
340	-0.20	0.00	-0.61	-0.54	-0.60	-0.49	-0.19	-0.09	0.00	0.09	0.42	0.55	0.54	0.92	1.37	2.28	2.69
365	0.00	0.00	0.00	0.00	-0.65	-0.55	-0.32	-0.18	-0.02	0.05	0.32	0.46	0.52	0.00	0.00	0.00	0.00
390	-0.68	-0.57	-0.92	-0.86	-0.75	-0.62	-0.41	-0.26	-0.11	0.01	0.24	0.39	0.46	0.85	1.23	2.11	2.51
415	0.00	0.00	0.00	0.00	-0.82	-0.70	-0.45	-0.28	-0.18	-0.03	0.11	0.33	0.46	0.00	0.00	0.00	0.00
440	-1.13	-1.07	-1.16	-1.08	-0.83	-0.69	-0.50	-0.35	-0.16	-0.03	0.16	0.37	0.50	0.99	1.48	2.13	2.43
490	-1.15	-1.36	-1.23	-1.09	-0.77	0.00	-0.53	0.00	-0.11	0.00	0.19	0.00	0.65	1.09	1.97	2.37	2.48
540	-1.25	-1.30	-1.29	-0.92	-0.88	0.00	-0.32	0.00	-0.12	0.00	0.34	0.00	0.58	1.32	1.81	2.29	2.43
590	-1.50	-1.40	-1.37	-0.90	-0.77	0.00	-0.24	0.00	-0.05	0.00	0.46	0.00	0.70	1.46	1.75	2.33	2.61
640	-1.31	-1.32	-1.39	-0.91	-0.76	0.00	-0.21	0.00	0.00	0.00	0.47	0.00	0.74	1.38	1.82	2.59	2.66
680	0.00	0.00	0.00	0.00	0.00	0.00	0.00	0.00	0.00	0.00	0.00	0.00	0.00	0.00	0.00	0.00	0.00

Note: X = the point in the direction parallel with longitudinal stiffeners (mm)  
 Y = the point in the direction perpendicular with longitudinal stiffeners (mm)

## Appendix-B Measurement of damaged plates before releasing boundary conditions (mm)

### SP-A2

X \ Y	0	20	70	120	170	195	220	245	270	295	320	345	370	420	470	520	550
0	-2.66	-2.84	-2.99	-2.99	-3.26	0.00	-3.25	0.00	-2.97	0.00	-3.05	0.00	-3.13	-3.06	-2.93	-2.91	0.00
40	0.59	0.62	1.06	0.99	1.24	0.00	1.12	0.00	1.40	0.00	1.42	0.00	1.52	1.56	1.61	1.32	1.15
90	6.33	6.70	7.06	7.25	7.49	0.00	7.54	0.00	8.06	0.00	7.95	0.00	8.23	7.98	8.42	8.15	7.91
140	12.41	12.71	13.18	13.49	13.65	0.00	14.07	0.00	14.16	0.00	14.35	0.00	14.54	14.51	14.85	14.59	14.53
190	18.38	18.54	18.97	19.75	19.93	0.00	20.40	0.00	20.56	0.00	20.95	0.00	20.88	21.25	21.21	21.12	20.75
240	23.73	24.39	25.62	26.32	26.76	26.97	27.10	27.83	28.57	28.82	27.93	27.67	27.60	28.07	28.43	27.84	27.86
265	0.00	0.00	0.00	0.00	29.92	30.17	30.56	31.75	32.62	32.80	31.16	31.16	31.36	0.00	0.00	0.00	0.00
290	29.25	29.87	31.98	32.61	33.20	33.49	33.81	35.68	37.09	36.57	34.73	34.49	34.75	35.09	35.34	34.51	34.65
315	0.00	0.00	0.00	0.00	37.15	36.95	37.36	39.89	42.03	41.09	38.54	38.44	39.04	0.00	0.00	0.00	0.00
340	34.30	34.70	39.96	38.53	41.21	40.94	40.33	43.94	49.52	48.22	42.10	42.54	42.78	42.15	43.42	41.34	43.00
365	0.00	0.00	0.00	0.00	42.58	42.02	40.87	45.37	53.44	52.46	43.11	43.84	45.61	0.00	0.00	0.00	0.00
390	32.22	33.43	37.81	36.79	38.38	38.25	38.52	42.11	46.53	46.82	40.27	40.39	40.84	40.61	42.97	40.50	42.73
415	0.00	0.00	0.00	0.00	34.01	34.16	34.57	36.86	38.34	38.21	36.01	36.11	36.67	0.00	0.00	0.00	0.00
440	26.66	27.51	29.05	29.62	30.08	30.51	30.84	32.29	32.98	32.83	31.93	32.33	32.51	33.16	33.41	33.53	33.89
490	20.59	20.72	21.45	22.03	22.65	0.00	23.60	0.00	24.25	0.00	24.27	0.00	25.05	25.23	25.49	25.58	25.91
540	13.71	13.96	14.50	14.97	15.75	0.00	16.14	0.00	16.58	0.00	17.06	0.00	17.55	17.98	18.14	18.65	18.32
590	7.03	7.02	7.82	8.09	8.75	0.00	9.11	0.00	9.69	0.00	9.64	0.00	10.37	10.50	10.87	11.24	11.05
640	0.14	0.44	0.75	0.95	1.08	0.00	1.80	0.00	2.23	0.00	2.51	0.00	2.93	2.92	3.32	3.52	3.63
680	-3.83	-3.97	-3.74	-2.90	-3.26	0.00	-2.67	0.00	-2.31	0.00	-1.86	0.00	-1.78	-1.43	-1.13	-0.37	-0.92

### SP-A3

X \ Y	0	20	70	120	170	195	220	245	270	295	320	345	370	420	470	520	550
0	1.06	0.94	0.34	0.15	0.05	0.00	-0.35	0.00	-0.98	0.00	-1.40	0.00	-1.53	-2.16	-2.66	-2.86	0.00
40	3.36	3.12	2.91	2.39	2.34	0.00	1.79	0.00	1.65	0.00	1.15	0.00	0.98	0.30	0.24	-0.26	-0.44
90	7.14	7.09	6.92	6.33	6.12	0.00	5.71	0.00	5.55	0.00	5.05	0.00	4.87	4.17	4.35	3.95	3.82
140	10.61	10.86	10.79	10.34	10.14	0.00	9.85	0.00	9.71	0.00	9.37	0.00	9.22	8.61	8.61	7.98	7.36
190	14.43	14.46	14.30	14.21	13.92	0.00	13.91	0.00	13.69	0.00	13.35	0.00	13.15	12.75	12.49	12.14	11.72
240	17.62	17.39	17.63	17.67	17.74	17.92	17.81	18.32	18.52	18.04	17.46	16.97	17.04	16.77	16.48	16.23	15.90
265	0.00	0.00	0.00	0.00	19.73	19.84	20.05	20.99	21.40	20.49	19.71	19.21	19.14	0.00	0.00	0.00	0.00
290	20.03	20.30	21.54	21.41	22.11	22.09	22.18	24.03	24.72	23.19	21.70	21.63	21.56	20.88	20.85	19.93	19.85
315	0.00	0.00	0.00	0.00	24.44	24.37	24.49	28.08	30.20	27.14	24.06	23.79	23.86	0.00	0.00	0.00	0.00
340	21.59	21.96	26.17	24.24	26.87	25.88	26.11	31.93	37.31	30.65	26.01	26.47	26.54	24.73	25.92	22.90	24.27
365	0.00	0.00	0.00	0.00	25.02	25.03	25.61	31.45	36.59	30.12	25.26	25.68	25.88	0.00	0.00	0.00	0.00
390	19.05	19.46	21.04	21.37	22.63	22.72	23.37	26.18	27.60	25.72	22.99	23.16	22.96	22.14	22.37	20.52	20.31
415	0.00	0.00	0.00	0.00	20.04	20.22	20.66	22.21	22.67	21.70	20.64	20.60	20.68	0.00	0.00	0.00	0.00
440	16.28	16.48	17.07	17.62	18.10	18.13	18.41	19.23	19.05	18.72	18.52	18.29	18.20	17.77	17.53	16.74	16.78
490	13.28	13.18	13.13	13.33	13.50	0.00	13.59	0.00	13.67	0.00	13.70	0.00	13.50	12.91	12.82	12.57	12.37
540	9.28	9.40	9.30	9.24	9.43	0.00	9.25	0.00	9.21	0.00	8.93	0.00	8.75	8.41	8.52	8.23	7.95
590	5.39	5.38	5.05	5.03	5.17	0.00	4.83	0.00	4.96	0.00	4.52	0.00	4.41	4.28	4.19	3.77	3.80
640	1.02	0.90	0.84	0.77	0.69	0.00	0.52	0.00	-0.01	0.00	-0.19	0.00	-0.44	-0.58	-0.62	-0.80	-1.03
680	-1.81	-1.95	-2.35	-2.44	-4.41	0.00	-2.88	0.00	-2.94	0.00	-3.22	0.00	-3.63	-3.80	-3.81	-4.02	-4.02

SP-B2

X \ Y	0	20	70	120	170	195	220	245	270	295	320	345	370	420	470	520	550
0	0.05	1.15	0.86	0.60	0.67	0.00	0.35	0.00	0.28	0.00	0.15	0.00	0.17	-0.05	-0.15	-0.19	0.00
40	3.27	3.15	3.20	2.79	2.94	0.00	2.59	0.00	2.61	0.00	2.29	0.00	2.36	1.79	2.14	1.83	2.02
90	6.57	6.69	6.73	6.09	6.26	0.00	5.91	0.00	5.84	0.00	5.45	0.00	5.37	5.08	5.33	4.72	4.86
140	9.89	10.01	9.78	9.64	9.47	0.00	9.42	0.00	9.00	0.00	8.76	0.00	8.39	8.13	7.75	7.38	6.73
190	12.97	13.03	13.06	12.98	12.78	0.00	12.64	0.00	12.55	0.00	11.96	0.00	11.53	11.14	10.54	10.15	9.64
240	15.34	15.45	15.94	15.84	16.16	16.18	16.39	17.48	18.11	16.25	15.07	14.92	14.61	13.92	13.35	12.37	11.94
265	0.00	0.00	0.00	0.00	17.90	17.75	18.31	19.82	20.63	18.49	16.69	16.25	16.08	0.00	0.00	0.00	0.00
290	17.20	17.61	18.76	18.70	19.79	19.78	20.18	22.46	23.35	20.77	17.96	17.70	17.47	16.36	15.76	14.08	13.47
315	0.00	0.00	0.00	0.00	22.07	21.93	22.25	27.83	28.17	23.38	19.58	19.44	19.01	0.00	0.00	0.00	0.00
340	19.12	18.95	21.22	20.94	24.67	23.99	23.97	33.41	34.32	26.75	20.91	21.16	21.40	18.30	17.96	15.00	14.33
365	0.00	0.00	0.00	0.00	23.33	23.29	24.58	35.71	37.40	27.47	20.80	20.97	20.88	0.00	0.00	0.00	0.00
390	18.40	18.68	21.63	19.55	20.71	20.95	21.95	27.54	28.64	24.10	19.06	18.82	18.49	16.96	16.48	14.20	13.72
415	0.00	0.00	0.00	0.00	18.28	18.41	18.98	21.21	21.79	19.35	16.90	16.71	16.48	0.00	0.00	0.00	0.00
440	15.29	15.30	16.28	15.53	15.83	15.88	16.26	17.29	17.17	16.26	14.91	14.84	14.63	13.73	12.98	11.87	11.42
490	10.95	10.84	10.80	10.89	10.96	0.00	10.90	0.00	10.64	0.00	10.47	0.00	10.27	9.90	9.49	9.02	8.56
540	5.89	5.98	6.33	6.43	6.23	0.00	6.46	0.00	6.31	0.00	6.11	0.00	6.24	5.97	5.79	5.41	5.24
590	1.19	1.32	1.64	1.94	1.98	0.00	1.97	0.00	2.31	0.00	2.18	0.00	2.40	2.28	2.16	1.95	1.96
640	-3.67	-3.74	-2.89	-2.82	-2.52	0.00	-2.16	0.00	-2.23	0.00	-2.00	0.00	-1.71	-1.91	-1.80	-2.07	-1.89
680	-6.08	-5.99	-5.55	-5.43	-5.25	0.00	-5.34	0.00	-5.96	0.00	-4.60	0.00	-4.53	-4.60	-4.55	-4.32	-4.57

SP-B3

X \ Y	0	20	70	120	170	195	220	245	270	295	320	345	370	420	470	520	550
0	-1.10	-1.05	-1.28	-1.30	-1.40	0.00	-1.52	0.00	-1.61	0.00	-1.71	0.00	-1.77	-2.32	-2.00	-1.95	0.00
40	-0.17	-0.20	0.02	-0.13	0.05	0.00	-0.03	0.00	-0.06	0.00	-0.23	0.00	-0.13	-0.37	-0.27	-0.72	-0.68
90	1.85	1.88	2.06	1.95	2.19	0.00	2.14	0.00	2.28	0.00	2.11	0.00	2.21	2.13	1.84	1.71	1.50
140	3.73	3.68	3.82	3.97	4.25	0.00	4.40	0.00	4.38	0.00	4.56	0.00	4.41	4.44	4.31	4.04	3.81
190	4.94	5.25	5.53	5.85	6.09	0.00	6.44	0.00	6.52	0.00	6.64	0.00	6.65	6.57	6.52	6.36	6.16
240	5.19	5.81	7.21	7.82	8.54	8.54	8.99	9.55	9.82	9.51	9.27	9.38	9.21	8.82	8.76	8.12	8.01
265	0.00	0.00	0.00	0.00	9.56	9.72	10.31	11.40	12.03	11.20	10.54	10.42	10.47	0.00	0.00	0.00	0.00
290	5.00	6.09	8.29	9.47	10.61	10.71	11.48	14.14	15.70	13.82	11.82	11.64	11.57	11.04	10.66	9.70	9.44
315	0.00	0.00	0.00	0.00	11.09	11.55	12.80	19.04	21.86	17.59	13.16	12.63	12.41	0.00	0.00	0.00	0.00
340	4.60	5.52	7.94	9.33	11.24	11.72	13.68	23.65	28.96	22.14	13.86	13.23	13.01	12.32	12.04	10.79	10.51
365	0.00	0.00	0.00	0.00	10.72	11.23	12.90	20.88	25.34	19.61	13.37	13.17	13.30	0.00	0.00	0.00	0.00
390	3.81	4.72	7.47	8.17	9.56	10.13	11.19	14.68	17.07	14.98	12.42	12.40	12.50	12.46	13.30	11.69	11.36
415	0.00	0.00	0.00	0.00	8.48	8.99	10.28	12.40	13.98	12.53	11.24	11.45	11.59	0.00	0.00	0.00	0.00
440	2.53	3.31	4.87	6.04	7.33	7.78	8.71	10.36	11.67	10.78	10.00	10.40	10.62	11.06	11.51	11.37	11.47
490	1.22	1.55	2.60	4.06	5.02	0.00	6.06	0.00	7.33	0.00	7.90	0.00	8.54	9.33	10.11	10.62	11.03
540	-0.77	-0.42	0.60	1.63	2.93	0.00	3.70	0.00	4.66	0.00	5.46	0.00	6.54	7.03	8.04	8.52	8.74
590	-3.01	-2.53	-1.35	-0.54	0.84	0.00	1.40	0.00	2.63	0.00	3.34	0.00	4.37	5.11	6.16	6.61	6.85
640	-5.10	-4.87	-3.66	-2.89	-1.47	0.00	-0.64	0.00	0.40	0.00	1.18	0.00	2.16	2.73	3.88	4.31	4.56
680	-6.47	-6.54	-5.28	-4.56	-3.37	0.00	-2.29	0.00	-1.33	0.00	-0.53	0.00	0.51	1.17	2.07	2.84	3.15

## Appendix-C Measurement of damaged plates after releasing boundary conditions (mm)

### SP-A2

X \ Y	0	20	70	120	170	195	220	245	270	295	320	345	370	420	470	520	550
0	-0.56	-0.22	-0.52	-0.34	-0.28	0.00	-0.20	0.00	-0.19	0.00	-0.03	0.00	0.05	0.44	0.37	0.62	0.86
40	4.36	4.48	4.53	4.67	4.89	0.00	4.91	0.00	5.34	0.00	5.30	0.00	5.12	5.31	5.61	5.43	5.52
90	12.66	13.02	13.49	13.43	13.61	0.00	13.54	0.00	13.73	0.00	13.64	0.00	13.79	13.80	13.84	13.54	13.65
140	20.85	21.05	21.57	21.56	21.95	0.00	22.00	0.00	22.02	0.00	21.84	0.00	22.18	21.94	21.87	21.79	21.71
190	29.15	29.57	29.77	29.81	30.13	0.00	30.29	0.00	30.03	0.00	30.43	0.00	30.24	29.97	29.78	29.94	29.65
240	37.75	37.84	38.35	38.53	38.80	38.86	38.90	39.83	40.09	39.65	38.64	38.69	38.37	38.58	38.29	37.39	36.50
265	0.00	0.00	0.00	0.00	43.03	42.92	42.96	45.27	46.67	44.72	42.85	42.70	42.73	0.00	0.00	0.00	0.00
290	47.44	45.44	48.68	46.99	47.95	47.62	47.28	54.59	55.20	50.92	47.04	47.48	47.39	46.50	48.13	44.35	43.51
315	0.00	0.00	0.00	0.00	52.87	51.50	50.77	59.66	61.86	54.29	49.85	51.09	52.21	0.00	0.00	0.00	0.00
340	48.55	46.69	49.60	49.07	50.59	50.16	50.03	56.31	58.17	52.81	49.46	50.58	50.73	49.11	51.19	46.38	45.91
365	0.00	0.00	0.00	0.00	46.59	46.48	46.72	49.67	51.21	48.76	46.64	46.69	47.03	0.00	0.00	0.00	0.00
390	39.89	40.32	41.59	42.31	42.77	42.82	43.40	45.17	45.86	44.99	43.38	43.53	43.43	43.64	43.74	41.87	41.55
415	0.00	0.00	0.00	0.00	39.09	39.23	39.64	41.49	41.87	40.88	40.20	40.26	40.46	0.00	0.00	0.00	0.00
440	33.28	33.76	34.81	35.50	35.91	35.94	36.39	37.74	37.84	37.33	37.09	37.24	37.49	37.59	37.48	36.78	36.70
490	26.33	27.26	28.01	28.65	29.01	0.00	29.74	0.00	30.04	0.00	30.44	0.00	30.89	31.19	31.02	31.43	31.31
540	19.88	20.55	21.44	21.93	22.63	0.00	23.04	0.00	23.64	0.00	24.29	0.00	24.65	24.94	25.34	25.62	25.55
590	13.35	14.68	14.76	15.34	16.04	0.00	16.76	0.00	17.33	0.00	17.81	0.00	18.42	18.99	19.67	19.75	19.68
640	6.25	6.89	8.44	8.73	9.24	0.00	9.92	0.00	10.90	0.00	11.39	0.00	12.08	12.53	13.50	13.66	13.84
680	2.20	2.41	3.35	3.72	4.67	0.00	5.22	0.00	6.43	0.00	6.68	0.00	7.49	8.26	9.18	10.03	10.04

### SP-A3

X \ Y	0	20	70	120	170	195	220	245	270	295	320	345	370	420	470	520	550
0	0.67	0.52	0.50	0.21	0.08	0.00	0.01	0.00	0.05	0.00	-0.09	0.00	-1.57	-0.14	-0.25	-0.06	0.08
40	4.22	3.97	3.86	3.83	3.68	0.00	3.76	0.00	3.80	0.00	3.84	0.00	3.66	3.59	3.42	3.33	3.26
90	9.19	8.98	9.13	8.98	8.71	0.00	8.80	0.00	8.87	0.00	8.56	0.00	8.53	8.25	7.99	7.88	8.05
140	13.57	13.81	13.66	13.68	13.50	0.00	13.48	0.00	13.49	0.00	13.23	0.00	13.16	12.86	12.60	12.52	12.26
190	18.18	18.38	18.43	18.32	18.29	0.00	18.36	0.00	18.25	0.00	18.00	0.00	17.67	17.28	16.95	16.57	16.52
240	22.46	22.54	23.00	23.28	23.41	23.32	23.33	23.58	23.81	23.36	22.87	22.66	22.29	21.66	21.13	20.11	19.83
265	0.00	0.00	0.00	0.00	25.69	25.70	25.67	26.36	27.31	26.57	25.32	24.90	24.47	0.00	0.00	0.00	0.00
290	25.99	26.25	27.66	27.65	28.23	28.15	28.08	29.97	32.97	30.94	27.81	27.14	26.95	25.64	25.01	23.47	22.90
315	0.00	0.00	0.00	0.00	30.78	30.73	30.33	35.20	41.26	36.31	30.28	29.44	29.49	0.00	0.00	0.00	0.00
340	29.76	28.47	31.68	29.96	31.79	31.53	30.77	35.17	42.27	37.20	30.90	30.48	31.39	28.46	30.31	25.90	25.33
365	0.00	0.00	0.00	0.00	29.02	28.80	28.84	31.57	34.38	32.82	29.17	28.73	28.69	0.00	0.00	0.00	0.00
390	25.33	25.33	25.95	25.95	26.32	26.31	26.57	27.90	29.20	28.72	26.96	26.43	26.38	25.68	25.65	24.31	24.09
415	0.00	0.00	0.00	0.00	23.86	24.08	24.14	24.91	25.76	25.24	24.33	24.18	23.98	0.00	0.00	0.00	0.00
440	21.01	21.07	21.27	21.47	21.65	21.77	21.85	22.41	22.88	22.43	22.25	21.95	21.82	21.72	21.62	21.36	21.45
490	16.34	16.69	16.77	17.02	17.33	0.00	17.51	0.00	17.98	0.00	17.90	0.00	18.04	18.14	18.10	18.34	18.42
540	11.69	11.99	12.72	12.77	13.26	0.00	13.14	0.00	13.62	0.00	13.74	0.00	13.95	14.06	14.32	14.52	14.26
590	7.38	7.55	7.87	8.02	8.39	0.00	8.35	0.00	8.95	0.00	9.04	0.00	9.48	9.61	10.27	10.39	10.36
640	2.64	2.78	3.17	3.41	3.79	0.00	4.05	0.00	4.55	0.00	4.57	0.00	5.27	5.23	5.83	5.81	6.22
680	-0.15	-0.28	-0.34	-0.05	0.62	0.00	0.99	0.00	1.42	0.00	1.69	0.00	2.37	2.51	3.03	3.11	3.51

SP-B2

X \ Y	0	20	70	120	170	195	220	245	270	295	320	345	370	420	470	520	550
0	0.22	0.35	0.22	-0.41	0.21	0.00	0.00	0.00	-0.02	0.00	-0.04	0.00	-0.15	-0.35	-0.06	-0.08	0.11
40	2.47	2.38	2.83	2.70	2.88	0.00	2.77	0.00	2.90	0.00	2.84	0.00	2.91	2.69	2.65	2.00	1.88
90	6.23	6.38	6.76	6.93	7.04	0.00	7.09	0.00	7.20	0.00	7.38	0.00	7.31	7.27	7.43	6.97	6.88
140	9.42	9.76	10.28	10.56	10.88	0.00	11.03	0.00	11.36	0.00	11.56	0.00	11.59	11.75	11.83	11.69	11.80
190	12.60	13.08	13.69	14.34	14.85	0.00	15.15	0.00	15.65	0.00	15.98	0.00	16.13	16.34	16.27	16.47	16.55
240	15.05	15.70	17.09	17.91	18.92	19.23	19.41	20.76	21.82	22.19	21.21	20.85	20.90	20.67	21.42	20.92	20.85
265	0.00	0.00	0.00	0.00	20.63	20.93	21.30	23.83	26.75	26.24	23.92	23.35	23.29	0.00	0.00	0.00	0.00
290	17.17	17.82	20.46	21.10	22.60	23.04	23.43	28.19	33.68	33.07	26.59	25.69	25.69	24.64	27.16	24.22	23.89
315	0.00	0.00	0.00	0.00	24.78	24.94	24.85	31.35	41.44	40.15	29.00	27.90	28.24	0.00	0.00	0.00	0.00
340	17.46	18.20	21.44	21.89	25.17	25.04	24.80	30.35	38.63	38.05	28.72	28.46	29.41	25.78	26.01	24.15	24.00
365	0.00	0.00	0.00	0.00	22.86	23.18	23.51	27.31	31.95	31.87	26.52	26.29	26.82	0.00	0.00	0.00	0.00
390	16.57	17.18	18.90	19.81	21.03	21.61	21.90	24.62	27.15	26.67	24.36	24.07	24.14	23.42	23.46	22.58	22.21
415	0.00	0.00	0.00	0.00	19.53	19.97	20.47	22.15	24.50	23.71	22.58	22.14	22.10	0.00	0.00	0.00	0.00
440	14.55	15.08	16.28	16.98	17.96	18.30	18.62	20.03	21.87	21.39	20.47	20.26	20.22	20.37	20.51	20.28	20.25
490	12.07	12.68	13.31	14.12	14.66	0.00	15.25	0.00	16.03	0.00	16.39	0.00	16.66	17.00	17.24	17.50	17.47
540	8.69	9.33	10.07	10.63	11.17	0.00	11.80	0.00	12.26	0.00	12.77	0.00	13.12	13.50	13.83	14.21	14.18
590	6.53	6.48	7.26	7.22	7.79	0.00	8.12	0.00	8.66	0.00	8.91	0.00	9.54	9.73	10.13	10.42	10.60
640	3.12	3.07	3.87	3.54	4.19	0.00	4.43	0.00	5.02	0.00	5.15	0.00	5.83	5.77	6.50	6.69	6.86
680	0.31	0.67	0.95	1.30	1.75	0.00	1.95	0.00	2.35	0.00	2.71	0.00	3.16	3.31	3.77	4.34	4.59

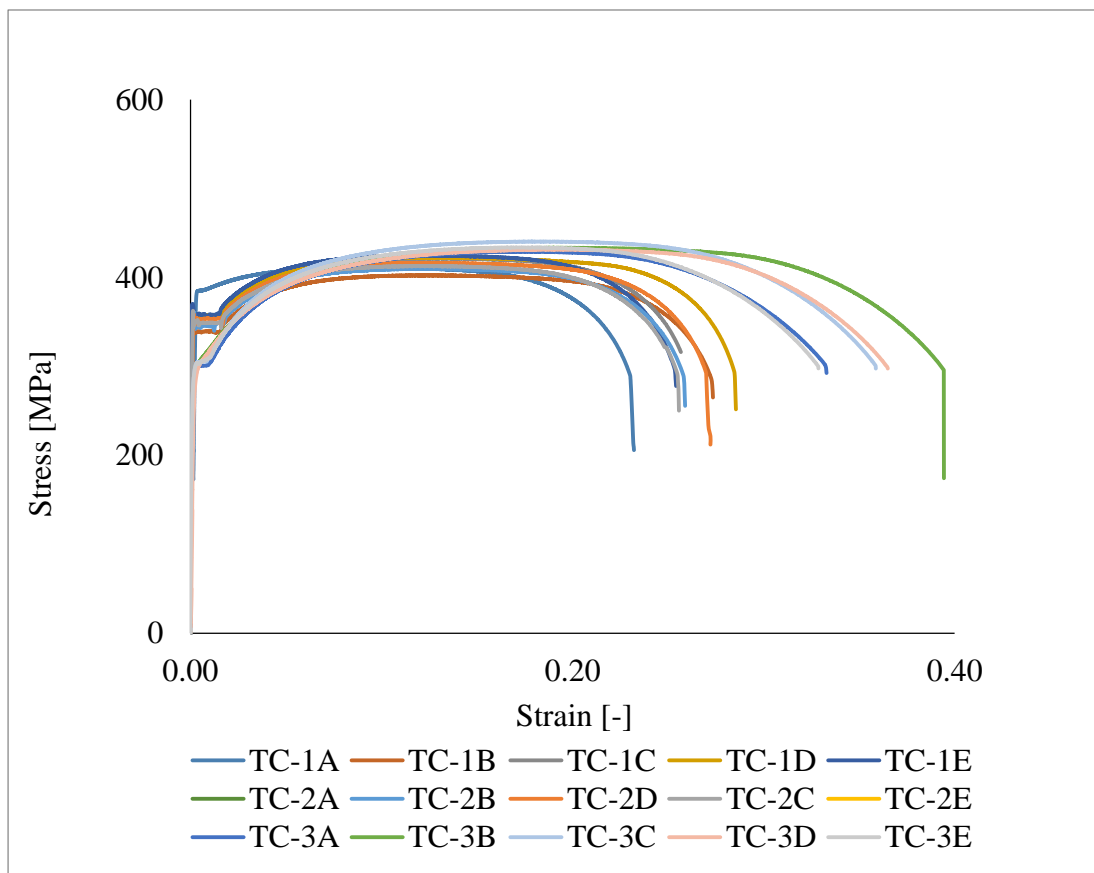
SP-B3

X \ Y	0	20	70	120	170	195	220	245	270	295	320	345	370	420	470	520	550
0	-0.84	-0.61	-0.88	-0.53	-0.55	0.00	-0.53	0.00	-0.03	0.00	0.16	0.00	0.34	0.38	0.72	1.11	1.25
40	0.32	0.36	0.85	0.87	1.37	0.00	1.48	0.00	1.86	0.00	1.96	0.00	2.37	2.34	2.51	2.58	2.67
90	2.75	2.86	3.39	3.63	4.02	0.00	4.34	0.00	4.56	0.00	4.80	0.00	5.03	5.16	5.20	5.32	5.31
140	5.12	5.32	5.65	6.13	6.51	0.00	6.91	0.00	7.25	0.00	7.58	0.00	7.80	8.03	8.04	8.16	7.92
190	6.93	7.33	7.84	8.43	8.85	0.00	9.52	0.00	9.80	0.00	10.28	0.00	10.50	10.58	10.72	10.93	10.76
240	7.72	8.43	10.09	10.89	11.85	12.00	12.48	13.32	13.67	13.48	13.35	13.46	13.52	13.48	13.55	13.15	13.18
265	0.00	0.00	0.00	0.00	13.07	13.36	13.90	15.49	16.04	15.72	14.76	14.90	14.99	0.00	0.00	0.00	0.00
290	7.96	9.10	11.60	12.97	14.46	14.68	15.34	18.43	20.12	18.55	16.38	16.23	16.27	16.08	15.92	15.12	15.13
315	0.00	0.00	0.00	0.00	15.15	15.72	17.00	23.07	26.29	22.76	17.90	17.44	17.37	0.00	0.00	0.00	0.00
340	8.12	9.13	11.73	13.43	15.48	16.19	18.29	28.66	33.79	27.21	18.94	18.31	18.23	17.74	17.66	16.65	16.58
365	0.00	0.00	0.00	0.00	15.24	15.92	17.63	25.23	30.52	25.12	18.77	18.47	18.74	0.00	0.00	0.00	0.00
390	7.72	8.76	11.65	12.66	14.30	15.01	16.32	20.25	22.46	20.64	17.76	17.87	18.19	18.35	19.47	17.97	17.85
415	0.00	0.00	0.00	0.00	13.44	14.04	15.29	17.63	19.43	17.97	16.93	17.21	17.43	0.00	0.00	0.00	0.00
440	7.07	7.85	9.66	11.22	12.48	13.13	14.17	15.84	17.37	16.60	16.00	16.44	16.82	17.44	18.07	18.15	18.38
490	6.11	6.52	7.77	9.46	10.76	0.00	12.10	0.00	13.46	0.00	14.25	0.00	15.19	16.13	17.06	17.84	17.93
540	4.64	5.09	6.38	7.52	9.06	0.00	10.15	0.00	11.39	0.00	12.31	0.00	13.54	14.40	15.47	16.38	16.54
590	2.85	3.50	4.80	5.88	7.33	0.00	8.38	0.00	9.64	0.00	10.62	0.00	11.92	12.86	14.09	14.78	15.15
640	1.12	1.58	2.96	4.08	5.55	0.00	6.58	0.00	7.77	0.00	8.79	0.00	9.97	10.88	12.19	12.84	13.18
680	-0.24	0.02	1.55	2.72	4.05	0.00	5.09	0.00	6.10	0.00	7.05	0.00	8.40	9.34	10.58	11.53	11.69

Note: X = the point in the direction parallel with longitudinal stiffeners (mm)  
 Y = the point in the direction perpendicular with longitudinal stiffeners (mm)

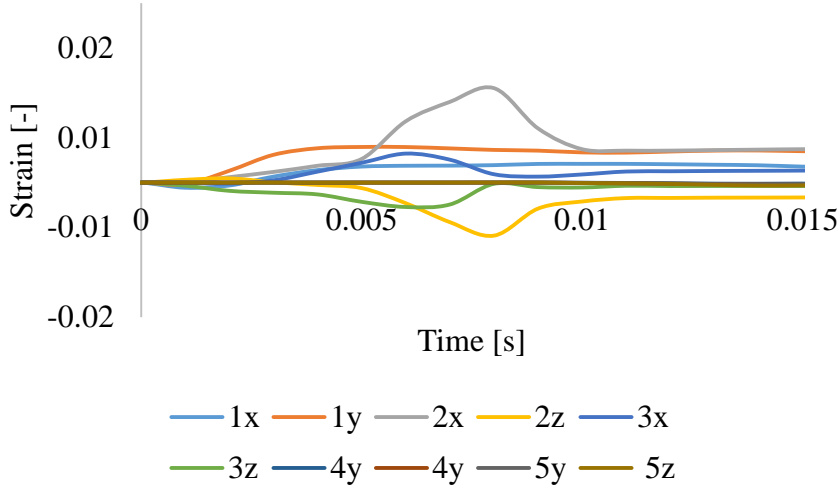
## Appendix-D Tensile test results

Coupons	E	$\sigma_Y$	$\epsilon_Y$	$\sigma_T$
	(MPa)	(MPa)		(MPa)
TC-1A	-	-	-	410.98
TC-1B	229847	335.58	0.0015	402.44
TC-1C	233786	352.55	0.0015	421.35
TC-1D	229008	357.71	0.0016	422.32
TC-1E	222758	358.79	0.0016	424.61
<b>Average</b>	228849.75	351.16	0.0015	416.34
TC-2A	236176	353.32	0.0015	416.22
TC-2B	216668	342.77	0.0016	409.66
TC-2C	227094	340.19	0.0015	412.82
TC-2D	230702	347.44	0.0015	416.36
TC-2E	260786	352.58	0.0014	421.89
<b>Average</b>	234285.20	347.26	0.0015	415.39
TC-3A	209738	305.80	0.0015	428.88
TC-3B	225053	300.67	0.0013	433.42
TC-3C	218540	304.64	0.0014	440.35
TC-3D	170943	300.86	0.0018	431.23
TC-3E	260786	70.95	0.0003	433.71
<b>Average</b>	217012.00	256.59	0.0012	433.52

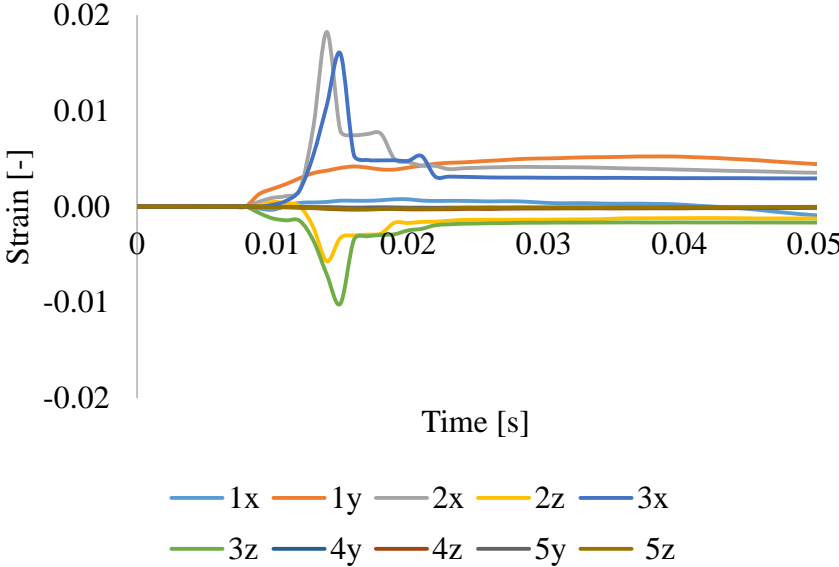


**Appendix-E Strain history of lateral collision tests (SP-A2 and SP-A3)**

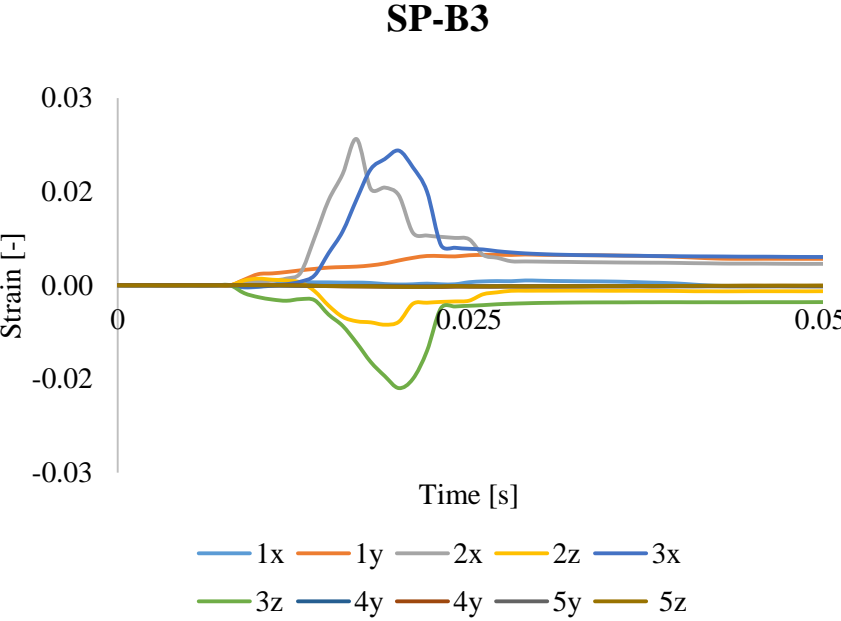
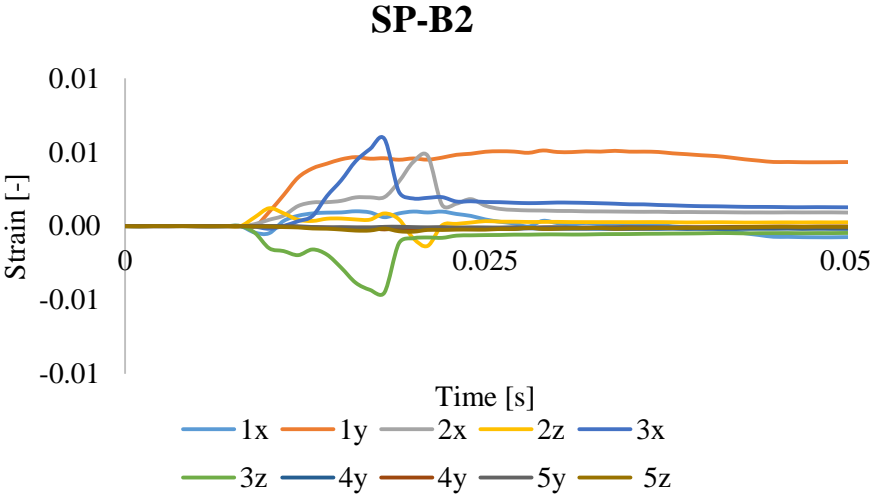
**SP-A2**



**SP-A3**

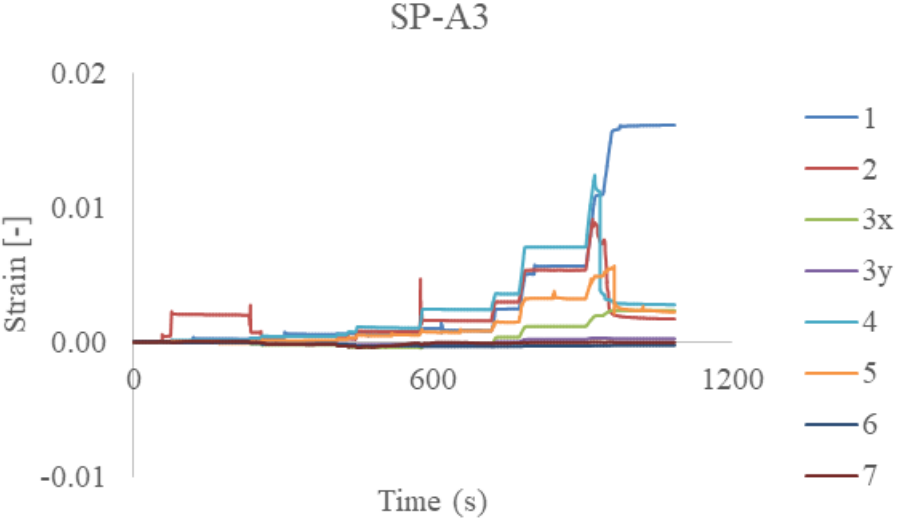
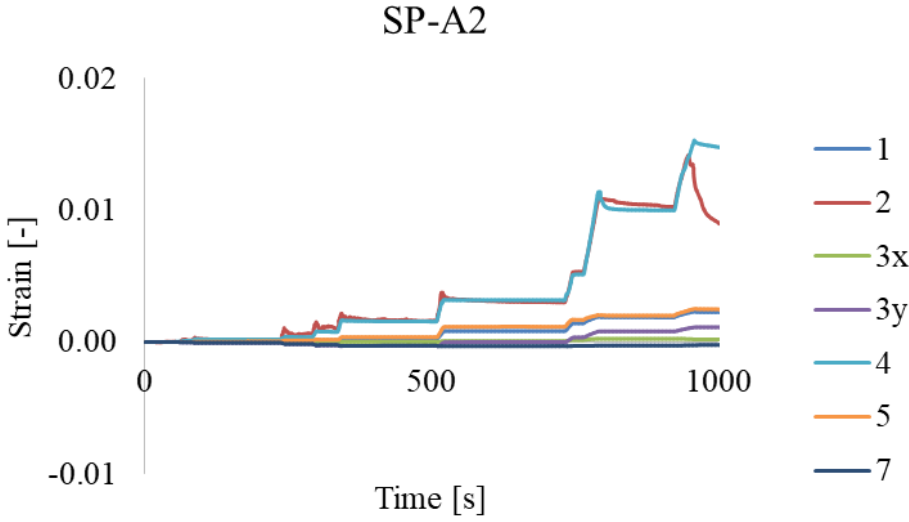


**Appendix-F Strain history of lateral collision tests (SP-B2 and SP-B3)**

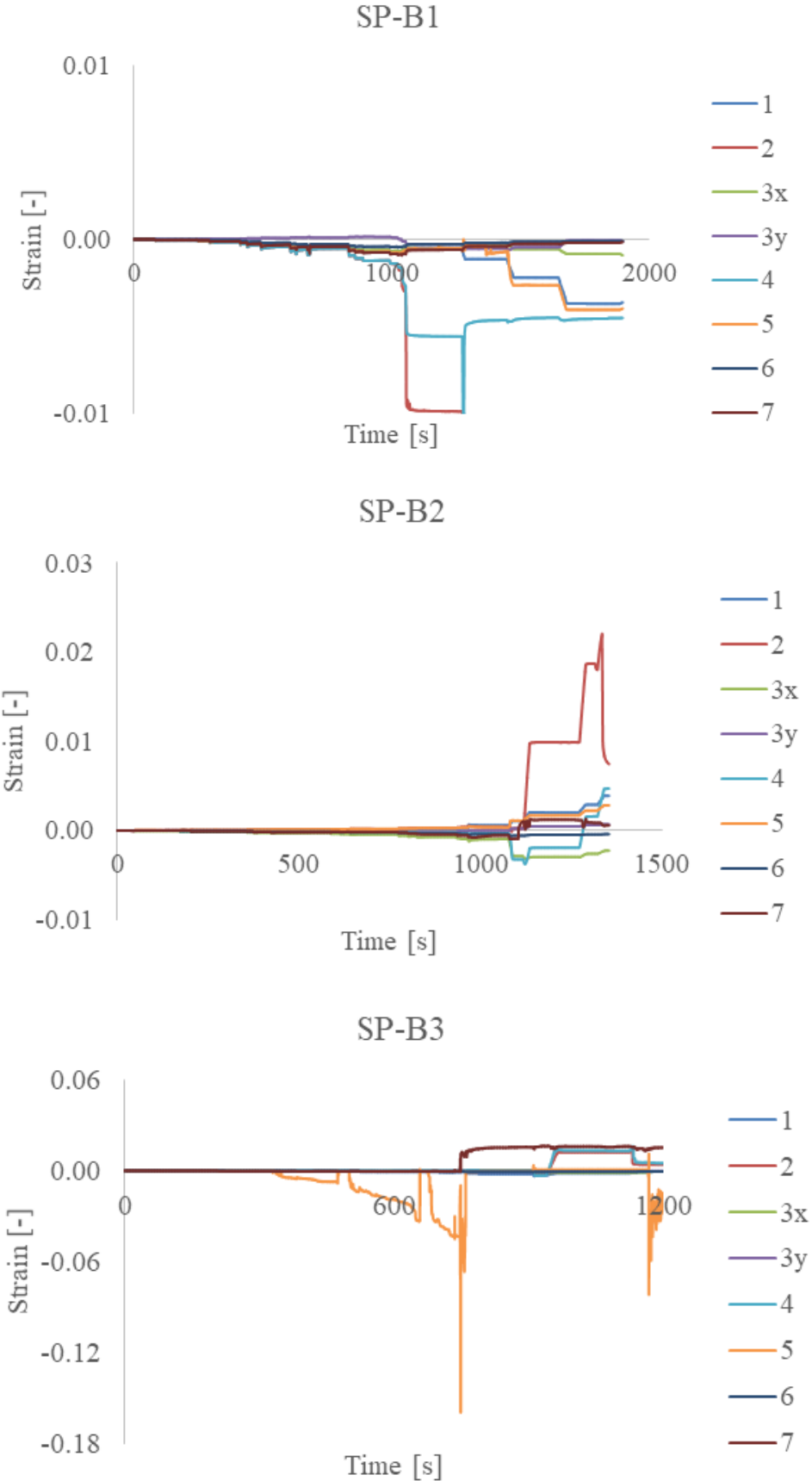




**Appendix-G Strain history of axial compression test (SP-A1, SP-A2 and SP-A3)**



**Appendix-H Strain history of axial compression test (SP-B1, SP-B2 and SP-B3)**



## Appendix-I Details of existing design formulations

### CSR-H

$$\frac{\gamma_c \sigma_a + \sigma_b + \sigma_w}{R_{eH}} S = 1$$

$$\sigma_a = \sigma_x \frac{st_p + A_s}{b_{eff1} t_p + A_s}$$

$$\sigma_b = \frac{M_0 + M_1}{1000Z}$$

$$\sigma_w = E y_w \left( \frac{t_f}{2} + h_w \right) \phi_0 \left( \frac{\pi}{l} \right)^2 \left[ \frac{1}{1 - \frac{0.4 R_{eH-s}}{\sigma_{ET}}} - 1 \right]$$

$$S = 1$$

$$\gamma_c = 1.25$$

### DNV

$$\frac{\sigma_{cr}}{\sigma_F} = \frac{1 + \mu + \lambda^2 - \sqrt{(1 + \mu + \lambda^2)^2 - 4\lambda^2}}{2\lambda^2}$$

$$\mu = 0.35(\lambda - 0.2)$$

$$\lambda = \sqrt{\frac{\sigma_Y}{\sigma_E}}$$

### Ref. [33]

$$\left( \frac{\sigma_{xa}}{\rho_c \sigma_{ec}} + \frac{\sigma_{xa} + \sigma_{xbs}}{\rho_t \sigma_{et}} + \frac{\sigma_{xa}}{\rho_{oa} \sigma_{eoax}} \right)^2 + \left( \frac{\sigma_{xa} + \sigma_{xb}}{\sigma_Y} \right)^2 = 1$$

$$\sigma_{ec} = \frac{\pi^2 EI}{Al^2}$$

$$\sigma_{et} = \frac{1}{I_o} \left( GJ + \frac{4\pi^2 EC_w}{l^2} \right)$$

$$\sigma_{eoax} = \frac{n^2 \pi^2 D_y}{\alpha_x B^2} \left[ \frac{D_x B^2}{D_y l^2} + \frac{2m^2 D_{xy}}{n^2 D_y} + \frac{m^4 l^2}{n^4 B^2} \right]$$

$$\sigma_{xb} = M_e \times \frac{Pba^2}{16}$$

$$\rho_c = 1.69\beta^{-0.69}\lambda_c^{1.63}\lambda_t^{0.09}$$

$$\rho_t = 0.332\beta^{0.47}\lambda_c^{-3.51}\lambda_t^{-1.14}$$

$$\rho_{oa} = 1$$

**Ref. [32]**

Ref. [32] procedure is the same with Ref. [33].

$$\rho_c = 0.2 + 0.6\beta^{0.5}\lambda_c^{1.2}\lambda_t^{0.4}$$

$$\rho_t = 0.6 + 9\beta^{-3.3}\lambda_c\lambda_t$$

$$\rho_{oa} = 1$$

## Appendix-J Summary of data

Ref.	Model	$L_{oa}$	$B_{oa}$	$t_p$	$l_{spa}$	$lh_w$	$lt_w$	$lw_f$	$lt_f$	$t_{spa}$	$th_w$	$tt_w$	$tw_f$	$tt_f$	E	$\varepsilon$	$\sigma_{YP}$	$\sigma_{YI}$	$\sigma_{Yg}$	$\sigma_u$
		mm	mm	mm	mm	mm	mm	mm	mm	mm	mm	mm	mm	mm	MPa		mm	MPa	MPa	MPa
[34]	1a	6115	3210	8.03	611.5	139.9	7.24	79.2	14.27	1223	240	9.4	125.9	18.35	207000	0.3	247.6	252.1	279.3	187.2
[34]	2b	6115	3210	7.39	305.8	105.1	5.4	44.8	9.56	1528.8	188	8.36	102.9	16.31	207000	0.3	258.1	273.2	234	221.9
[34]	3b	6115	3210	6.42	305.8	71.1	4.66	28	6.37	1528.8	140.1	6.91	79.5	14.27	207000	0.3	250.6	221.9	271.7	147.9
[34]	4a	6115	3210	6.45	254.8	70.6	4.87	27.8	6.37	1223	186.3	8.66	102.7	16.31	207000	0.3	258.1	232.5	255.1	200.8
[34]	5	6115	3210	6.45	611.5	106.9	5.35	46.4	9.56	1528.8	140.4	6.78	77.5	14.27	207000	0.3	246	229.4	268.7	172.1
[34]	6	6115	3210	6.34	611.5	70.1	4.56	27.5	6.37	1223	105.4	5.38	46.4	9.56	207000	0.3	255.1	240	264.2	122.3
[34]	7	6115	3210	6.32	611.5	105.9	5.17	45.4	9.56	1528.8	140.1	6.68	80	14.27	207000	0.3	288.3	303.4	262.7	181.1
[35]	T1-30	950	350	1.49	175	29.81	1.49	0	0	475	149	7.45	0	0	207000	0.3	181	181	18	82.2
[35]	T1-45	950	350	1.5	175	28.5	1.5	0	0	475	142.5	7.5	0	0	207000	0.3	155	155	155	75.8
[35]	T2-31	950	350	1.49	126	29.8	1.49	0	0	475	149	7.45	0	0	207000	0.3	181	181	181	102.8
[35]	T2-33	950	350	1.5	126	30	1.5	0	0	475	150	7.5	0	0	207000	0.3	174	174	174	105.4
[35]	T3-34	950	350	1.5	95.5	30	1.5	0	0	475	150	7.5	0	0	207000	0.3	176	176	176	135.8
[35]	T3-35	950	350	1.5	95.5	30	1.5	0	0	475	150	7.5	0	0	207000	0.3	176	176	176	126.2
[36]	P1R1T	325	325	4.4	162.5	30	5.1	0	0	162.5	36.4	4.7	35.3	4.7	207000	0.3	219	326	326	162.1
[36]	P1L1T	325	325	4.4	162.5	25	5.2	14.8	5.2	162.5	35.6	4.8	34.2	4.8	207000	0.3	225	326	326	160
[36]	P1T1T	325	325	4.4	162.5	25.4	4.6	25.3	4.6	162.5	35.5	4.9	35.2	4.9	207000	0.3	219	273	273	157.9
[36]	P2R1T	325	216	4.4	72	30	5.1	0	0	162.5	36	4.7	35.7	4.7	207000	0.3	219	326	326	194
[36]	P2L1T	325	217	4.4	72.3	25.1	5.1	14.6	5.1	162.5	36	4.6	35.9	4.6	207000	0.3	227	326	326	192
[36]	P2T1T	325	217	4.4	72.3	24.1	4.7	25	4.7	162.5	34.9	4.7	34.8	4.7	207000	0.3	220	273	273	196
[36]	P2R2T	216	216	4.4	72	30.1	5	0	0	72	35.7	4.7	35.7	4.7	207000	0.3	225	326	326	193.9
[36]	P2L2T	217	217	4.4	72.3	24.9	5.1	14.9	5.1	72.3	35.9	4.7	35.5	4.7	207000	0.3	227	326	326	221.1
[36]	P1T2T	216	216	4.4	72	25.2	4.6	24.8	4.6	72	35.8	4.8	35.5	4.8	207000	0.3	218	273	273	225
[36]	SP-A1	680	550	3	100	30	3	15	3	340	90	10	30	10	207000	0.3	351.74	347.83	256.9	252.3
[36]	SP-B1	680	550	4	100	40	3	20	3	340	90	10	30	10	207000	0.3	351.74	347.83	256.9	221.2
[37]	H	3200	2440	9.85	533	136.1	7.36	28.6	15.9	3200	1361	73.6	286	159	207000	0.3	377	377	377	266
[37]	J	3200	2440	9.95	533	136.1	7.36	28.6	15.9	3200	1361	73.6	286	159	207000	0.3	377	377	377	235
[37]	K	3200	2440	9.78	533	136.1	7.36	28.6	15.9	3200	1361	73.6	286	159	207000	0.3	377	377	377	235
[37]	R	3200	2440	9.95	533	136.1	7.36	28.6	15.9	3200	1361	73.6	286	159	207000	0.3	377	377	377	271
[37]	S	3200	2440	9.8	533	136.1	7.36	28.6	15.9	3200	1361	73.6	286	159	207000	0.3	377	377	377	254
[37]	T	3200	2440	9.8	610	87.7	6.6	22.2	14.3	1600	877	66	222	143	207000	0.3	340	340	340	170
[37]	U	3200	2440	9.66	610	87.7	6.6	22.2	14.3	1600	877	66	222	143	207000	0.3	312	312	312	174
[37]	W	3200	2440	9.6	457	436.1	7.36	28.6	15.9	3200	4361	73.6	286	159	207000	0.3	400	400	400	249
[37]	M	1600	2440	4.8	267	68.1	3.68	14.3	7.9	1600	681	36.8	143	79	207000	0.3	324	324	324	223

[38]	6	915	1523	9.5	457	152.5	16	0	0	915	1525	150	0	0	207000	0.3	259.5	264	264	241.2
[38]	1	915	1523	9.5	457	152.5	16	0	0	915	1525	160	0	0	207000	0.3	259.5	264	264	228.2
[38]	4	915	1523	9.5	457	152.5	16	0	0	915	1525	160	0	0	207000	0.3	259.5	264	264	234.8
[38]	2	915	1523	9.5	457	152.5	16	0	0	915	1525	160	0	0	207000	0.3	259.5	264	264	218
[38]	7	1830	1523	9.5	457	152.5	16	0	0	1830	1525	160	0	0	207000	0.3	254.7	268.1	268.1	206.3
[38]	14	1830	1523	9.5	457	152.5	16	0	0	1830	1525	160	0	0	207000	0.3	254.7	268.1	268.1	216.5
[38]	12	1830	1523	9.5	457	152.5	16	0	0	1830	1525	160	0	0	207000	0.3	254.7	268.1	268.1	206.4
[38]	8	1830	1523	9.5	457	152.5	16	0	0	1830	1525	160	0	0	207000	0.3	254.7	268.1	268.1	223.4
[38]	13	1830	1523	9.5	457	152.5	16	0	0	1830	1525	160	0	0	207000	0.3	275.5	262	262	202.7
[38]	11	1830	1523	9.5	457	152.5	16	0	0	1830	1525	160	0	0	207000	0.3	275.5	262	262	214.3
[38]	D22	1830	1523	10	457	80	12	0	0	1830	800	120	0	0	207000	0.3	244.3	287	287	150.9
[38]	D21	1830	1523	10	457	80	12	0	0	1830	800	120	0	0	207000	0.3	243	256	256	140.8
[38]	D23	1830	1523	10	457	80	12	0	0	1830	800	120	0	0	207000	0.3	243	289.4	289.4	109.1
[38]	D12	1830	1523	10	457	80	12	0	0	1830	800	120	0	0	207000	0.3	233.6	252.3	252.3	153.5
[38]	D11	1830	1523	10	457	80	12	0	0	1830	800	120	0	0	207000	0.3	282.9	290.7	290.7	179.8
[38]	B22	915	1523	6.5	457	152.5	9.5	0	0	915	1525	95	0	0	207000	0.3	352.2	344.5	344.5	216.3
[38]	B21	915	1523	6.5	457	152.5	9.5	0	0	915	1525	95	0	0	207000	0.3	345.2	351.6	351.6	232.9
[38]	B12	915	1523	6.5	457	152.5	9.5	0	0	915	1525	95	0	0	207000	0.3	349.3	332.7	332.7	224.7
[38]	B11	915	1523	6.5	457	152.5	9.5	0	0	915	1525	95	0	0	207000	0.3	367.4	333.9	333.9	223.9
[38]	A23	1830	1523	6.5	457	152.5	9.5	0	0	1830	1525	95	0	0	207000	0.3	352.2	323.9	323.9	208.6
[38]	A21	1830	1523	6.5	457	152.5	9.5	0	0	1830	1525	95	0	0	207000	0.3	345	334.7	334.7	219.6
[38]	A22	1830	1523	6.5	457	152.5	9.5	0	0	1830	1525	95	0	0	207000	0.3	334	323.9	323.9	186.4
[38]	A12	1830	1523	6.5	457	152.5	9.5	0	0	1830	1525	95	0	0	207000	0.3	349.3	354.5	354.5	199.7
[38]	A11	1830	1523	6.5	457	152.5	9.5	0	0	1830	1525	95	0	0	207000	0.3	367.4	334.7	334.7	194
[38]	E23	1830	1523	6.5	457	152.5	9.5	0	0	1830	1525	95	0	0	207000	0.3	329.8	369.5	369.5	151.9
[38]	E21	1830	1523	6.5	457	152.5	9.5	0	0	1830	1525	95	0	0	207000	0.3	335.6	353.3	353.3	149.9
[38]	E22	1830	1523	6.5	457	152.5	9.5	0	0	1830	1525	95	0	0	207000	0.3	343.2	389.6	389.6	119.1
[38]	E12	1830	1523	6.5	457	152.5	9.5	0	0	1830	1525	95	0	0	207000	0.3	334.7	377.9	377.9	164.2
[38]	E11	1830	1523	6.5	457	152.5	9.5	0	0	1830	1525	95	0	0	207000	0.3	335.9	374	374	162.3
[38]	3	915	1523	9.5	457	152.5	9.5	0	0	915	1525	95	0	0	207000	0.3	259.5	275.1	275.1	224.3
[38]	5	915	1523	9.5	457	152.5	9.5	0	0	915	1525	95	0	0	207000	0.3	259.5	275.1	275.1	215.6
[38]	9	1830	1523	9.5	457	152.5	9.5	0	0	1830	1525	95	0	0	207000	0.3	262.1	272.5	272.5	206.9
[38]	15	1830	1523	9.5	457	152.5	9.5	0	0	1830	1525	95	0	0	207000	0.3	275.5	272.5	272.5	187.5
[38]	10	1830	1523	9.5	262.1	152.5	9.5	0	0	1830	1525	95	0	0	207000	0.3	262.1	272.5	272.5	191